The Dissertation Committee for Scott Jason Zimmer Certifies that this is the approved version of the following dissertation:

Reducing Spacecraft State Uncertainty Through Indirect Trajectory Optimization

Committee:

Cesar Ocampo, Supervisor

Robert Bishop

David Hull

E. Glenn Lightsey

Timothy Crain

Reducing Spacecraft State Uncertainty Through Indirect Trajectory Optimization

by

Scott Jason Zimmer, B.S.

Dissertation

Presented to the Faculty of the Graduate School of

The University of Texas at Austin

in Partial Fulfillment

of the Requirements

for the Degree of

Doctor of Philosophy

The University of Texas at Austin

December 2005

Dedication

To Erin

To Mom and Dad

To Teachers

Acknowledgements

I have been blessed to know many outstanding teachers throughout my life. First and foremost my parents taught me the importance of education. They are most responsible for inspiring me to pursue this degree. In high school, two teachers, Toni Feeley and Barbara Markelz, challenged me to think critically for the first time. While I was an undergraduate at the University of Illinois, Todd Cerven and Professor Wayne Solomon welcomed me to their research groups even though I was not able to contribute to their research at the time I joined their groups. At Texas, Professor Cesar Ocampo introduced me to trajectory optimization through his Optimal Space Trajectories course. His passion for the topic and challenging assignments convinced me to pursue trajectory optimization. Throughout my time at Texas, Dr. Ocampo has always been eager to share research ideas, answer questions about trajectory optimization, and discuss whatever was on my mind. Robert Bishop has also been extremely helpful in sharing his knowledge of spacecraft navigation and covariance analysis. I would like to also thank Professor David Hull, Professor Glenn Lightsey, and Tim Crain for their valuable comments on this dissertation. Jean Philippe Munoz and Eric Monda taught me a great deal and made studying for the written qualifying exams at least somewhat enjoyable. Chris Ranieri read a draft of this dissertation and made many valuable suggestions. I would also like to thank all of the other graduate students at Texas that I have bounced ideas off or shared a beer with.

Most importantly, I would like to thank Erin. I cannot express how important you are in just a couple of lines, but I'll try. You help me be the person that I want to be.

Reducing Spacecraft State Uncertainty Through Indirect Trajectory Optimization

Publication No._____

Scott Jason Zimmer, PhD

The University of Texas at Austin, 2005

Supervisor: Cesar Ocampo

The exact position and velocity of a spacecraft is never known; instead, an estimate of the spacecraft location is determined based on observations of the spacecraft state. The accuracy of this state estimate depends on numerous factors including the number, quality, frequency, and types of measurements; the accuracy with which the equations of motion are modeled; and the trajectory of the spacecraft relative to the observer.

Many choices of trajectories are available to transfer a spacecraft from an initial set of constraints to a final set of constraints. Most efforts to optimize these transfers involve determining the minimum propellant or minimum time transfer. This dissertation provides a technique to determine trajectories that lead to a more accurate estimate of the spacecraft state.

The calculus of variations is used to develop the necessary theory and derive the optimality conditions for a spacecraft to transfer between a set of initial and final

conditions while minimizing a combination of fuel consumption and a function of the estimation error covariance matrix associated with the spacecraft Cartesian position and velocity components. The theory is developed in a general manner that allows for multiple observers, moving observers, a wide variety of observation types, multiple gravity bodies, and uncertainties in the spacecraft equations of motion based on the thrust related parameters of the spacecraft. A series of example trajectories from low Earth orbit (LEO) to a near geosynchronous Earth orbit (GEO) shows that either the trace or the integral of the trace of the covariance matrix associated with the Cartesian position and velocity can be reduced significantly with a small increase in the integral of the spacecraft thrust acceleration squared.

A method to minimize the uncertainty of the spacecraft state in a set of coordinates other than the one in which the spacecraft equations of motion and covariance are expressed is also introduced. The technique allows one to minimize the uncertainty in non-Cartesian components such as the spacecraft semimajor axis, flight path angle, or range without developing the equations of motion for the spacecraft or covariance in a non-Cartesian frame. Example problems with transfers from LEO to near GEO and LEO to lunar orbit demonstrate that the covariance associated with the semi-major axis can be reduced significantly with only a slight increase in fuel consumption.

Table of Contents

LIST OF FIGURES

LIST OF TABLES

CHAPTER 1 INTRODUCTION

Motivation

The objective of this investigation is to demonstrate a technique that determines trajectories which minimize a combination of fuel consumption and spacecraft state uncertainty. Most current research first seeks a mass or time optimal transfer, followed by a second, independent study to determine if the optimal trajectory can be navigated. One must determine the number, quality, frequency, and types of measurements of the spacecraft state which must be taken in order to navigate the spacecraft with the required precision. Because no effort was made to improve observability during the optimization process, observability along the optimal trajectory may be significantly worse than the observability along another trajectory that has only a slightly greater fuel or time cost.

It is well understood that the exact location and velocity of a spacecraft is never known. Because the exact spacecraft state cannot be determined, a nominal spacecraft location is determined along with estimates of the probability the spacecraft is within a given distance of the nominal location. The equations of motion for the spacecraft are idealized to remove terms such as differences between the prescribed and actual thrust level, gravity forces which are not modeled, and other perturbation terms. An estimate of the spacecraft state is determined based on the nominal state and measurements of function of the spacecraft state which are always corrupted by noise. The quality of these measurements depends on the spacecraft state and location of the observers. The nominal

spacecraft location at a given time is obtained by propagating the best available estimate of the initial spacecraft state forward in time using the nominal equations of motion.

The phrase ‘more observable’ is used throughout this dissertation to describe trajectories. It is important to note that this phrase is used to describe trajectories that have less uncertainty with respect to a user defined function of the spacecraft state over a user defined period of time. The trajectories described by this phrase may have more uncertainty associated with other functions of the spacecraft state or more uncertainty associated with the user defined function of the spacecraft state at times outside of the user defined time period of interest.

The uncertainty associated with the spacecraft state at a given time depends on the path the spacecraft traverses to reach that location. In Figure 1.1 two potential trajectories are shown which connect the same initial and final states. The spacecraft has an uncertainty shown by the orange circle if it traverses the red path and an uncertainty shown by the green oval if it traverses the blue path even though the uncertainty at the initial time is given by the yellow oval for both transfer paths. In this example, the two transfer paths are quite different. In many spacecraft transfers, modifying the transfer path slightly results in significant changes to the spacecraft uncertainty at the end of the transfer.

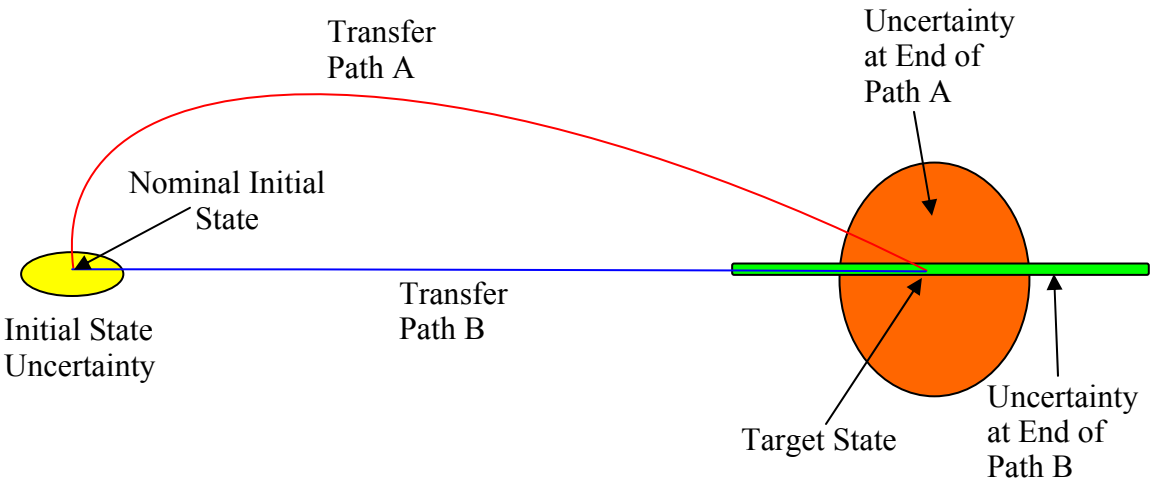

Figure 1.1 The Effect of Transfer Path on Spacecraft Uncertainty

These transfers illustrate one of the difficulties associated with minimizing the uncertainty associated with the spacecraft state at the end of a trajectory. Which path leads to the better spacecraft uncertainty at the final time? The blue path leads to a smaller area inside the uncertainty ellipse while the red path leads to a smaller maximum error distance. The optimal path depends on the specific spacecraft mission. If the goal is to minimize the horizontal error in final position, the red path would be optimal. If, instead, the goal is to minimize the vertical error in final position, the blue path would be optimal. This dissertation presents a method of minimizing the uncertainty associated with any function of the spacecraft state.

Previous Work

Numerous researchers have determined trajectories that 'optimally' transfer spacecraft from an initial state to a final state. Constraints may be imposed on these

transfers requiring certain launch windows, periods when the spacecraft must not fire its engine, or any other mission requirements. The definition of optimal has sometimes meant the transfer trajectory that consumes the least fuel, requires the least time, or a combination of the two. These optimal trajectories have been studied for decades with numerous methods available for solving the optimization problem. Betts provides an excellent summary of the techniques available for determining optimal trajectories.[1] This current investigation relied on indirect[2,3] trajectory optimization techniques.

Ideally, the optimization process should allow one to determine a trajectory that optimizes fuel efficiency or mission duration and observability simultaneously. Previous efforts to simultaneously improve the observability along a trajectory have been limited. In 1968, Vander Stoep[4] presented a method of transferring from a specified initial state to a specified final state in a fixed period of time. During this transfer both the continuous observations and the equations of motion were corrupted by white noise. The cost function for this study was an integral of a function of the control, state, covariance, and time combined with a weighted sum of elements of the Cartesian covariance matrix at the final time. In 1970, Schmidt[5] extended Vander Stoep's method to allow free final time as well as both free and linearly constrained final states. Schmidt's work focused on determining the optimal controls for a closed-loop feedback control system instead of designing a trajectory to minimize open-loop estimation errors.

Between 1984 and 1990 Speyer et. al.[6] and Hull et. al.[7,8] presented a method of improving the observability in the homing missile problem by minimizing the trace of the Fisher information matrix. They showed that the likelihood of missile intercept in the homing missile problem could be increased by altering the intercept trajectory away from

proportional navigation. In 1999, Oshman and Davidson[9] presented a method of optimizing the trajectory of an observer who is attempting to determine the location of a fixed target by taking observations of the angle between the local horizontal and the target. The cost function in this study was the determinant of the Fisher information matrix plus a penalty function that was based on the observer location. In addition, constraints were placed on the observer location. In this study, the control was discretized, and an approximate optimal control was determined.

Between 1996 and 2004 Seywald[10,11,12] investigated a technique to determine trajectories that were less sensitive to uncertainties in the initial spacecraft state. Seywald used the state transition matrix to estimate the first order error in the final state caused by errors in the initial spacecraft state. He included these errors in the cost function along with a measure of the fuel efficiency of the transfer. This technique would provide the same results as the current dissertation if the equations of motion were modeled without noise and no measurements were employed. In 2005, Mishne[13] applied the same technique to optimally reconfiguring a satellite formation when there is uncertainty in the initial state of the satellites.

Contributions

This dissertation provides a foundation upon which trajectory optimization can be accomplished with observability included as part of the cost function. It unifies the work of three separate papers[14,15,16] on utilizing a function of the covariance matrix in the cost function in order to determine trajectories that are more observable. The results from two

additional papers[17,18] also provide a necessary tool to determine many of the numerical solutions presented. The key contributions of each paper are summarized below.

In the first paper (Reference 14), the calculus of variations[19] is used to develop the necessary theory and derive the optimality conditions for a spacecraft to transfer from a set of initial conditions to a set of final conditions while minimizing a combination of fuel consumption and a function of the covariance matrix associated with the spacecraft Cartesian position and velocity components. The theory is developed in a general manner that allows for multiple observers, moving observers, any observation type, multiple gravity bodies, and uncertainties in the spacecraft equations of motion based on the thrust parameters. A series of example trajectories from low Earth orbit (LEO) to a near geosynchronous Earth orbit (GEO) shows that either the trace or the integral of the trace of the covariance matrix associated with the Cartesian position and velocity can be reduced by approximately 12 percent with an increase of less than one-half of one percent in the integral of the spacecraft thrust acceleration squared.

The second paper (Reference 15) provides a method to minimize the uncertainty of the spacecraft state in a frame other than the one in which the spacecraft equations of motion and covariance are expressed. The technique allows one to minimize the uncertainty in the spacecraft semimajor axis, flight path angle, range, or any other function of the spacecraft state without developing the equations of motion for the spacecraft or covariance in a non-Cartesian frame. Example problems demonstrate that the covariance associated with the semimajor axis at the end of a mass optimal transfer can be reduced by over ten percent with only a one-half of one percent increase in the integral of the thrust acceleration squared.

The third paper (Reference 16) expands the theory from Reference 14 to allow for the case where the observations are discrete instead of continuous measurements. Because the optimality conditions derived with the calculus of variations require the covariance matrix be included in the spacecraft state, each discrete observation provides a discontinuity in the spacecraft state. The theory is developed via the calculus of variations to determine the required relationship between the costates before and after each discrete measurement. A comparison is made between observations that are modeled as continuous and discrete.

References 17 and 18 provide a method of using the state transition matrix to determine the derivatives of a function of the spacecraft state at the final time with respect to parameters that determine the spacecraft state at an earlier time. These techniques provide an original method that allows the derivatives to be calculated even when the spacecraft state or equations of motion are discontinuous at a finite number of intermediate locations. Both papers show that the derivatives are accurate to the order of the integrator used to propagate the spacecraft equations of motion. These derivatives are also shown to allow the optimization process to converge to the optimal solution more quickly and more robustly than finite difference derivatives. These derivatives are employed throughout the examples in this dissertation in order to converge to optimal solutions.

The theory from References 14, 15, and 16 is also applied to a planar transfer from an Earth orbit to a lunar orbit. The gravitational effects of both the Earth and the moon are included throughout the trajectory. The trajectory is optimized for fuel consumption as well as the covariance associated with the spacecraft semimajor axis in

the final lunar orbit. Additionally, the observations are modeled as continuous measurements from three rotating observers located 120 degrees apart on the surface of the Earth. Alternating periods of continuous measurements and periods without measurements are employed during the transfer.

Dissertation Organization

Chapter Summaries

This dissertation is organized into five chapters and three appendices. The first chapter provides an introduction for the topic and illustrates the motivation for this research. The current chapter also provides a summary of the previous work in this area and discusses the contributions of this dissertation. The second chapter provides the framework for optimizing trajectories for both spacecraft uncertainty and fuel consumption. This chapter provides a technique that can be applied to any spacecraft transfer with any measurement type or types in order to minimize an arbitrary function of the covariance associated with any function of the spacecraft state. The example problems shown in the second chapter all involve planar transfers from LEO to near GEO. The third chapter demonstrates a technique to minimize the covariance associated with a non-Cartesian frame. The fourth chapter takes the techniques from the second and third chapters and applies them to more complicated transfers and terms in the covariance propagation. In this chapter, transfers where the observer rotates with the surface of the Earth and the noise in the dynamics is a function of the thrust level are solved. Additionally, transfers from Earth orbit to lunar orbit are solved where both bodies'

gravitational force affects the spacecraft throughout the transfer. The final chapter summarizes the key results of this work and discusses the conclusions that can be drawn from the dissertation. The first appendix demonstrates a technique of calculating semi-analytic derivatives which is needed in order to determine some of the solutions presented in this dissertation. The second appendix provides a summary of the adjoint control transformation which is used to determine the initial value of the position and velocity costates. The third appendix illustrates the patched conic gravity assist model that is employed in the first appendix.

Chapter Organization

Each chapter begins with a short summary of the key concepts from the chapter as well as the most interesting results. The remainder of each chapter consists of alternating theory and example transfers. Each chapter ends with a conclusion that summarizes the key results of the chapter and any conclusions that should be drawn from the example transfers. The second chapter includes a nomenclature section which defines all variables used in the first five chapters. Vectors in the nomenclature are specified by bold, lower case letters, and matrices are specified by bold, capital letters. The first appendix also includes a nomenclature section that defines the variables used in the appendices. Note that the meaning of a variable may be different in the appendices than in the first five chapters.

CHAPTER 2 MINIMIZING CARTESIAN STATE UNCERTAINTY

Chapter Summary

This chapter provides a method of determining trajectories that optimizes a combination of fuel consumption and observability. The measure of observability in this study is an arbitrary function of the estimation error covariance matrix associated with the spacecraft position and velocity vectors. The calculus of variations is employed to derive the first order optimality conditions between arbitrary initial and final constraints. The formulation is general and allows for arbitrary models of the observations and noise in the equations of motion. Example transfers from LEO to GEO show this technique can reduce the trace of the spacecraft estimation error covariance at the end of a mass optimal transfer by over thirty percent with less than a one-half of one percent increase in the integral of the thrust acceleration squared.

Nomenclature

a	semimajor axis
A	derivative of **y** state with respect to **x** state
B	relates covariance before and after a discrete measurement
e	eccentricity
F	derivative of time derivative of Cartesian spacecraft position and velocity with respect to Cartesian spacecraft position and velocity
g	gravitational acceleration acting on spacecraft
G	derivative of time derivative of **y** frame state with respect to **y** frame state

$\mathbf{H}$	derivative of observation with respect to spacecraft position and velocity
H_a	Hamiltonian function
J	one-half of the integral of spacecraft thrust acceleration squared
$\mathbf{L}$	derivative of measurement constraint with respect to covariance
m	spacecraft mass
n	number of discrete times a function of the spacecraft covariance is included in the cost function
$\mathbf{n}$	random vector of errors in observation
p	number of discrete measurements
$\mathbf{p}$	vector from central body to observer
P	power
$\mathbf{P}$	covariance matrix for spacecraft position and velocity
q	integral of the trace of the spacecraft covariance
$\mathbf{Q}$	spectral density matrix for errors in equations of motion
r	radial position
$\mathbf{r}$	spacecraft position
$\mathbf{R}$	spectral density matrix for observation noise
$\tilde{\mathbf{R}}$	covariance matrix for observation noise
$\mathbf{r}_s$	vector from observer to spacecraft
s	term that appears in the $\mathbf{L}$ matrix
t	time
T_1	error in thrust acceleration
u	thrust acceleration

$\mathbf{u}$	thrust direction unit vector
$\mathbf{v}$	velocity
$\mathbf{w}$	random vector of errors in equations of motion
W	cost function
w_1^2	constant term in spectral density matrix for equations of motion
x_s	x component of vector from observer to spacecraft
$\mathbf{x}$	Cartesian frame
$\mathbf{X}$	spacecraft Cartesian state including only position and velocity
$\tilde{\mathbf{X}}$	spacecraft state including covariance
y_s	y component of vector from observer to spacecraft
$\mathbf{y}$	arbitrary frame
$\mathbf{Y}$	spacecraft state in non-Cartesian frame
$\mathbf{z}$	observation
α	thrust direction
α_1	error in thrust direction
$\boldsymbol{\alpha}$	free variables in planar orbit to orbit transfer
$\boldsymbol{\beta}$	Lagrange multiplier
$\boldsymbol{\gamma}$	Lagrange multiplier
Γ	thrust acceleration magnitude
δ	Dirac delta function
$\boldsymbol{\eta}$	Lagrange multiplier
θ	polar angle
$\boldsymbol{\theta}$	constraints on the spacecraft state at the initial time

κ	true anomaly
λ_r	spacecraft radial position costate
$\boldsymbol{\lambda_r}$	spacecraft position costate
$\lambda_{\dot{r}}$	spacecraft radial position costate
$\boldsymbol{\lambda_v}$	spacecraft velocity costate
λ_J	thrust acceleration costate
λ_θ	spacecraft polar position costate
$\lambda_{\dot{\theta}}$	spacecraft polar velocity costate
$\lambda_{1\text{-}21}$	spacecraft covariance costate
μ	gravitational parameter of central body
$\boldsymbol{\upsilon}$	Lagrange multiplier
ξ	constant
$\boldsymbol{\rho}$	parameter vector used in constraints
$\boldsymbol{\sigma}$	constraint relating covariance before and after a discrete measurement
φ	scalar weight
$\boldsymbol{\chi}$	function of the covariance added to the cost function
$\boldsymbol{\psi}$	constraints on the spacecraft state at the final time
ω	longitude of perigee

Subscripts

0	initial
f	final
int	integrator

max	maximum
nom	nominal
r	radial
s	prescribed
t	cross-track

Superscripts

*	true value
&	targeted value
~	augmented state including the covariance terms
ˆ	function equivalent in different frame
_	covariance terms or covariance costates associated with **y** frame

General Theory

In order to use calculus of variations to optimize a trajectory, a scalar cost function must be defined to measure the trajectory's merit. Because the goal is to maximize a combination of the observability along a trajectory and the trajectory's fuel efficiency, the cost function must include both mass and observability terms. Improving the observability along a trajectory is important because the ability to deliver the spacecraft to the target orbit or constraint is dependent on how well the spacecraft state can be estimated. For a mass optimal solution the choice of cost function is straightforward with the mass of the spacecraft at the final time providing one obvious choice. Determining a scalar representation of the observability along a trajectory is

more difficult. Bishop et. al.[20] presented a method based on the inverse function theorem to estimate the state observability along a trajectory using the determinant of the observability matrix. This measure was rejected for this study because its effectiveness in measuring the observability along a trajectory is relatively unknown, and it yields an abstruse function that must be incorporated in the cost function.

The observability term for this study is a function of the estimation error covariance matrix associated with the spacecraft position and velocity because it provides an estimate of the mean square errors in the spacecraft position and velocity as well as the correlation between the errors in different components of the position and velocity vectors. A general cost function incorporating covariance is given by Eq. (2.1), where ε_i is an arbitrary function of the covariance, position, and velocity at discrete times, t_i, and χ is an arbitrary function of covariance, position, and velocity. The choice of ε_i and t_i allow one to minimize a given function of the covariance at any discrete time(s) such as immediately before an impulsive maneuver, gravity assist, or atmospheric entry. The function χ allows one to minimize the integral of a function of the covariance along the trajectory. Note that the covariance matrix included in the cost function is the covariance associated with Cartesian position and velocity. As explained in Chapter 3, one could select the functions ε and χ so the covariance associated with another coordinate frame such as orbital elements is included in the cost function.

$$W = J_f + \sum_{i=1}^{n} \varepsilon_i[\mathbf{r}(t_i), \mathbf{v}(t_i), \mathbf{P}(t_i)] + \int_{t_0}^{t_f} \chi[\mathbf{r}(t), \mathbf{v}(t), \mathbf{P}(t)]\, dt \tag{2.1}$$

The mass term in the cost function, J, is defined to be one-half the integral of the thrust acceleration squared as specified by Eq. (2.2). For a power limited propulsion

(PLP) engine, minimizing J is equivalent to maximizing the final mass since J and the fuel required are ordered and one to one.[21] The mass at any time can be determined from the initial mass and the power available to the engine using Eq. (2.3). Utilizing J, instead of mass, allows one to solve optimization problems when the initial spacecraft mass or the power available to the engine is not known. One can make this PLP formulation mimic a constant specific impulse formulation by constraining either the engine's thrust or specific impulse. The variable q is defined to be the integral of χ as shown in Eq. (2.4).

$$J(t) = \int_{t_0}^{t} \frac{\Gamma^2}{2} dt \tag{2.2}$$

$$m(t) = \frac{m(t_0)\, P_{max}}{P_{max} + m(t_0)\, J(t)} \tag{2.3}$$

$$q(t) = \int_{t_0}^{t} \chi[\mathbf{r}(t), \mathbf{v}(t), \mathbf{P}(t)]\, dt \tag{2.4}$$

In order to make the cost function depend only on the state, time, and constant parameters, define the augmented state, $\tilde{\mathbf{X}}$, as in Eq. (2.5) where P_i are defined in Eq. (2.6). The covariance terms are only associated with the position and velocity states and are defined in Eq. (2.6) for the three dimensional case. Because the covariance matrix is symmetric, there are only 21 unique elements for the three dimensional case.

$$\tilde{\mathbf{X}}^T = \left(\mathbf{r}^T\ \mathbf{v}^T\ J\ P_1\ \ldots\ P_{21}\ q\right) \tag{2.5}$$

$$\mathbf{P}_X \equiv \begin{pmatrix} P_{xx} & P_{xy} & P_{xz} & P_{x\dot{x}} & P_{x\dot{y}} & P_{x\dot{z}} \\ P_{xy} & P_{yy} & P_{yz} & P_{y\dot{x}} & P_{y\dot{y}} & P_{y\dot{z}} \\ P_{xz} & P_{yz} & P_{zz} & P_{z\dot{x}} & P_{z\dot{y}} & P_{z\dot{z}} \\ P_{x\dot{x}} & P_{y\dot{x}} & P_{z\dot{x}} & P_{\dot{x}\dot{x}} & P_{\dot{x}\dot{y}} & P_{\dot{x}\dot{z}} \\ P_{x\dot{y}} & P_{y\dot{y}} & P_{z\dot{y}} & P_{\dot{x}\dot{y}} & P_{\dot{y}\dot{y}} & P_{\dot{y}\dot{z}} \\ P_{x\dot{z}} & P_{y\dot{z}} & P_{z\dot{z}} & P_{\dot{x}\dot{z}} & P_{\dot{y}\dot{z}} & P_{\dot{z}\dot{z}} \end{pmatrix} \equiv \begin{pmatrix} P_1 & P_2 & P_3 & P_4 & P_5 & P_6 \\ P_2 & P_7 & P_8 & P_9 & P_{10} & P_{11} \\ P_3 & P_8 & P_{12} & P_{13} & P_{14} & P_{15} \\ P_4 & P_9 & P_{13} & P_{16} & P_{17} & P_{18} \\ P_5 & P_{10} & P_{14} & P_{17} & P_{19} & P_{20} \\ P_6 & P_{11} & P_{15} & P_{18} & P_{20} & P_{21} \end{pmatrix} \tag{2.6}$$

The time derivatives of the spacecraft position and velocity are given by Eqs. (2.7) and (2.8). In order to find the time derivative of the covariance matrix, the linearized time derivative of the position and velocity given by Eq. (2.9) is needed. The noise in the equations of motion is accounted for by **w,** which is a zero-mean Gaussian white noise process with spectral density **Q**. The model for the observation is given by Eq. (2.10). The noise in the observation measurement is accounted for by **n,** which is a zero-mean Gaussian white noise process with spectral density **R**. The time derivative of the covariance for periods of continuous measurements is given by the matrix Riccati equation given in Eq. (2.11)[22]. If no measurements are being taken, the time derivative of the covariance is given by Eq. (2.12). The relationship between the covariance after a discrete measurement and the covariance before the measurement is given by Eq. (2.13) where t_k is the time of the measurement.[22] The covariance at any time can be determined from the initial value of the covariance and Eqs. (2.11) to (2.13).

$$\dot{\mathbf{r}} = \mathbf{v} \tag{2.7}$$

$$\dot{\mathbf{v}} = \mathbf{g}(\mathbf{r}) + \Gamma\mathbf{u} \tag{2.8}$$

$$\begin{pmatrix} \dot{\mathbf{r}} \\ \dot{\mathbf{v}} \end{pmatrix} = \mathbf{F}\begin{pmatrix} \mathbf{r} \\ \mathbf{v} \end{pmatrix} + \mathbf{w};\ \mathbf{F} = \left.\frac{\partial\begin{pmatrix} \dot{\mathbf{r}} \\ \dot{\mathbf{v}} \end{pmatrix}}{\partial\begin{pmatrix} \mathbf{r} & \mathbf{v} \end{pmatrix}}\right|_{\mathbf{r},\mathbf{v}=\mathbf{r}_{nom},\mathbf{v}_{nom}} \tag{2.9}$$

$$\mathbf{z} = \mathbf{H}\begin{pmatrix}\mathbf{r}\\ \mathbf{v}\end{pmatrix} + \mathbf{n}; \quad \mathbf{H} = \left.\frac{\partial \mathbf{z}(\mathbf{r},\mathbf{v})}{\partial\begin{pmatrix}\mathbf{r} & \mathbf{v}\end{pmatrix}}\right|_{\mathbf{r},\mathbf{v}=\mathbf{r}_{nom},\mathbf{v}_{nom}} \tag{2.10}$$

$$\dot{\mathbf{P}} = \mathbf{F}\ \mathbf{P} + \mathbf{P}\ \mathbf{F}^{T} + \ \mathbf{Q}\ - \mathbf{P}\ \mathbf{H}^{T}\mathbf{R}^{-1}\mathbf{H}\ \mathbf{P} \tag{2.11}$$

$$\dot{\mathbf{P}} = \mathbf{F}\ \mathbf{P} + \mathbf{P}\ \mathbf{F}^{T} + \ \mathbf{Q} \tag{2.12}$$

$$\boldsymbol{\sigma} \equiv \mathbf{P}(t_{k+}) - \mathbf{P}(t_{k-}) + \mathbf{P}(t_{k-})\mathbf{H}^{T}(t_{k})[\mathbf{H}(t_{k})\mathbf{P}(t_{k-})\mathbf{H}^{T}(t_{k}) + \tilde{\mathbf{R}}]^{-1}\mathbf{H}(t_{k})\mathbf{P}(t_{k-}) = \mathbf{0} \tag{2.13}$$

It is important to note that both **Q** and **R** may be functions of the time, spacecraft state, or controls. Although extended Kalman filter theory does not allow these spectral densities to be a function of the spacecraft state or control, empirical evidence suggests this model is valid. The values of spectral density matrix, **R**, are based on the type of measurements taken, sensors used, and other factors related to a specific mission. For a discrete measurement, $\tilde{\mathbf{R}}$ is the covariance associated with the errors in the observation measurements. The values of the spectral density matrix, **Q**, are determined by how well the dynamic equations of motion are modeled as well as how accurately the engine can produce the desired thrust level.

The spectral density matrices, **Q** and **R**, and the initial covariance, $\mathbf{P}(t_0)$, must be determined a priori. Only the relative value of these matrices is important because they can be scaled by the same factor without altering the solutions obtained from the optimization process. Because the covariance throughout the trajectory will be scaled by that factor, the functions ε and χ should be divided by that same factor. The time derivative of the full spacecraft state can easily be determined from Eqs. (2.2), (2.4), (2.7), (2.8), (2.11), (2.12), and (2.13). The costates associated with the state defined by Eq. (2.5) are specified in Eq. (2.14). The Hamiltonian, H_a, omitted here because of its

length, can be determined using the equations for the time derivative of the state and Eq. (2.15).

$$\boldsymbol{\lambda}^T = (\boldsymbol{\lambda}_\mathbf{r}^T \; \boldsymbol{\lambda}_\mathbf{v}^T \; \lambda_J \; \lambda_1 \; \ldots \; \lambda_{21} \; \lambda_q)^T \tag{2.14}$$

$$H_a = \boldsymbol{\lambda}^T \dot{\tilde{\mathbf{X}}} \tag{2.15}$$

The optimal control problem is to transfer the spacecraft from an initial state constraint, given by Eq. (2.16), to the final state constraint, given by Eq. (2.17). The constraints may or may not include parameters, $\boldsymbol{\rho}$. Note the constraint may specify a prescribed initial and final orbit, a prescribed initial and final state, or some other function of the initial and final states. These constraints are adjoined to the cost function to form the augmented performance index in Eq. (2.18).

$$\boldsymbol{\theta}(t_0, x_0, \boldsymbol{\rho}) = \mathbf{0} \tag{2.16}$$

$$\boldsymbol{\psi}(t_f, x_f, \boldsymbol{\rho}) = \mathbf{0} \tag{2.17}$$

$$W' = W + \boldsymbol{\nu}^T \boldsymbol{\theta} + \boldsymbol{\eta}^T \boldsymbol{\psi} \tag{2.18}$$

The first variation of the augmented performance index is given by Eq. (2.19). Requiring the first variation of W' to be zero in order to minimize W' yields the conditions in Eqs. (2.20) to (2.28). These equations, along with Eqs. (2.16) and (2.17), form the constraints required to set up a two point boundary value problem (TPBVP). If the covariance associated with the error in the linearized dynamics and measurements is independent of the controls, then Eqs. (2.21) and (2.22) take on the familiar form of Eqs. (2.29) and (2.30).

$$\delta W' = \left(\frac{\partial W'}{\partial \tilde{\mathbf{X}}_f} - \boldsymbol{\lambda}_f^T \right) \delta \tilde{\mathbf{X}}_f + \left[H_a(t_f) + \frac{\partial W'}{\partial t_f} \right] \delta t_f + \left(\frac{\partial W'}{\partial \tilde{\mathbf{X}}_0} + \boldsymbol{\lambda}_0^T \right) \delta \tilde{\mathbf{X}}_0$$

$$+ \left[H_a(t_0) - \frac{\partial W'}{\partial t_0} \right] \delta t_0 + \frac{\partial W'}{\partial \boldsymbol{\rho}} \delta \boldsymbol{\rho} + \sum_{i=1}^{n} \left[\frac{\partial \varepsilon_i}{\partial \tilde{\mathbf{X}}(t_i)} - \boldsymbol{\lambda}(t_{i-}) + \boldsymbol{\lambda}(t_{i+}) \right] \delta \tilde{\mathbf{X}}(t_i)_{t_i \neq t_f} \qquad (2.19)$$

$$+ \int_{t_0}^{t_f} \{ (\frac{\partial H_a}{\partial \tilde{\mathbf{X}}} + \dot{\boldsymbol{\lambda}}^T) \delta \tilde{\mathbf{X}} + \frac{\partial H_a}{\partial \Gamma} \delta \tilde{\Gamma} + \frac{\partial H_a}{\partial \mathbf{u}} \delta \tilde{\mathbf{u}} \} \, dt$$

$$H_a(t_0) = \frac{\partial W'}{\partial t_0} \qquad (2.20)$$

$$\frac{\partial H_a}{\partial \Gamma} = 0 \qquad (2.21)$$

$$\frac{\partial H_a}{\partial \mathbf{u}} = \mathbf{0} \qquad (2.22)$$

$$\frac{\partial W'}{\partial \tilde{\mathbf{X}}_f} = \boldsymbol{\lambda}_f^T \qquad (2.23)$$

$$H_a(t_f) = -\frac{\partial W'}{\partial t_f} \qquad (2.24)$$

$$\boldsymbol{\lambda}_0^T = -\frac{\partial W'}{\partial \tilde{\mathbf{X}}_0} \qquad (2.25)$$

$$\frac{\partial W'}{\partial \boldsymbol{\rho}} = \mathbf{0} \qquad (2.26)$$

$$\frac{\partial \varepsilon_i}{\partial \tilde{\mathbf{X}}(t_i)} - \boldsymbol{\lambda}(t_{i-}) + \boldsymbol{\lambda}(t_{i+}) = \mathbf{0} \Big|_{i=1 \to n} \qquad (2.27)$$

$$\dot{\boldsymbol{\lambda}}^T = -\frac{\partial H_a}{\partial \tilde{\mathbf{X}}} \qquad (2.28)$$

$$\mathbf{u} = \frac{\boldsymbol{\lambda}_v}{\lambda_v} \qquad (2.29)$$

$$\Gamma = -\frac{\lambda_v}{\lambda_J} \tag{2.30}$$

Discrete Measurements

Because the optimality conditions derived with the calculus of variations require the covariance matrix to be included in the spacecraft state, each discrete observation provides a discontinuity in the spacecraft state. Consequently, the constraint relating the covariance after the measurement to the covariance before the measurement must be included in the cost function as shown in Eq. (2.31). The summation indicates that the covariance must be constrained at each of the p measurements. This discontinuity in the spacecraft state causes the optimal costates to be discontinuous across each measurement as well. Because discrete observations each add either 10 constraints for a planar transfer or 21 constraints for a three dimensional transfer, the state will have 10 or 21 times the number of observations discontinuities. These constraints require the unique elements of the covariance matrix to satisfy Eq. (2.13). While these jumps do not provide a theoretical difficulty, they do make it more difficult to numerically find solutions to the problem.

$$W' = J(t_f) + \sum_{i=1}^{n} \varepsilon_i[\mathbf{x}(t_i), \mathbf{P}_x(t_i)] + \int_{t_0}^{t_f} \chi[\mathbf{x}(t), \mathbf{P}_x(t)]dt + \boldsymbol{\upsilon}^T\boldsymbol{\theta} + \boldsymbol{\eta}^T\boldsymbol{\psi} + \sum_{k=1}^{p}\left(\boldsymbol{\gamma}^T\boldsymbol{\sigma}\right)_k \tag{2.31}$$

The costates before and after each measurement must satisfy Eqs. (2.32) to (2.36). Because of the formulation of the constraints in Eq. (2.13) where $\mathbf{P}(t_{k+})$ appears linearly, the costates after the measurement must satisfy Eq. (2.37). Consequently, one can formulate the constraint expressed in Eq. (2.38) where the **L** matrix is defined in Eq.

(2.39). The covariance costates after each measurement can be uniquely determined from the covariance costates before the measurement and the augmented spacecraft state, $\tilde{\mathbf{X}}$, as long as the **L** matrix can be inverted. If the **L** matrix is singular, then there exist an infinite number of possible values for the covariance costates after the measurement that satisfy the first order extremal conditions. As a result, no unique solution exists for the TPBVP if **L** is singular.

$$\lambda_i(t_{k-}) = \frac{\partial W}{\partial P_i(t_{k-})} \tag{2.32}$$

$$\lambda_i(t_{k+}) = -\frac{\partial W}{\partial P_i(t_{k+})} \tag{2.33}$$

$$\boldsymbol{\lambda}_r(t_{k+}) - \boldsymbol{\lambda}_r(t_{k-}) + \frac{\partial W}{\partial \mathbf{r}(t_k)} = \mathbf{0} \tag{2.34}$$

$$\boldsymbol{\lambda}_v(t_{k+}) - \boldsymbol{\lambda}_v(t_{k-}) + \frac{\partial W}{\partial \mathbf{v}(t_k)} = \mathbf{0} \tag{2.35}$$

$$\boldsymbol{\lambda}_J(t_{k+}) = \boldsymbol{\lambda}_J(t_{k-}) \tag{2.36}$$

$$\lambda_i(t_{k+}) = -\gamma_i \tag{2.37}$$

$$\mathbf{L}\ \bar{\boldsymbol{\lambda}}(t_{k+}) = \bar{\boldsymbol{\lambda}}(t_{k-}) \tag{2.38}$$

$$\mathbf{L}(i, j) = \frac{\partial \sigma_j}{\partial P_i} \tag{2.39}$$

In order to verify the existence of $\mathbf{L}^{-1}$, one could alternatively express the constraints from Eq. (2.13) as the constraints in Eq. (2.40) where the **B** matrix is defined in Eq. (2.41). If the **B** matrix is invertible, then the **L** matrix must also be invertible. Consider the case where the solution to the TPBVP is sought by integrating backwards in

time. At the time just after the last measurement, the entire augmented state and costate are known. The position, velocity, and integral of thrust acceleration squared do not change during the measurement, and the covariance before the measurement can be determined by inverting **B** in Eq. (2.40). The covariance costates before the measurement can be determined from Eq. (2.38) and the other costates before the measurement can be determined from Eqs. (2.34) to (2.36). This known, complete set of states and costates can then be integrated back in time until the time of the previous measurement, and the process can be repeated until the initial time is reached. The set of optimal costates will be unique in this solution. Because the solution is unique when the TPBVP is solved by integrating backwards in time, the costates must be unique when integrating forward in time and the inverse of **L** must exist.

$$\mathbf{P}(t_{k+}) = \mathbf{B}(t_{k+})\,\mathbf{P}(t_{k-}) \tag{2.40}$$

$$\mathbf{B} \equiv \mathbf{I} - \mathbf{P}(t_{k+})\mathbf{H}^{T}(t_{k})\tilde{\mathbf{R}}^{-1}\mathbf{H}(t_{k}) \tag{2.41}$$

Solution Process

The above equations provide a general method to determine optimal trajectories between any initial and final constraints. Note the term optimal means trajectories that maximize a combination of fuel efficiency and trajectory observability. By varying the relative values of the terms in the cost function, either fuel efficiency or observability can be emphasized.

A major difficulty associated with solving this type of TPBVP is the sensitivity of the solution process to the initial estimate of the costates. One might assume that including observability in the cost function makes determining an initial estimate quite

difficult since including observability requires the estimate of 14 initial costates instead of 4 initial costates for the mass optimal solution in two dimensions or 27 costates instead of 6 in three dimensions. In fact, it is no more difficult to estimate the costates with observability than without. The first step of the solution process should always be to solve the mass optimal problem and obtain the value of the costates for that problem. This solution, with all of the covariance costates set to zero, is an excellent initial guess if the observability terms in the cost function are multiplied by a small scalar weight. By slowly increasing these scalar weights for the observability terms in the cost function, one can 'walk' a mass optimal solution to a solution that optimizes for observability and fuel efficiency without needing to guess the initial costates for the covariance terms. Using the state transition matrix to compute derivatives (See Appendix A) instead of finite differences provides a faster, more robust method to 'walk' from solutions that ignore observability to ones that incorporate observability.[17,18]

The above method can be applied to any observation type using any number of observers. The observers may be fixed in space or their positions may be an arbitrary function of time. The errors in the measurements and the uncertainty in the dynamic equations may be constants or may be functions of the controls, spacecraft state, observer location, and time.

Planar Orbit to Orbit Transfer Optimality Conditions

The first application is a planar transfer through a central body gravity field from an initial orbit with eccentricity e_0, semimajor axis a_0, and argument of perigee ω_0 to a target orbit with eccentricity e_f, semimajor axis a_f, and argument of perigee ω_f. The

initial time is specified to be zero, and the final time is specified to be t_f. The location of the spacecraft in the initial and final orbit is free because the initial and final true anomalies are free variables. The constraints requiring the spacecraft transfer between the initial and final orbit are specified by Eqs. (2.42) and (2.43). The initial covariance is defined to be $\mathbf{P}_0$ and the spectral density of the uncertainty in the dynamic equations is given by the constant matrix **Q**. The measurements are continuous scalar range measurements from a single observer to the spacecraft. The observer's location is specified by **p**(t), which is a vector from the center of the central body to the observer. The spectral density of the uncertainty in the measurement is given by the constant matrix **R** which is a scalar. Utilizing these conditions, Eqs. (2.5) to (2.10) and (2.14) can now be written as Eqs. (2.44) to (2.47). The specific cost function for the examples in this chapter is given by Eq. (2.48) where q is the integral of the trace of the covariance.

$$\boldsymbol{\theta} = \begin{pmatrix} \mathbf{r}(t_0) - \dfrac{a_0(1-e_0^2)}{1+e_0\cos(\kappa_0)} \begin{pmatrix} \cos(\kappa_0+\omega_0) \\ \sin(\kappa_0+\omega_0) \end{pmatrix} \\ \mathbf{v}(t_0) + \sqrt{\dfrac{\mu_{cb}}{a_0(1-e_0^2)}} \begin{pmatrix} \sin(\kappa_0+\omega_0)+e_0\sin(\omega_0) \\ -\cos(\kappa_0+\omega_0)-\cos(\omega_0) \end{pmatrix} \\ t_0 - t_{0s} \end{pmatrix} \tag{2.42}$$

$$\boldsymbol{\psi} = \begin{pmatrix} \mathbf{r}(t_f) - \dfrac{a_f(1-e_f^2)}{1+e_f\cos(\kappa_f)} \begin{pmatrix} \cos(\kappa_f+\omega_f) \\ \sin(\kappa_f+\omega_f) \end{pmatrix} \\ \mathbf{v}(t_f) + \sqrt{\dfrac{\mu_{cb}}{a_f(1-e_f^2)}} \begin{pmatrix} \sin(\kappa_f+\omega_f)+e_0\sin(\omega_f) \\ -\cos(\kappa_f+\omega_f)-\cos(\omega_f) \end{pmatrix} \\ t_f - t_{fs} \end{pmatrix} \tag{2.43}$$

$$\begin{pmatrix}\dot{\mathbf{r}}(t)\\ \dot{\mathbf{v}}(t)\end{pmatrix}=\begin{pmatrix}\mathbf{0} & \mathbf{I}\\ \dfrac{\partial \mathbf{g}}{\partial \mathbf{r}} & \mathbf{0}\end{pmatrix}\begin{pmatrix}\mathbf{r}\\ \mathbf{v}\end{pmatrix}+\begin{pmatrix}0\\ 0\\ w_x\\ w_y\end{pmatrix} \tag{2.44}$$

$$\mathbf{z}(t)=\begin{pmatrix}\dfrac{\mathbf{r}_s^{\,T}}{r_s} & \mathbf{0}^{T}\end{pmatrix}\begin{pmatrix}\mathbf{r}(t)\\ \mathbf{v}(t)\end{pmatrix}+n_1 \tag{2.45}$$

$$\tilde{\mathbf{X}}^{T}=\left(\mathbf{r}^{T}\ \mathbf{v}^{T}\ J\ P_1\ P_2\ P_3\ P_4\ \ P_5\ P_6\ P_7\ \ P_8\ P_9\ \ P_{10}\ q\right) \tag{2.46}$$

$$\boldsymbol{\lambda}^{T}=\left(\boldsymbol{\lambda}_{\mathbf{r}}^{T}\ \boldsymbol{\lambda}_{\mathbf{v}}^{T}\ \lambda_J\ \lambda_2\ \lambda_3\ \lambda_4\ \lambda_5\ \lambda_6\ \lambda_7\ \lambda_8\ \lambda_9\ \lambda_{10}\ \lambda_q\right) \tag{2.47}$$

$$W=\phi_1 P_{xx}(t_f)+\phi_2 P_{yy}(t_f)+\phi_3 P_{\dot{x}\dot{x}}(t_f)+\phi_4 P_{\dot{y}\dot{y}}(t_f)+\phi_5 J(t_f)+\phi_6 q(t_f) \tag{2.48}$$

The six scalars in the cost function denoted by φ determine the relative importance of each element of the trace of the covariance at the final time, the integral of the trace of the covariance, and the propellant. The mass optimal solution is obtained by setting all of the φ_i to zero except for φ_5. In order to place more emphasis on the trajectory's observability at the final time, φ_1 to φ_4 can be increased. Increasing φ_6 will place more emphasis on minimizing the trace of the covariance along the entire trajectory. Because the magnitudes of the φ_i are irrelevant and only the relative values of the φ_i are important, φ_5 will always be set to one. If all the scalars are positive, the goal is to minimize the cost function; if the scalars are negative the goal is to maximize the cost function.

The problem can now be solved as a TPBVP with the 18 unknowns given by Eq. (2.49). The combination of **α** and Eq. (2.42) specifies the initial states and costates of the system given by Eqs. (2.46) and (2.47). The initial position and velocity costates are

determined using the adjoint control transformation discussed in Appendix B. Utilizing Eqs. (2.15) and (2.28), the time derivative of the costates along the optimal path can be written. The explicit expression is omitted here because of its length. The inclusion of Eqs. (2.29) and (2.30) specifies the equations of motion for the entire system (states and costates).

$$\boldsymbol{\alpha}^{\mathrm{T}} = \left(\boldsymbol{\lambda}_{\mathbf{r}}^{\mathrm{T}}(\mathrm{t}_0)\ \boldsymbol{\lambda}_{\mathbf{v}}^{\mathrm{T}}(\mathrm{t}_0)\ \lambda_{\mathrm{J}}(\mathrm{t}_0)\ \lambda_1(\mathrm{t}_0)\ \ldots\ \lambda_{10}(\mathrm{t}_0)\ \lambda_{\mathrm{q}}\ \kappa_0\ \kappa_{\mathrm{f}}\right) \tag{2.49}$$

The constraints that form the TPBVP are determined from Eqs. (2.23), (2.26), and (2.43). Eq. (2.23) provides the 12 constraints given by Eq. (2.50), and Eq. (2.43) provides four additional constraints. The final two constraints given by Eq. (2.51) are provided by Eqs. (2.23) and (2.26). Any trajectory satisfying these equations will be first order extremal.

$$\begin{aligned}
&\lambda_{\mathrm{J}}(\mathrm{t}_{\mathrm{f}}) = \phi_5 \\
&\lambda_1(\mathrm{t}_{\mathrm{f}}) = \phi_1 \\
&\lambda_5(\mathrm{t}_{\mathrm{f}}) = \phi_2 \\
&\lambda_8(\mathrm{t}_{\mathrm{f}}) = \phi_3 \\
&\lambda_{10}(\mathrm{t}_{\mathrm{f}}) = \phi_4 \\
&\lambda_{\mathrm{q}}(\mathrm{t}_{\mathrm{f}}) = \phi_6 \\
&\lambda_2(\mathrm{t}_{\mathrm{f}}) = \lambda_3(\mathrm{t}_{\mathrm{f}}) = \lambda_4(\mathrm{t}_{\mathrm{f}}) = \lambda_6(\mathrm{t}_{\mathrm{f}}) = \lambda_7(\mathrm{t}_{\mathrm{f}}) = \lambda_9(\mathrm{t}_{\mathrm{f}}) = 0
\end{aligned} \tag{2.50}$$

$$\begin{aligned}
&\boldsymbol{\lambda}_{\mathbf{r}}^{\mathrm{T}}(\mathrm{t}_0)\frac{\partial \mathbf{r}(\mathrm{t}_0)}{\partial \kappa_0} + \boldsymbol{\lambda}_{\mathbf{v}}^{\mathrm{T}}(\mathrm{t}_0)\frac{\partial \mathbf{v}(\mathrm{t}_0)}{\partial \kappa_0} = 0 \\
&\boldsymbol{\lambda}_{\mathbf{r}}^{\mathrm{T}}(\mathrm{t}_{\mathrm{f}})\frac{\partial \mathbf{r}(\mathrm{t}_{\mathrm{f}})}{\partial \kappa_{\mathrm{f}}} + \boldsymbol{\lambda}_{\mathbf{v}}^{\mathrm{T}}(\mathrm{t}_{\mathrm{f}})\frac{\partial \mathbf{v}(\mathrm{t}_{\mathrm{f}})}{\partial \kappa_{\mathrm{f}}} = 0
\end{aligned} \tag{2.51}$$

Example Transfers

Continuous Scalar Range Measurements

The example used to illustrate this technique is a 20,000 second planar transfer from an initial LEO with eccentricity equal to 0.05, semimajor axis equal to 7,000 kilometers, and argument of perigee equal to zero to a near GEO with eccentricity equal to 0.1, semimajor axis equal to 42,200 kilometers, and argument of perigee equal to zero. Unless specified, all distance units are kilometers and all time units are seconds. The Earth is the central gravity body and all third body effects are ignored. The observer is located at the center of the Earth in this example. In all of the examples that follow, φ_1, φ_2, φ_3, and φ_4 will always have the same value defined to be φ. Unless specified, the spectral density matrices for all the examples and the initial value of the covariance are given by Eqs. (2.52) to (2.54). These values are determined based on the sensors on the spacecraft and the models of the equations of motion that are employed. Additionally, q(t) will always be the integral of the equally weighted sum of the diagonal elements of the covariance matrix. Because these problems are solved with distance units of kilometers and time units of seconds, the magnitudes of the covariance elements associated with position are orders of magnitude larger than the magnitudes of the covariance elements associated with velocity. In effect, this choice of scaling places a much greater emphasis on decreasing P_1 and P_5 than on decreasing P_8 and P_{10}. To emphasize all elements of the covariance matrix equally, one could easily choose φ_3 and φ_4 to be orders of magnitude larger than φ_1 and φ_2 and could determine q(t) from Eq. (2.55) instead of as the trace of the covariance.

$$\mathbf{P}(t_0) = \begin{pmatrix} 10^{-5} & 0 & 0 & 0 \\ 0 & 10^{-5} & 0 & 0 \\ 0 & 0 & 10^{-8} & 0 \\ 0 & 0 & 0 & 10^{-8} \end{pmatrix} \tag{2.52}$$

$$\mathbf{Q} = \begin{pmatrix} w_1^2 & 0 \\ 0 & w_1^2 \end{pmatrix} = \begin{pmatrix} 10^{-16} & 0 \\ 0 & 10^{-16} \end{pmatrix} \tag{2.53}$$

$$\mathbf{R} = 10^{-1} \tag{2.54}$$

$$q(t) = \int_{t_0}^{t} \left(P_{xx} + P_{yy} + 10^8 \; P_{\dot{x}\dot{x}} + 10^8 \; P_{\dot{y}\dot{y}} \right) \, dt \tag{2.55}$$

In Figures 2.1 to 2.7, φ is zero and the value of φ_6 is increased in order to decrease the integral of the trace of the spacecraft's covariance. In Figure 2.1 it is clear that the paths followed on the optimal trajectories obtained with the integral of trace of the covariance increasingly contributing to the cost function are quite similar. In fact, at the scale of Figure 2.1, the trajectories appear to be the same. In Figure 2.2, one can observe that the trajectories that weight the integral of the trace of the covariance more heavily remain closer to the central body during most of the trajectory.

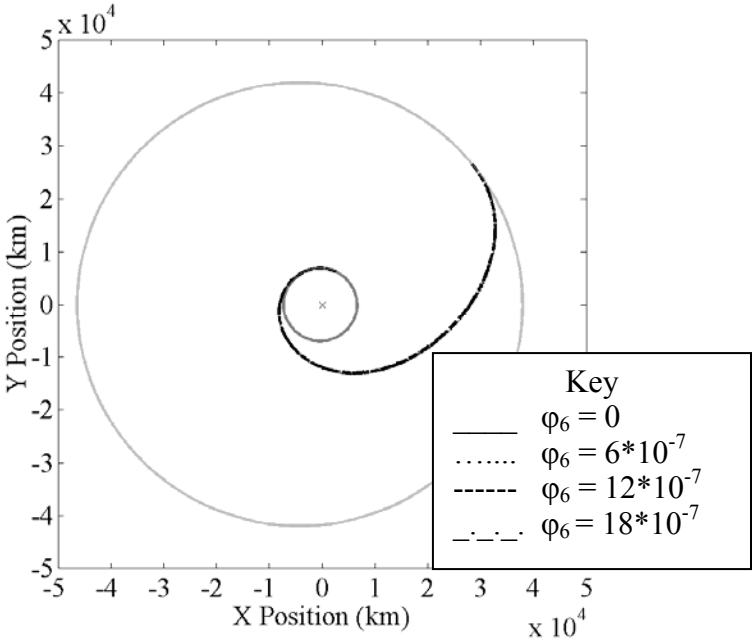

Figure 2.1 Optimal Trajectories

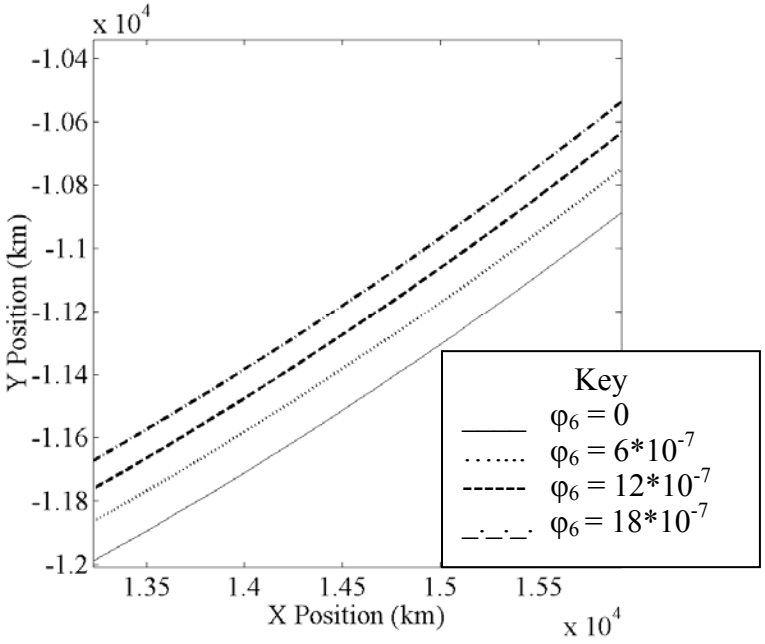

Figure 2.2 Magnified Portion of Optimal Trajectories

Figure 2.3 shows that the optimal thrust acceleration magnitudes for the trajectories are similar as well. Figure 2.4 shows that the difference between the thrust acceleration magnitude on trajectories that include observability in the cost function and the trajectory that is mass optimal is on the order of ten percent of the thrust acceleration.

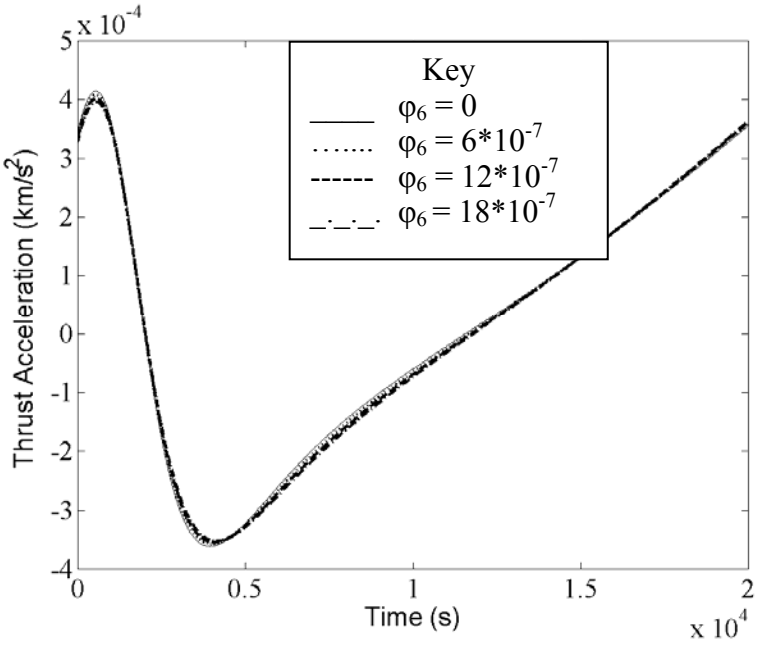

Figure 2.3 Thrust Acceleration Magnitude vs Time

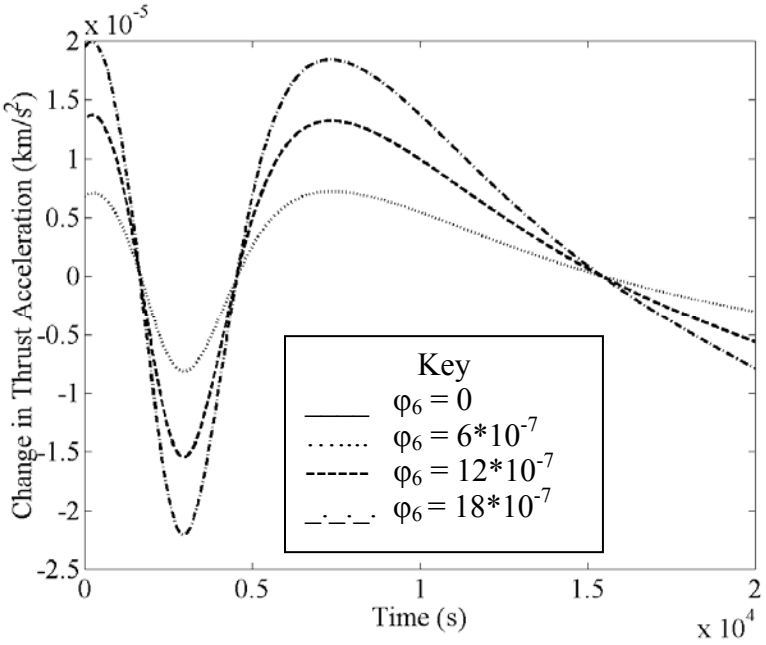

Figure 2.4 Perturbation to Thrust Acceleration Magnitude Caused by Including Observability in the Cost Function

Figure 2.5 shows the major difference between the optimal trajectories that incorporate covariance into the cost function. As the value of φ_6 is increased, the trace of the covariance is decreased significantly. Table 2.1 illustrates that a small increase in fuel consumption can significantly reduce the covariance. Between the mass optimal solution and the solution with φ_6 equal to $18*10^{-7}$, the integral of the trace of the covariance is reduced by over 12 percent while the integral of the thrust acceleration squared is only increased by about one-half of one percent. Notice the diminishing returns that are obtained by increasing the value of φ_6. As φ_6 is increased from 0 to $6*10^{-7}$, it takes less additional fuel to reduce the integral of the trace of the covariance than it does as φ_6 is increased from 6 to $12*10^{-7}$.

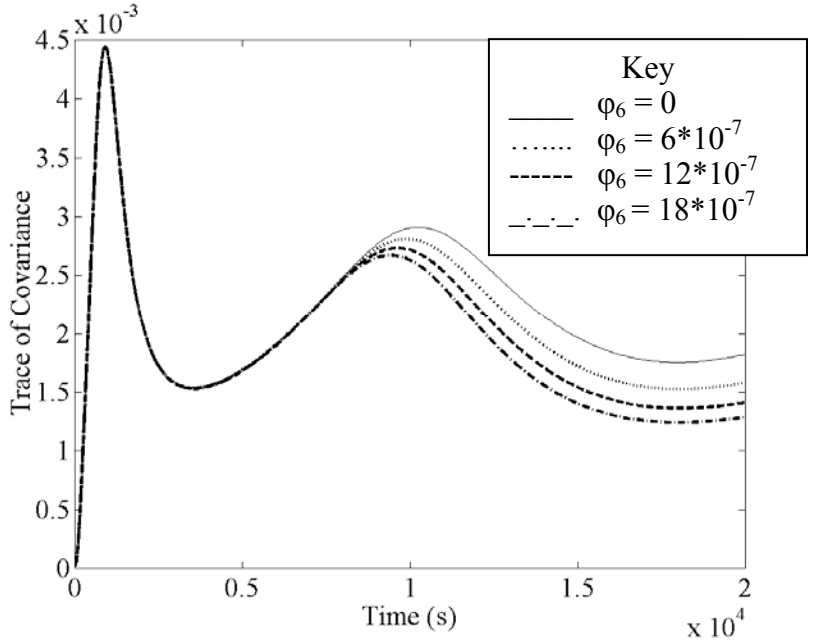

Figure 2.5 Trace of Covariance vs Time

Table 2.1 Observability and Fuel Usage for Trajectories Minimizing the Integral of the Trace of the Covariance

φ6 *10^{-7}	Integral of Thrust Acceleration Squared *10^{-4}	Change in Integral of Thrust Acceleration Squared *10^{-7}	Integral of Trace of Covariance	Change in Integral of Trace of Covariance	Trace of Covariance at Final Time *10^{-3}	Change in Final Trace *10^{-4}
0	16.9774	N/A	43.7312	N/A	1.8217	N/A
6	16.9910	13.6	41.3646	-2.3666	1.5806	-2.411
12	17.0230	45.6	39.5520	-4.1792	1.4122	-4.095
18	17.0662	88.8	38.1030	-5.6282	1.2876	-5.341

Figures 2.6 and 2.7 show a sampling of the behavior of the costates associated with the elements of the covariance matrix. As the value of φ_6 is increased, the graphs of the costates retain the same shape with the amplitude increasing. This observation is true for all of the costates, not just the sample illustrated in these figures.

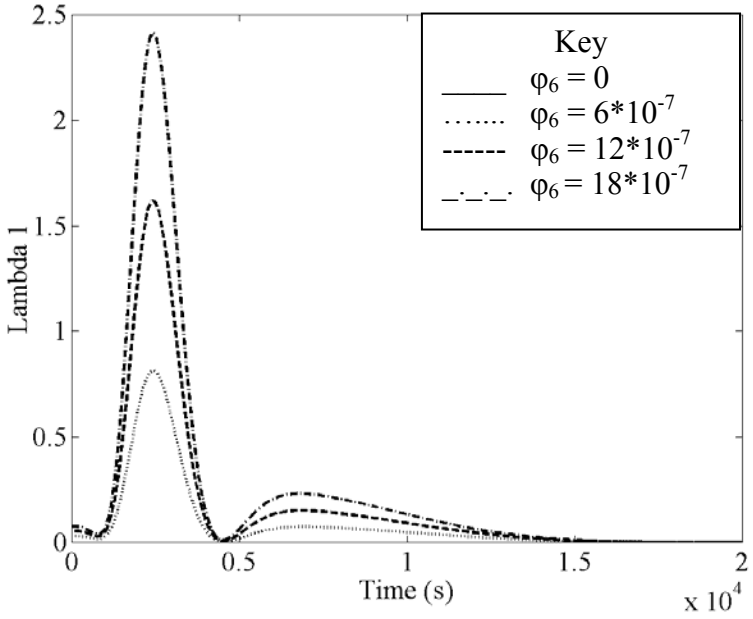

Figure 2.6 λ_1 vs Time

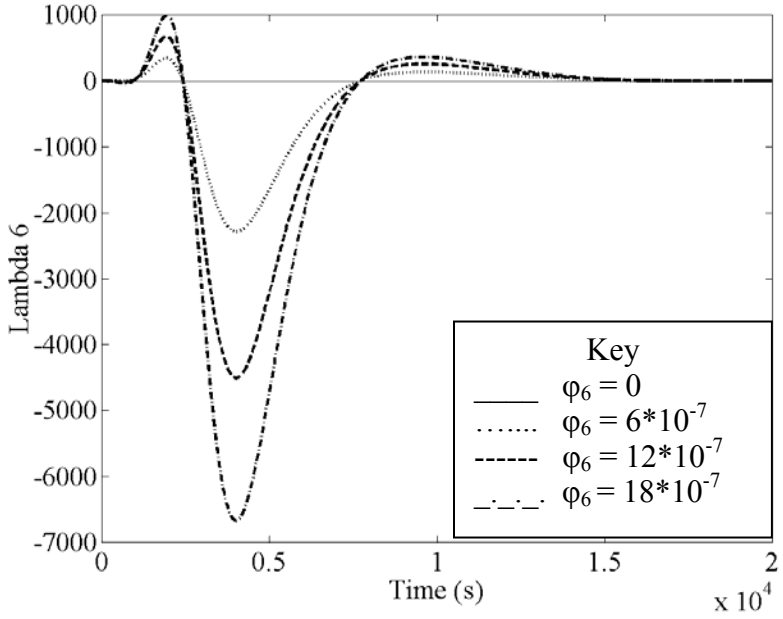

Figure 2.7 λ_6 vs Time

In the above example, φ was set to zero and the value of φ_6 was increased in order to incorporate observability into the optimization process. Alternatively, one could set φ_6 to zero and increase the value of φ in order to minimize the trace of the covariance at the final time instead of the integral of the trace of the covariance. This technique provides similar results to the above example. In fact, plots of the trajectories, controls, and costates are similar to those shown above with one exception. As φ is increased, the trajectories no longer remain closer to the central body during the majority of the trajectory as they did in the examples where φ_6 was increased. In fact, there is no correlation between the distance the spacecraft is from the central body during the majority of the trajectory and the value of φ.

Table 2.2 provides a summary of the fuel consumption and observability along each trajectory. The trace of the covariance at the final time can be reduced by over 31 percent with less than a .6 percent increase in the integral of the thrust acceleration squared. For this specific transfer problem, either method (increasing φ or increasing φ_6) will result in a trajectory where both the integral of the trace of the covariance and the trace of the covariance at the final time are reduced. As expected, increasing φ more efficiently reduces the trace of the covariance at the final time, while increasing φ_6 allows the integral of the trace of the covariance to be reduced with a smaller fuel penalty. In other transfer problems, increasing φ_6 may cause the trace of the covariance to be greater at the final time even though it reduces the integral of the trace of the covariance. Similarly, increasing φ may cause the integral of the trace of the covariance to increase even though it reduces the trace of the covariance at the final time. The values φ and φ_6

that produce the optimal trajectory (trajectory that balances observability and fuel efficiency optimally for a particular mission) will depend on the mission.

Table 2.2 Observability And Fuel Usage for Trajectories Minimizing the Trace of the Covariance at the Final Time

φ $*10^{-4}$	Integral of Thrust Acceleration Squared $*10^{-4}$	Change in Integral of Thrust Acceleration Squared $*10^{-7}$	Integral of Trace of Covariance	Change in Integral of Trace of Covariance	Trace of Covariance at Final Time $*10^{-}3$	Change in Final Trace $*10^{-4}$
0	16.977	N/A	43.7312	N/A	1.8217	N/A
55	16.989	11.6	41.5930	-2.1382	1.5894	-2.323
110	17.013	35.6	40.1272	-3.6040	1.4411	-3.806
165	17.042	64.6	39.0203	-4.7109	1.3348	-4.869
200	17.062	84.2	38.4371	-5.2941	1.2807	-5.410
220	17.073	95.6	38.1359	-5.5953	1.2533	-5.684

Periods Without Measurements

The optimality conditions derived using the calculus of variations for the case of continuous observations throughout the transfer are largely unchanged if there are periods when no observations are taken. The times when observations begin and end are not optimized and must be determined a priori. The time derivative of the covariance matrix will instantaneously change between Eqs. (2.11) and (2.12) when observations begin and end. Consequently, the Hamiltonian defined by Eq. (2.56) will change as well. Because the optimality conditions require the time derivative of the costates be given by Eq. (2.57), the time derivative of the costates will change as well. Both the augmented state and costate vectors will be continuous at the times when observations start or stop. The other optimality conditions determined by the calculus of variations are unchanged.

$$H_a = \boldsymbol{\lambda}^T \dot{\tilde{\mathbf{X}}} \tag{2.56}$$

$$\dot{\boldsymbol{\lambda}} = \frac{-\partial H_a}{\partial \tilde{\mathbf{X}}} \tag{2.57}$$

The same transfer as the first example with all of the parameters unchanged except for the spectral density associated with the measurement is used to illustrate the changes necessary when there are periods without observations. Continuous scalar range measurements are taken when the thousands digit of the elapsed time is an even number. Because the measurements are only taken half of the time, the spectral density associated with the measurement error was reduced by one-half. This value of the spectral density causes the final value of the trace of the covariance on the mass optimal solution to be nearly the same in this example and the first example.

$$\mathbf{R} = .05 \tag{2.58}$$

The results from optimizing the trajectory with periods that have no measurements are similar to the results obtained in the first example when observations were made continuously throughout the trajectory. Table 2.3 provides a summary of the fuel cost and trace of the covariance at the final time for various values of φ. Notice that φ_6 is zero in this example. The trace of the covariance can be reduced by 30 percent for about a one-half percent increase in the integral of the thrust acceleration squared. The results indicate that the fuel cost of reducing the covariance at the final time is the same whether the measurements are continuous throughout the transfer or there are periods without measurements. Figures 2.8 to 2.12 show the optimal trajectory, trace of the covariance, thrust acceleration magnitude, and costates for various values of φ. These figures are remarkably similar to the figures for the same variables for the case of

continuous measurements. The costates follow a curve with the same shape and phase behavior as the results from the first example.

Table 2.3 Integral of Thrust Acceleration Squared and Trace of Covariance at Final Time with Periods of No Observations

φ	Integral of Thrust Acceleration Squared $*10^{-4}$	Change in Integral of Thrust Acceleration Squared $*10^{-10}$	Trace of Covariance at Final Time $*10^{-3}$	Change in Final Trace $*10^{-6}$	$\frac{\Delta Tr[\mathbf{P}]}{\Delta J}$
0	16.97740	N/A	1.77833	N/A	N/A
.0001	16.97741	6	1.77285	-5.5	913.35
.0005	16.97753	134	1.75157	-26.8	166.25
.0010	16.97791	510	1.72632	-52.0	67.15
.0050	16.98720	9804	1.56459	-213.7	17.4
.0100	17.00772	30320	1.42504	-353.3	6.8
.0150	17.03281	55408	1.32372	-454.6	4.05
.0200	17.06007	82674	1.24538	-533.0	2.85
.0300	17.11718	139784	1.12974	-648.6	2
.0400	17.17500	197600	1.04657	-731.8	1.45
.0500	17.23222	254816	0.98271	-795.6	1.1

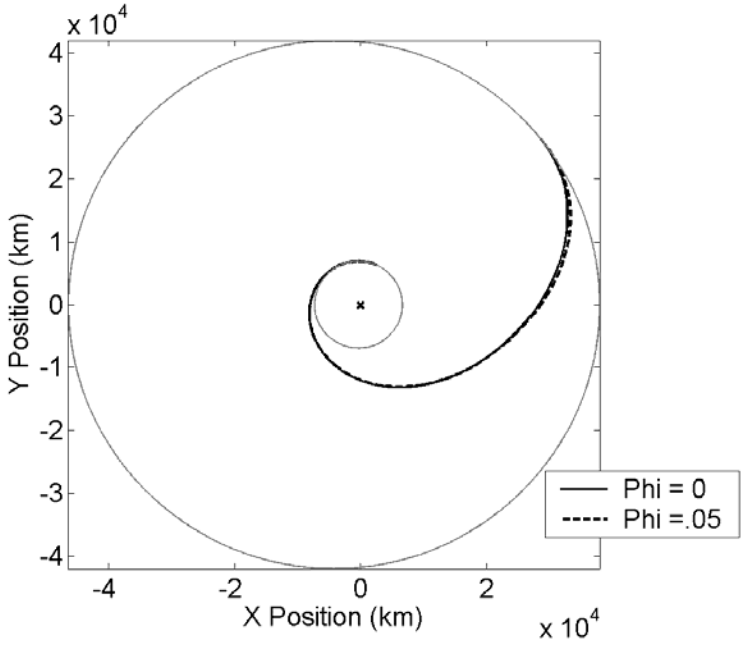

Figure 2.8 Optimal Trajectories

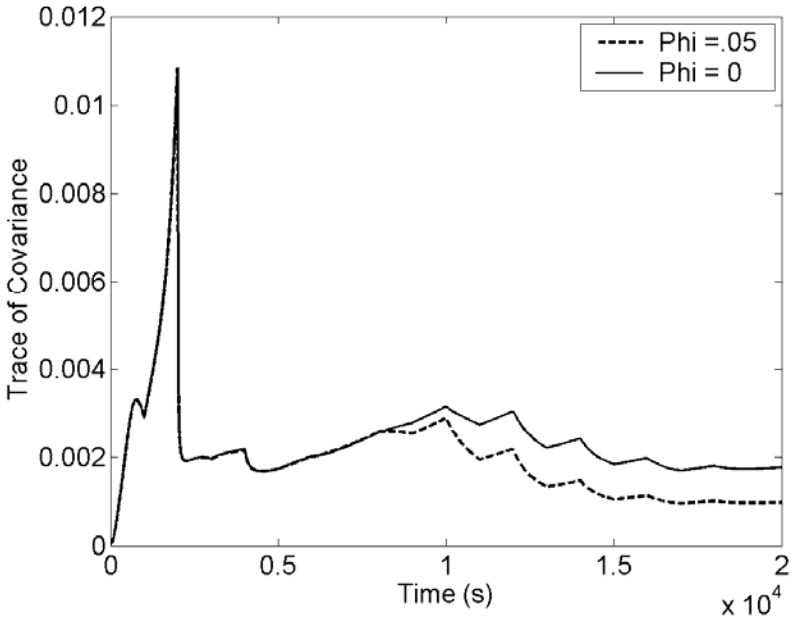

Figure 2.9 Trace of Covariance vs Time

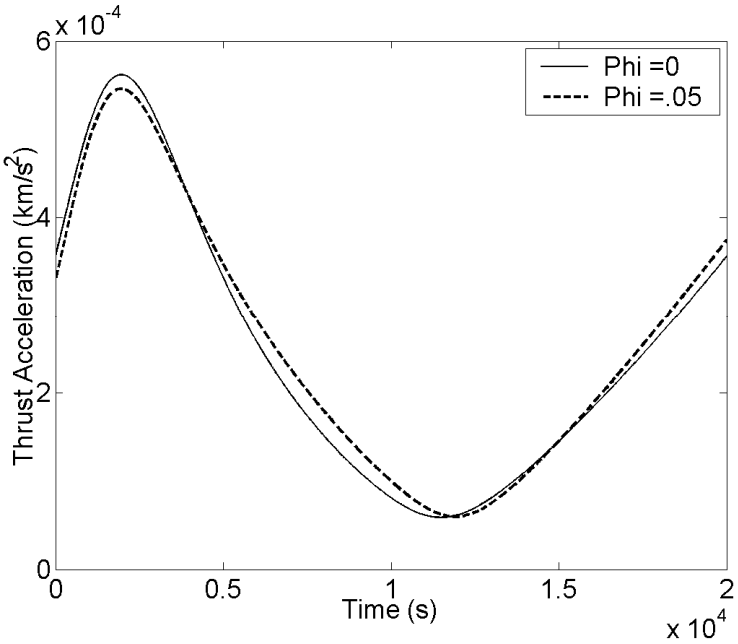

Figure 2.10 Thrust Acceleration Magnitude vs Time

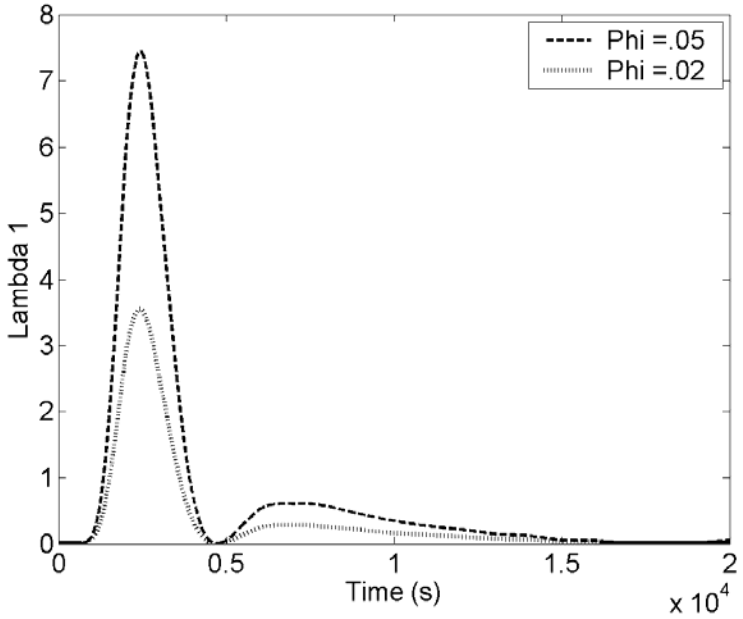

Figure 2.11 λ_1 vs Time

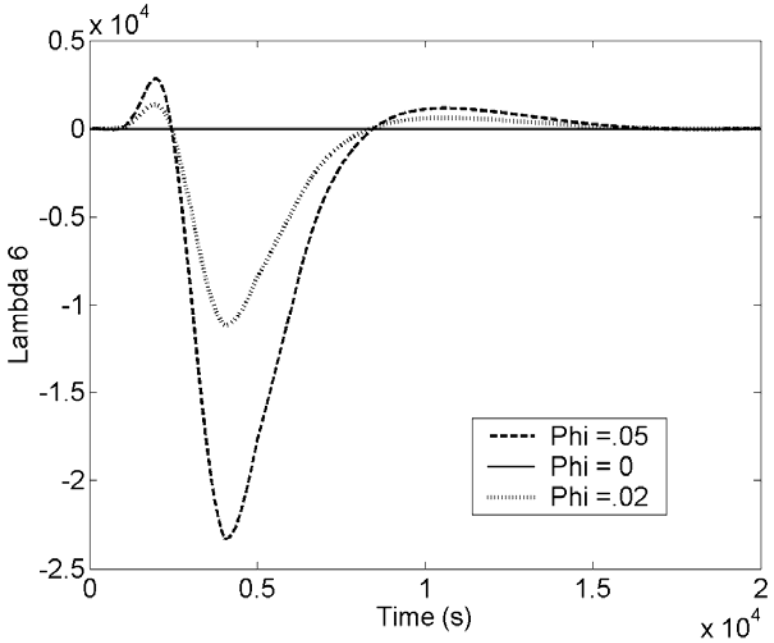

Figure 2.12 λ_6 vs Time

Discrete Scalar Range Measurements

The same transfer as the previous two examples is used to illustrate the discrete measurements case. The covariance associated with the noise in the measurement given by Eq. (2.59) is different than the spectral density specified in Eq. (2.54) because the covariance term is not integrated over the time between each measurement. The value of the covariance associated with the noise in the measurement was selected so that the final value of the covariance for the mass optimal case was of the same order of magnitude as the mass optimal solution from the first example that used continuous measurements. A discrete scalar range measurement from the center of the Earth to the spacecraft is taken every 400 seconds beginning at t = 400 and ending at t = 19,600.

$$\tilde{R} = .00025 \tag{2.59}$$

To illustrate the constraints specified by **σ**, Eq. (2.60), where s is defined in Eq. (2.61), gives the third unique constraint from Eq. (2.13). The expression represented by s is a scalar because the measurements can always be processed one at a time. The value of one element of the **L** matrix is given by Eq. (2.62). The other elements of **σ** and **L** can be determined from Eqs. (2.13) and (2.39). When the observations are scalar range measurements, the determinant of **B** is given by Eq. (2.63) which can never be zero as long as there is noise in the measurement and the observer never occupies the same location as the spacecraft. As a result, one can solve Eq. (2.38) to determine the unique costates after each discrete measurement.

$$\sigma_3 = P_{x\dot{x}}(t_{k+}) - P_{x\dot{x}}(t_{k-}) + \frac{s}{x_s^2 + y_s^2}\left[P_{xx}(x_s^2 P_{x\dot{x}} + x_s y_s P_{y\dot{x}}) + P_{xy}(x_s y_s P_{x\dot{x}} + y_s^2 P_{y\dot{x}})\right]\Big|_{t_{k-}} \tag{2.60}$$

$$s = \left(\mathbf{H}(t_k)\mathbf{P}(t_{k-})\mathbf{H}^T(t_k) + \mathbf{R} \right)^{-1} \tag{2.61}$$

$$L(6,3) = \frac{s}{x_s^2 + y_s^2} \left[P_{xx} x_s y_s + P_{xy} y_s^2 \right] \Bigg|_{t_{k-}} \tag{2.62}$$

$$|\mathbf{B}| = \frac{\tilde{R}\left(x_s^2 + y_s^2 \right)}{P_{xx} x_s^2 + P_{xy} x_s y_s + P_{yy} y_s^2 + \tilde{R}\left(x_s^2 + y_s^2 \right)} \tag{2.63}$$

The results for this discrete measurement example are similar to the results for continuous measurements. The integral of the thrust acceleration squared and the final value of the trace of the Cartesian covariance for the optimal trajectories for various values of φ are shown in Table 2.4. The trace of the covariance at the final time can be reduced by about 20 percent with an increase of less than two-tenths of one percent in the integral of the thrust acceleration squared. Just as in the case of the continuous measurements, the fuel cost of further reducing the trace of the covariance at the final time increases significantly as φ is increased. The optimal trajectories, controls, covariance, and costates for various values of φ are shown in Figures 2.13 to 2.17. Although the plot of the trace of the covariance is discontinuous, the shape of the graph and the time when the covariance on the mass optimal solution diverges from the covariance on the φ=.5 solution is nearly the same as the previous example with continuous observations. The results are similar for the control and the costates as well. Even though the covariance and costates are discontinuous at each measurement time, the controls still remain continuous at the measurement times. The plots for the other covariance elements and other costates are omitted because they are similar to the plots

that are shown. The only elements that are significantly different are the plots for λ_8, λ_9, and λ_{10} which are continuous.

Table 2.4 Observability And Fuel Usage for Trajectories Minimizing the Trace of the Covariance at the Final Time with Discrete Observations

φ	Integral of Thrust Acceleration Squared $*10^{-4}$	Change in Integral of Thrust Acceleration Squared $*10^{-10}$	Trace of Covariance at Final Time $*10^{-3}$	Change in Final Trace $*10^{-6}$	$\frac{\Delta Tr[\mathbf{P}]}{\Delta J}$
0	16.97740	N/A	1.82928	N/A	N/A
.0001	16.97741	12	1.82355	-6.1	510
.0005	16.97754	136	1.80220	-27.5	172.2
.0010	16.97791	512	1.77683	-52.8	67.45
.0050	16.98729	9888	1.61344	-216.2	17.45
.0100	17.00815	30752	1.47149	-358.2	6.8
.0150	17.03384	56436	1.36794	-461.7	4.05
.0200	17.06177	84374	1.28765	-542.0	2.85
.0300	17.12041	143010	1.16891	-660.8	2.05
.0400	17.17986	202458	1.08339	-746.3	1.45
.0500	17.23872	261324	1.01769	-812.0	1.1

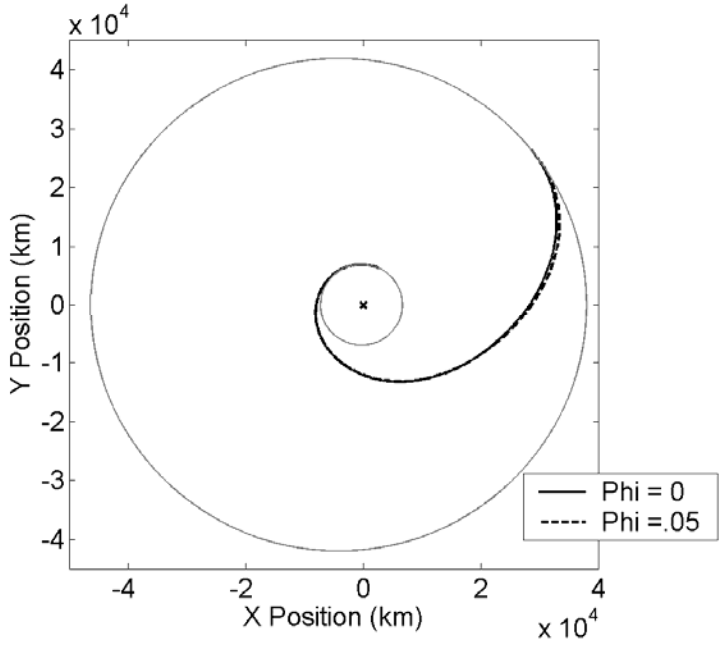

Figure 2.13 Optimal Trajectories

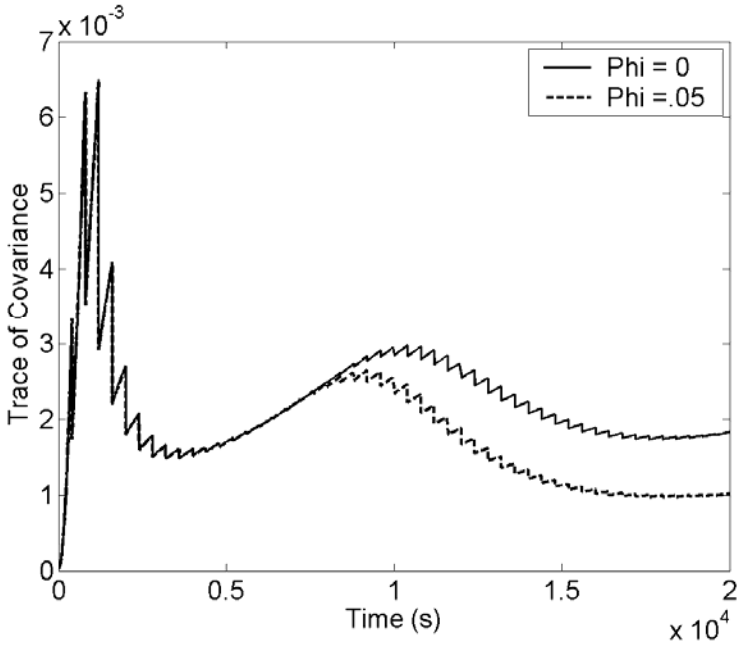

Figure 2.14 Trace of Covariance vs Time

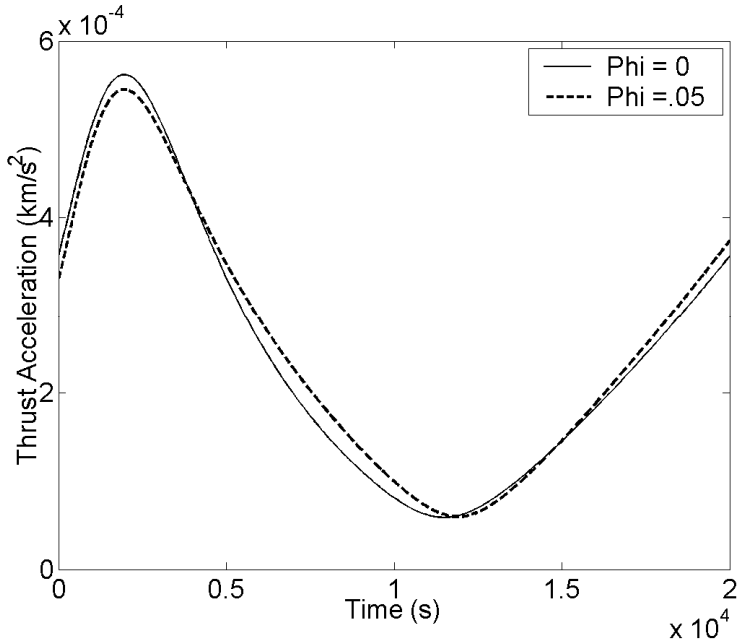

Figure 2.15 Thrust Acceleration Magnitude vs Time

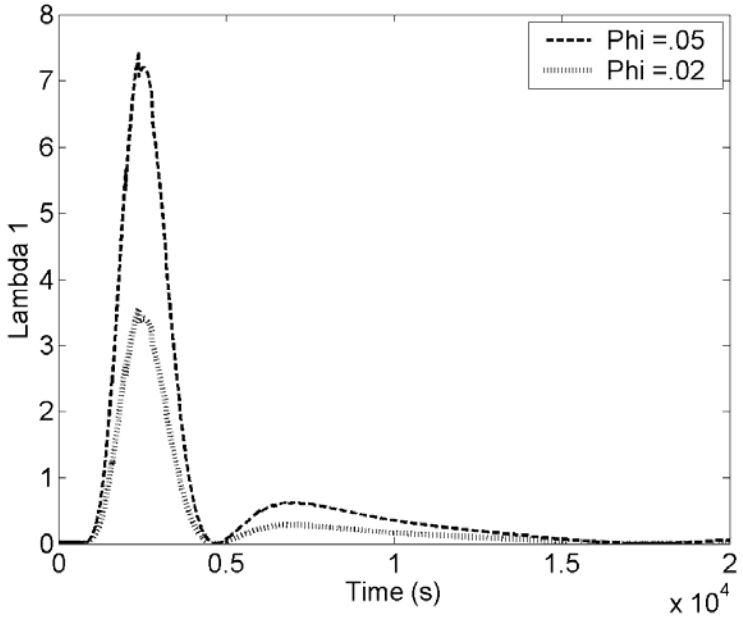

Figure 2.16 λ_1 vs Time

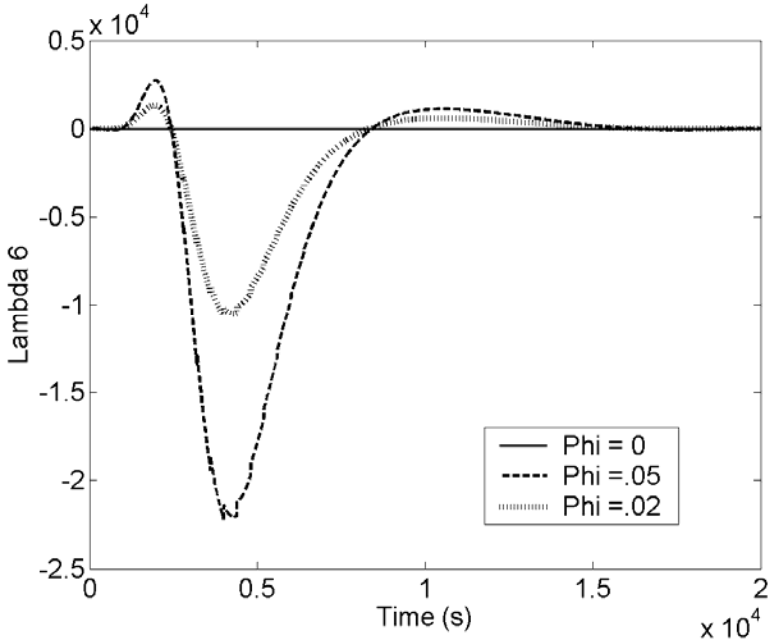

Figure 2.17 λ_6 vs Time

Chapter Conclusions

Adding either the trace of the covariance at discrete times or the integral of the trace of the covariance to the cost function allows one to determine trajectories with significantly improved observability with very little additional propellant required. These results indicate that the cost of further improving the observability increases as observability is increased.

The amount of fuel required to improve the observability along a trajectory by a given percentage will depend on numerous factors including the initial and final orbits as well as the transfer time. This research has not attempted to determine which trajectories require less propellant to improve observability. The models for the error in observations and errors in dynamic equations will also affect the results. The effect of changing the ratio of terms in $\mathbf{R}$, $\mathbf{Q}$, and $\mathbf{P}(t_0)$ has not been investigated. Additionally, these results assume scalar range measurements. Transitioning to different measurement types, multiple observers, or missions between different orbits may yield different results.

The differences between the optimal trajectories with continuous measurements throughout the trajectory, alternating periods of continuous measurements and no measurements, and discrete measurements are minimal for the example transfer from LEO to GEO. The optimal control histories and optimal costates are also similar for these three types of measurements. The results indicate that the exact times of the observations do not need to be known a priori in order to determine the fuel cost of decreasing the covariance by a given amount using this technique. The results do indicate that one must know the quality and quantity of the measurements that will be taken. Additionally, this study only examined trajectories in which the temporal spacing

of the observations was equal. Further study is necessary to determine the effect of different measurement spacing.

The similarity between the results using discrete observations and the results using continuous observations indicates that the continuous model is sufficient to determine optimal trajectories including observability. While one could theoretically use the method presented in this paper to solve an optimization problem with any number of discrete observations, one major difficulty limits the practical application of this method. In order to solve the TPBVP, one must compute the derivatives of the states and costates at the final time with respect to the costates at the initial time. As the number of observations increases, the number of jumps in the augmented state increases as well. These jumps in the state elements and the corresponding jumps in the costate elements make it difficult to compute the derivatives with enough accuracy to determine optimal trajectories with thousands of discrete measurements. Therefore, the similar results between discrete and continuous observations indicate the continuous model should be used in order to avoid the numerical difficulties of the discrete model unless an extremely high level of accuracy is necessary.

CHAPTER 3 MINIMIZING UNCERTAINTY IN ALTERNATE COORDINATE SYSTEMS

Chapter Summary

This chapter presents a method to transfer a spacecraft with continuous thrust while minimizing a combination of fuel consumption and the uncertainty of the spacecraft state in a frame other than the one in which the spacecraft equations of motion and covariance are expressed. The technique allows one to minimize the uncertainty in the spacecraft semimajor axis, flight path angle, range, or any other function of the spacecraft state without developing the equations of motion for the spacecraft or covariance in a non-Cartesian frame. An example problem demonstrates that this technique yields the same optimal trajectory as formulating the entire problem in the state space of the covariance term that is minimized. Another example demonstrates that the covariance associated with the semimajor axis at the end of a LEO to near GEO transfer can be reduced significantly with only a slight increase in fuel consumption.

Introduction

The previous chapter provided a method to minimize a combination of the propellant mass and the sum of the expected mean square errors in the spacecraft Cartesian position and velocity. Instead of, or in addition to, minimizing the covariance associated with the spacecraft Cartesian position and velocity, this chapter demonstrates a technique to minimize the covariance associated with non-Cartesian frames. The optimization problem is again solved using the calculus of variations to set up a

TPBVP.[19] One could formulate the entire problem in the non-Cartesian frame and derive the spacecraft equations of motion, time derivative of the covariance, and optimality conditions in that frame.

This chapter presents a method to solve the problem without formulating the entire problem in the non-Cartesian frame. The technique allows one to minimize the uncertainty in any function of the spacecraft state without developing the equations of motion for the spacecraft or covariance in a non-Cartesian frame. The first example problem demonstrates this method's accuracy by solving a transfer problem that seeks to minimize the covariance associated with polar coordinates. The problem is first formulated and solved in polar coordinates. The problem is then formulated and solved in the Cartesian frame using the technique developed in this paper. The optimal control is shown to be equivalent using either method.

The second example is a spacecraft orbit transfer problem that seeks to decrease the covariance associated with the spacecraft semimajor axis following a LEO to near GEO transfer. Minimizing the covariance associated with the semimajor axis is especially interesting because the error in estimating the spacecraft state at some time after the spacecraft is inserted into the target orbit is dominated by the error in the spacecraft semimajor axis when it is inserted into the target orbit. Example problems demonstrate that the covariance associated with the semimajor axis can be reduced significantly with only a slight increase in fuel consumption when this technique is applied to a LEO to GEO transfer.

Frame Transformation

Instead of minimizing the covariance associated with the spacecraft Cartesian position and velocity, defined to be the **x** frame, one may wish to minimize a function of the covariance associated with the spacecraft orbital elements or any other non-Cartesian frame, defined to be the **y** frame, that can be expressed as in Eq. (3.1). The cost function given by Eq. (3.2) allows one to minimize a function of the covariance along the trajectory as well as at discrete times. One technique to employ the calculus of variations to determine an optimal trajectory with this cost function, which includes the covariance associated with the **y** frame, requires the entire problem be formulated in the **y** frame. This formulation requires that the spacecraft equations of motion, time derivative of the covariance matrix, time derivatives of the costates, and optimal values of the costates be derived in the **y** frame. Alternatively, one could express the **y** frame covariance using Eq. (3.3), where **A** is the derivative of the **y** state with respect to the **x** state. This derivative must be continuous with a continuous inverse and must not be an explicit function of time in order to use the following technique. Because **A** and **y** can be written as functions of **x,** the cost function from Eq. (3.2) can be expressed as Eq. (3.4). With Eq. (3.4) as the cost function, the entire problem can be solved in the **x** frame without deriving equations of motion or optimality conditions in the **y** frame.

$$\mathbf{y} = \mathbf{s}(\mathbf{x}) \tag{3.1}$$

$$W = J_f + \sum_{i=1}^{n} \varepsilon_i[\mathbf{y}(t_i), \mathbf{P}_y(t_i)] + \int_{t_0}^{t_f} \chi[\mathbf{y}(t), \mathbf{P}_y(t)]\, dt \tag{3.2}$$

$$\mathbf{P}_y = \mathbf{A}\mathbf{P}_x\mathbf{A}^T \tag{3.3}$$

$$W = J_f + \sum_{i=1}^{n} \hat{\varepsilon}_i[\mathbf{x}(t_i), \mathbf{P}_x(t_i)] + \int_{t_0}^{t_f} \hat{\chi}[\mathbf{x}(t), \mathbf{P}_x(t)]\, dt \tag{3.4}$$

Outline of Proof of Equivalency

The first step in proving that Eq. (3.3) provides the same value of the **y** frame covariance to the cost function as directly integrating the **y** frame covariance is demonstrating the equivalence at the initial time. For the optimization problem, the value of either the **x** frame or the **y** frame covariance at the initial time must be given. If the initial covariance of the state is provided as the **y** covariance, then the initial value of the **x** covariance used by the integrator in the optimization code is given by Eq. (3.5). Notice that the expression in Eq. (3.5) does not necessarily give the exact value of the **x** covariance at the initial time, but it does give the exact value of the **y** covariance when it is transformed back to the **y** frame using Eq. (3.3).

$$\mathbf{P}_x^{int}(t_0) = \mathbf{A}^{-1}(t_0)\mathbf{P}_y^{given}(t_0)\mathbf{A}^{-T}(t_0) \tag{3.5}$$

If the initial covariance of the state is given as the **x** covariance, then the **x** covariance must be transformed to be a given **y** covariance using whatever order transformation that is desired. The value of the **x** covariance used by the integrator is then obtained by transforming this **y** covariance using Eq. (3.5). The **x** covariance obtained by Eq. (3.5) will only be the initial given **x** covariance if a linear transformation is made to obtain the given **y** covariance. Figure 3.1 more clearly illustrates the transformation. In Figure 3.1, the given **x** covariance is transformed to be a given **y** covariance using an nth order transformation. The optimization technique requires the given **y** covariance to be transformed linearly to form an **x** covariance for the integrator.

Despite the initial **x** covariance used by the optimization routine not equaling the given initial **x** covariance, Eq. (3.3) and the initial **x** covariance used by the integrator provide the initial given **y** covariance.

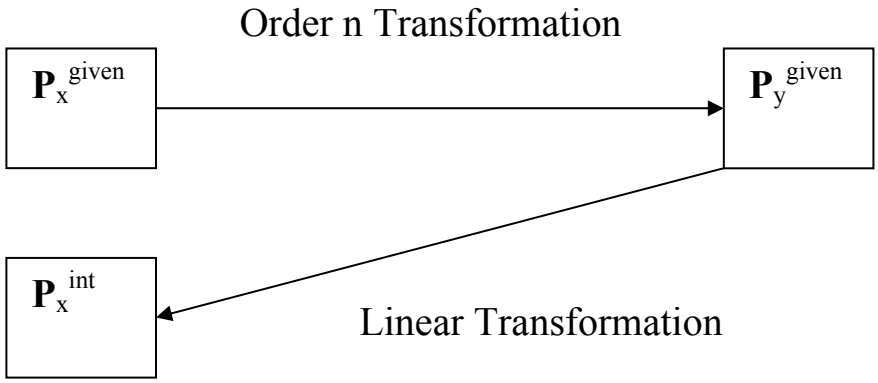

Figure 3.1 Transformation of Initial Value of Covariance

By definition, **x** varies with time according to Eq. (3.6) where $\mathbf{w}_x$ is a zero-mean Gaussian white noise process with spectral density $\mathbf{Q}_x$. The time derivative of **y** can be determined from the chain rule according to Eq. (3.7). The observation model is given by Eq. (3.8) where **n** is a zero-mean Gaussian white noise process with spectral density **R**. The observation model can be expressed in the **y** frame with a similar expression to Eq. (3.9) obtained for $\mathbf{H}_y$. Notice that **R** does not depend on whether **h** is expressed in the **x** or **y** frame. By linearizing about the nominal solution, the matrix Riccati equations given by Eqs. (3.10) and (3.11) can be obtained for both the **x** and **y** covariance.[22] Notice that Eq. (3.11) is the time derivative of the **y** covariance for the case when the problem is formulated in the **y** frame.

$$\dot{\mathbf{x}} = \mathbf{f}(\mathbf{x}(t), t) + \mathbf{w}_x(t) \tag{3.6}$$

$$\dot{\mathbf{y}} = \mathbf{A}\dot{\mathbf{x}} \tag{3.7}$$

$$\mathbf{z}(t) = \mathbf{h}(\mathbf{x}(t), t) + \mathbf{n}(t) \tag{3.8}$$

$$\mathbf{H}_x \equiv \frac{\partial \mathbf{h}}{\partial \mathbf{x}} \tag{3.9}$$

$$\dot{\mathbf{P}}_x = \mathbf{F}\mathbf{P}_x + \mathbf{P}_x\mathbf{F}^T + \mathbf{Q}_x - \mathbf{P}_x\mathbf{H}_x^T\mathbf{R}^{-1}\mathbf{H}_x\mathbf{P}_x \tag{3.10}$$

$$\dot{\mathbf{P}}_y = \mathbf{G}\mathbf{P}_y + \mathbf{P}_y\mathbf{G}^T + \mathbf{Q}_y - \mathbf{P}_y\mathbf{H}_y^T\mathbf{R}^{-1}\mathbf{H}_y\mathbf{P}_y \tag{3.11}$$

Since Eq. (3.3) accurately expresses the **y** covariance at the initial time, demonstrating that the time derivative of it and the time derivative of the **y** covariance when the equations of motion are expressed in the **y** frame are equal, shows that Eq. (3.3) can be used to express the **y** covariance. Taking the time derivative of both sides of Eq. (3.3) yields Eq. (3.12) which can be expressed as Eq. (3.13) when Eqs. (3.3) and (3.10) are used. Eqs. (3.11) and (3.13) will be equivalent and Eq. (3.3) will accurately represent the **y** covariance so long as Eqs. (3.14) to (3.16) are satisfied.

$$\dot{\mathbf{P}}_y = \dot{\mathbf{A}}\mathbf{P}_x\mathbf{A}^T + \mathbf{A}\dot{\mathbf{P}}_x\mathbf{A}^T + \mathbf{A}\mathbf{P}_x\dot{\mathbf{A}}^T \tag{3.12}$$

$$\dot{\mathbf{P}}_y = (\dot{\mathbf{A}}\mathbf{A}^{-1} + \mathbf{A}\mathbf{F}\mathbf{A}^{-1})\mathbf{P}_y + \mathbf{P}_y(\mathbf{A}^{-T}\mathrm{F}^T\mathbf{A}^T + \mathbf{A}^{-T}\dot{\mathbf{A}}^T) + \mathbf{A}\mathbf{Q}_x\mathbf{A}^T + \mathbf{P}_y\mathbf{A}^{-T}\mathbf{H}_x^T\mathbf{R}^{-1}\mathbf{H}_x\mathbf{A}^{-1}\mathbf{P}_y \tag{3.13}$$

$$\mathbf{G} = \dot{\mathbf{A}}\mathbf{A}^{-1} + \mathbf{A}\mathbf{F}\mathbf{A}^{-1} \tag{3.14}$$

$$\mathbf{Q}_y = \mathbf{A}\mathbf{Q}_x\mathbf{A}^T \tag{3.15}$$

$$\mathbf{H}_y = \mathbf{H}_x\mathbf{A}^{-1} \tag{3.16}$$

Outline of Proof of Eq. (3.14)

The derivative of a function expressed in the **x** coordinate system with respect to a coordinate in the **y** system can be determined from Eq. (3.17) which comes from the

chain rule. The jth column of $\frac{\partial}{\partial \mathbf{y}}(\dot{\mathbf{y}})$ is $\frac{\partial}{\partial y_j}(\mathbf{A}\dot{\mathbf{x}})$. Notice that $\mathbf{A}\dot{\mathbf{x}}$ is a function of $\mathbf{x}$. Using Eqs. (3.7) and (3.17), one can determine the jth column of $\frac{\partial}{\partial \mathbf{y}}(\dot{\mathbf{y}})$ which is given by Eq. (3.18). The i,j component of $\frac{\partial}{\partial \mathbf{y}}(\dot{\mathbf{y}})$ can be determined from Eq. (3.18) to be Eq. (3.19), where $\mathbf{a}_i$ is the ith row of $\mathbf{A}$.

$$\frac{\partial}{\partial \mathrm{y_j}}(\mathrm{g}(\mathbf{x})) = \sum_{\mathrm{k}} \frac{\partial \mathrm{x_k}}{\partial \mathrm{y_j}} \frac{\partial}{\partial \mathrm{x_k}}(\mathrm{g}(\mathbf{x})) \tag{3.17}$$

$$\frac{\partial}{\partial \mathrm{y_j}}(\mathbf{A}\dot{\mathbf{x}}) = \sum_{\mathrm{k}} \left[\frac{\partial \mathrm{x_k}}{\partial \mathrm{y_j}} \frac{\partial}{\partial \mathrm{x_k}}(\mathbf{A}\dot{\mathbf{x}}) \right] = \sum_{\mathrm{k}} \left[\frac{\partial \mathrm{x_k}}{\partial \mathrm{y_j}} \frac{\partial \mathbf{A}}{\partial \mathrm{x_k}} \right] \dot{\mathbf{x}} + \sum_{\mathrm{k}} \left[\frac{\partial \mathrm{x_k}}{\partial \mathrm{y_j}} \mathbf{A} \frac{\partial \dot{\mathbf{x}}}{\partial \mathrm{x_k}} \right] \tag{3.18}$$

$$\frac{\partial \dot{\mathbf{y}}}{\partial \mathbf{y}}(\mathrm{i,j}) = \sum_{\mathrm{k}} \left[\frac{\partial \mathrm{x_k}}{\partial \mathrm{y_j}} \frac{\partial \mathbf{a}_\mathrm{i}}{\partial x_\mathrm{k}} \right] \dot{\mathbf{x}} + \sum_{\mathrm{k}} \left[\frac{\partial \mathrm{x_k}}{\partial \mathrm{y_j}} \mathbf{a}_i \frac{\partial \dot{\mathbf{x}}}{\partial \mathrm{x_k}} \right] \tag{3.19}$$

The jth column of $\mathbf{AFA}^{-1}$ is given by Eq. (3.20) where $\mathbf{c}$ is defined in Eq. (3.21). Using Eqs. (3.20) and (3.21) and taking advantage of the fact that $\frac{\partial x_i}{\partial y_j}$ is a scalar, one can simplify $\mathbf{AFA}^{-1}$ as in Eq. (3.22).

$$\mathbf{AFA}^{-1}(\mathrm{col\ j}) = \mathbf{Ac} \tag{3.20}$$

$$\mathbf{c}_\mathrm{i} \equiv \mathbf{F}(\mathrm{row\ i}) \cdot \mathbf{A}^{-1}(\mathrm{col\ j}) = \sum_{\mathrm{k}} \frac{\partial \dot{\mathrm{x}}_\mathrm{i}}{\partial \mathrm{x_k}} \frac{\partial \mathrm{x_k}}{\partial \mathrm{y_j}} \tag{3.21}$$

$$\mathbf{AFA}^{-1}(\mathrm{col\ j}) = \mathbf{A} \sum_{\mathrm{k}} \frac{\partial \dot{\mathbf{x}}}{\partial \mathrm{x_k}} \frac{\partial \mathrm{x_k}}{\partial \mathrm{y_j}} = \sum_{\mathrm{k}} \frac{\partial \mathrm{x_k}}{\partial \mathrm{y_j}} \mathbf{A} \frac{\partial \dot{\mathbf{x}}}{\partial \mathrm{x_k}} \tag{3.22}$$

Using the chain rule, the time derivative of $\mathbf{A}$ can be determined as in Eq. (3.23), assuming the partial derivative of $\mathbf{A}$ with respect to time is zero. Therefore, the ith row of

$\dot{\mathbf{A}}$ can be expressed as in Eq. (3.24). The jth column of $\mathbf{A}^{-1}$ is given by Eq. (3.25). The i,j term of $\dot{\mathbf{A}}\mathbf{A}^{-1}$ is given by Eq. (3.26). Using Eqs. (3.22) and (3.26), the i,j term of $\dot{\mathbf{A}}\mathbf{A}^{-1} + \mathbf{A}\mathbf{F}\mathbf{A}^{-1}$ is given by Eq. (3.27) which is equivalent to Eq. (3.19). Because i and j are arbitrary, Eq. (3.14) has been proven.

$$\dot{\mathbf{A}}(\mathrm{i},\mathrm{j}) = \sum_{\mathrm{k}} \frac{\partial}{\partial \mathrm{x}_{\mathrm{k}}} \frac{\partial \mathrm{y}_{\mathrm{i}}}{\partial \mathrm{x}_{\mathrm{j}}} \dot{\mathrm{x}}_{\mathrm{k}} = \sum_{\mathrm{k}} \frac{\partial}{\partial \mathrm{x}_{\mathrm{j}}} \frac{\partial \mathrm{y}_{\mathrm{i}}}{\partial \mathrm{x}_{\mathrm{k}}} \dot{\mathrm{x}}_{\mathrm{k}} = \frac{\partial \mathbf{a}_{\mathrm{i}}}{\partial \mathrm{x}_{\mathrm{j}}} \dot{\mathbf{x}} \tag{3.23}$$

$$\dot{\mathbf{A}}(\text{row i}) = \left[\left(\frac{\partial \mathbf{a}_{\mathrm{i}}}{\partial \mathrm{x}_1} \dot{\mathbf{x}} \right) \left(\frac{\partial \mathbf{a}_{\mathrm{i}}}{\partial \mathrm{x}_2} \dot{\mathbf{x}} \right) \left(\frac{\partial \mathbf{a}_{\mathrm{i}}}{\partial \mathrm{x}_3} \dot{\mathbf{x}} \right) \left(\frac{\partial \mathbf{a}_{\mathrm{i}}}{\partial \mathrm{x}_4} \dot{\mathbf{x}} \right) \left(\frac{\partial \mathbf{a}_{\mathrm{i}}}{\partial \mathrm{x}_5} \dot{\mathbf{x}} \right) \ldots\ldots \right] \tag{3.24}$$

$$\mathbf{A}^{-1}(\text{col j}) = \left[\left(\frac{\partial \mathrm{x}_1}{\partial \mathrm{y}_{\mathrm{j}}} \right) \left(\frac{\partial \mathrm{x}_2}{\partial \mathrm{y}_{\mathrm{j}}} \right) \left(\frac{\partial \mathrm{x}_3}{\partial \mathrm{y}_{\mathrm{j}}} \right) \left(\frac{\partial \mathrm{x}_4}{\partial \mathrm{y}_{\mathrm{j}}} \right) \left(\frac{\partial \mathrm{x}_5}{\partial \mathrm{y}_{\mathrm{j}}} \right) \ldots\ldots \right]^{\mathrm{T}} \tag{3.25}$$

$$\dot{\mathbf{A}}\mathbf{A}^{-1}(\mathrm{i},\mathrm{j}) = \dot{\mathbf{A}}(\text{row i}) \cdot \mathbf{A}^{-1}(\text{col j}) = \sum_{\mathrm{k}} \frac{\partial \mathbf{a}_{\mathrm{i}}}{\partial \mathrm{x}_{\mathrm{k}}} \dot{\mathbf{x}} \frac{\partial \mathrm{x}_{\mathrm{k}}}{\partial \mathrm{y}_{\mathrm{j}}} \tag{3.26}$$

$$\dot{\mathbf{A}}\mathbf{A}^{-1}(\mathrm{i},\mathrm{j}) + \mathbf{A}\mathbf{F}\mathbf{A}^{-1}(\mathrm{i},\mathrm{j}) = \sum_{\mathrm{k}} \frac{\partial \mathbf{a}_{\mathrm{i}}}{\partial \mathrm{x}_{\mathrm{k}}} \dot{\mathbf{x}} \frac{\partial \mathrm{x}_{\mathrm{k}}}{\partial \mathrm{y}_{\mathrm{j}}} + \sum_{\mathrm{k}} \frac{\partial \mathrm{x}_{\mathrm{k}}}{\partial \mathrm{y}_{\mathrm{j}}} \mathbf{a}_{\mathrm{i}} \frac{\partial \dot{\mathbf{x}}}{\partial \mathrm{x}_{\mathrm{k}}} \tag{3.27}$$

Outline of Proof of Eq. (3.15)

The time derivative of **x** is expressed in Eq. (3.6), and the time derivative of **y** can be expressed either as Eq. (3.7) or in the form of Eq. (3.28). The spectral densities associated with with $\mathbf{w}_x$ and $\mathbf{w}_y$ are given by Eqs. (3.29) and (3.30). Substituting Eq. (3.6) into Eq. (3.7) gives Eq. (3.31). In order for both Eq. (3.28) and Eq. (3.31) to be satisfied, $\mathbf{w}_y$ must be given by Eq. (3.32). Utilizing Eqs. (3.30) and (3.32) to determine $\mathbf{Q}_y$, yields Eq. (3.33) which verifies Eq. (3.15).

$$\dot{\mathbf{y}} = \hat{\mathbf{f}}(\mathbf{y}(\mathrm{t}),\mathrm{t}) + \mathbf{w}_{\mathrm{y}}(t) \tag{3.28}$$

$$\mathbf{Q}_x(t)\delta(t-\tau) \equiv E[\mathbf{w}_x(t)\mathbf{w}_x^T(\tau)] \tag{3.29}$$

$$\mathbf{Q}_y(t)\delta(t-\tau) \equiv E[\mathbf{w}_y(t)\mathbf{w}_y^T(\tau)] \tag{3.30}$$

$$\dot{\mathbf{y}} = \mathbf{A}\mathbf{f}(\mathbf{x}(t), t) + \mathbf{A}\mathbf{w}_x(t) \tag{3.31}$$

$$\mathbf{w}_y = \mathbf{A}\mathbf{w}_x \tag{3.32}$$

$$\mathbf{Q}_y \equiv E[\mathbf{A}\mathbf{w}_x\mathbf{w}_x^T\mathbf{A}^T] = \mathbf{A}\mathbf{Q}_x\mathbf{A}^T \tag{3.33}$$

Outline of Proof of Eq. (3.16)

Because the observation and the derivative of the observation with respect to the **x** state are given by Eqs. (3.8) and (3.9), the i,j element of $\mathbf{H}_x\mathbf{A}^{-1}$ is given by Eq. (3.34). By applying the chain rule in Eq. (3.17), the derivative of h_i with respect to y_j is expressed in Eq. (3.35). Because these expressions are equivalent and i and j are arbitrary, Eq. (3.16) is proven.

$$\left(\frac{\partial \mathbf{h}}{\partial \mathbf{x}}\mathbf{A}^{-1}\right)(i, j) = \sum_k \frac{\partial x_k}{\partial y_j}\frac{\partial h_i}{\partial x_k} \tag{3.34}$$

$$\frac{\partial \mathbf{h}}{\partial \mathbf{y}}(i, j) = \sum_k \frac{\partial x_k}{\partial y_j}\frac{\partial h_i}{\partial x_k} \tag{3.35}$$

$$H_x\mathbf{A}^{-1} = \frac{\partial \mathbf{h}}{\partial \mathbf{x}}\mathbf{A}^{-1} = \frac{\partial \mathbf{h}}{\partial \mathbf{y}} = H_y \tag{3.36}$$

Equivalence of Solving Problem in Alternate Frames

In order to verify the equivalence of solving the optimization problem in a non-Cartesian frame and solving the problem in the Cartesian frame using Eq. (3.3), a simple transfer is sought where the cost function includes a function of the covariance associated

with the polar coordinates. The polar coordinate system state is defined in Eq. (3.37). The time derivative of the state can be derived from first principles to be Eq. (3.38) where u_r and u_t are the radial and tangential components of the thrust acceleration provided by the engine. The optimization problem is to transfer from a specified initial position, $\mathbf{Y}(t_0)$, to a specified final position, $\mathbf{Y}(t_f)$, where both the initial and final times are specified, subject to the cost function given by Eq. (3.39) where φ_1 is a scalar weight. The transfer is made in a gravity free environment. The J term in the cost function is the integral of the thrust acceleration squared provided by the controls as shown in Eq. (3.40). Minimizing this term minimizes the thrust acceleration provided by the engine. Minimizing the other term in the cost function will minimize the uncertainty associated with the final value of the polar angle, θ.

$$Y = \begin{pmatrix} r \\ \theta \\ \dot{r} \\ \dot{\theta} \end{pmatrix} \tag{3.37}$$

$$\dot{Y} = \begin{pmatrix} \dot{r} \\ \dot{\theta} \\ r\dot{\theta}^2 + u_r \\ -2\dot{r}\dot{\theta} + u_t \end{pmatrix} \tag{3.38}$$

$$W = J(t_f) + \phi_1 P_{\theta\theta}(t_f) \tag{3.39}$$

$$J(t) = \int_{t_0}^{t} \frac{u_t^2 + u_r^2}{2} dt \tag{3.40}$$

In order to use the calculus of variations to optimize this transfer, one needs to define a set of state variables that includes not only the traditional polar coordinate states given by Eq. (3.37) but also the covariance terms. The state, $\tilde{\mathbf{Y}}$, given by Eq. (3.41) where the covariance terms are defined in Eq. (3.43), is a state that can be used with the calculus of variations. The costates associated with $\tilde{\mathbf{Y}}$ are given by Eq. (3.42). The observations are continuous scalar range measurements from the observer which is located at the origin. The initial value of the covariance matrix is specified. The time derivative of the covariance is given by the matrix Riccati equation, Eq. (3.11) with the expressions needed in this equation specified in Eqs. (3.44) to (3.46). The complete expression for the Hamiltonian is omitted because of its length, but it can be determined from the information provided and Eq. (3.47).

$$\tilde{\mathbf{Y}} = \begin{pmatrix} \mathrm{r} & \theta & \dot{\mathrm{r}} & \dot{\theta} & \mathrm{J} & \overline{\mathrm{P}}_1 & \overline{\mathrm{P}}_2 & \overline{\mathrm{P}}_3 & \overline{\mathrm{P}}_4 & \overline{\mathrm{P}}_5 & \overline{\mathrm{P}}_6 & \overline{\mathrm{P}}_7 & \overline{\mathrm{P}}_8 & \overline{\mathrm{P}}_9 & \overline{\mathrm{P}}_{10} \end{pmatrix}^{\mathrm{T}} \tag{3.41}$$

$$\overline{\boldsymbol{\lambda}} = \begin{pmatrix} \lambda_{\mathrm{r}} & \lambda_{\theta} & \lambda_{\dot{\mathrm{r}}} & \lambda_{\dot{\theta}} & \lambda_{\mathrm{J}} & \overline{\lambda}_1 & \overline{\lambda}_2 & \overline{\lambda}_3 & \overline{\lambda}_4 & \overline{\lambda}_5 & \overline{\lambda}_6 & \overline{\lambda}_7 & \overline{\lambda}_8 & \overline{\lambda}_9 & \overline{\lambda}_{10} \end{pmatrix}^{\mathrm{T}} \tag{3.42}$$

$$\mathbf{P}_{\mathrm{Y}} \equiv \begin{pmatrix} \mathrm{P}_{\mathrm{rr}} & \mathrm{P}_{\mathrm{r}\theta} & \mathrm{P}_{\mathrm{r}\dot{\mathrm{r}}} & \mathrm{P}_{\mathrm{r}\dot{\theta}} \\ \mathrm{P}_{\mathrm{r}\theta} & \mathrm{P}_{\theta\theta} & \mathrm{P}_{\dot{\mathrm{r}}\theta} & \mathrm{P}_{\theta\dot{\theta}} \\ \mathrm{P}_{\mathrm{r}\dot{\mathrm{r}}} & \mathrm{P}_{\dot{\mathrm{r}}\theta} & \mathrm{P}_{\dot{\mathrm{r}}\dot{\mathrm{r}}} & \mathrm{P}_{\dot{\mathrm{r}}\dot{\theta}} \\ \mathrm{P}_{\mathrm{r}\dot{\theta}} & \mathrm{P}_{\theta\dot{\theta}} & \mathrm{P}_{\dot{\mathrm{r}}\dot{\theta}} & \mathrm{P}_{\dot{\theta}\dot{\theta}} \end{pmatrix} \equiv \begin{pmatrix} \overline{\mathrm{P}}_1 & \overline{\mathrm{P}}_2 & \overline{\mathrm{P}}_3 & \overline{\mathrm{P}}_4 \\ \overline{\mathrm{P}}_2 & \overline{\mathrm{P}}_5 & \overline{\mathrm{P}}_6 & \overline{\mathrm{P}}_7 \\ \overline{\mathrm{P}}_3 & \overline{\mathrm{P}}_6 & \overline{\mathrm{P}}_8 & \overline{\mathrm{P}}_9 \\ \overline{\mathrm{P}}_4 & \overline{\mathrm{P}}_7 & \overline{\mathrm{P}}_9 & \overline{\mathrm{P}}_{10} \end{pmatrix} \tag{3.43}$$

$$\mathbf{G} = \begin{pmatrix} 0 & 0 & 1 & 0 \\ 0 & 0 & 0 & 1 \\ \dot{\theta}^2 & \mathrm{u}_{\mathrm{t}} & 0 & 2\mathrm{r}\dot{\theta} \\ \dfrac{2\dot{\mathrm{r}}\dot{\theta} - \mathrm{u}_{\mathrm{t}}}{\mathrm{r}^2} & \dfrac{-\mathrm{u}_{\mathrm{r}}}{\mathrm{r}} & \dfrac{-2\dot{\theta}}{\mathrm{r}} & \dfrac{-2\dot{\mathrm{r}}}{\mathrm{r}} \end{pmatrix} \tag{3.44}$$

$$\mathbf{H}_{\mathrm{y}} = \begin{pmatrix} 1 & 0 & 0 & 0 \end{pmatrix} \tag{3.45}$$

$$\mathbf{Q}_y = \begin{pmatrix} 0 & 0 & 0 & 0 \\ 0 & 0 & 0 & 0 \\ 0 & 0 & q_3 & 0 \\ 0 & 0 & 0 & q_4 \end{pmatrix} \tag{3.46}$$

$$H_a = \bar{\boldsymbol{\lambda}}^T \dot{\tilde{\mathbf{Y}}} \tag{3.47}$$

The optimal controls, given by Eqs. (3.50) and (3.51), can be determined from the calculus of variations using Eqs. (3.48) and (3.49). The optimal time derivatives of the costates are again determined by the calculus of variations and are expressed in Eq. (3.52). The optimal values for the costates at the final time are given by Eq. (3.53) where the superscript * indicates the final value is not constrained. A TPBVP can be set up to minimize Eq. (3.39). The unknowns are the initial values of the costates; the constraints are given by Eq. (3.53) and the specified final state, $\mathbf{Y}(t_f)$.

$$\frac{\partial H_a}{\partial u_r} = 0 = \lambda_r + \lambda_J u_r - \frac{\bar{\lambda}_4 \bar{P}_2 + \bar{\lambda}_7 \bar{P}_5 + \bar{\lambda}_9 \bar{P}_6 + 2\bar{\lambda}_{10} \bar{P}_7}{r} \tag{3.48}$$

$$\frac{\partial H_a}{\partial u_t} = 0 = \frac{\lambda_{\dot{\theta}}}{r} + \lambda_J u_t + \bar{\lambda}_3 \bar{P}_2 + \bar{\lambda}_6 \bar{P}_5 + 2\bar{\lambda}_8 \bar{P}_6 + \bar{\lambda}_9 \bar{P}_7 - \frac{\bar{\lambda}_9 \bar{P}_3 + \bar{\lambda}_4 \bar{P}_1 + \bar{\lambda}_7 \bar{P}_2 + 2\bar{\lambda}_{10} \bar{P}_4}{r^2} \tag{3.49}$$

$$u_r = \frac{-r\lambda_{\dot{r}} + \bar{\lambda}_4 \bar{P}_2 + \bar{\lambda}_7 \bar{P}_5 + \bar{\lambda}_9 \bar{P}_6 + 2\bar{\lambda}_{10} \bar{P}_7}{r\lambda_J} \tag{3.50}$$

$$u_t = \frac{1}{\lambda_J}\left(-\frac{\lambda_{\dot{\theta}}}{r} - \bar{\lambda}_3 \bar{P}_2 - \bar{\lambda}_6 \bar{P}_5 - 2\bar{\lambda}_8 \bar{P}_6 - \bar{\lambda}_9 \bar{P}_7 + \frac{\bar{\lambda}_9 \bar{P}_3 + \bar{\lambda}_4 \bar{P}_1 + \bar{\lambda}_7 \bar{P}_2 + 2\bar{\lambda}_{10} \bar{P}_4}{r^2} \right) \tag{3.51}$$

$$\dot{\bar{\boldsymbol{\lambda}}} = \frac{-\partial H_a}{\partial \tilde{Y}} \tag{3.52}$$

$$\bar{\boldsymbol{\lambda}}(t_f) = \begin{pmatrix} * & * & * & * & -1 & 0 & 0 & 0 & 0 & \phi_1 & 0 & 0 & 0 & 0 & 0 \end{pmatrix}^T \tag{3.53}$$

To illustrate this technique, consider a transfer from the initial state given by Eq. (3.54) to the final state given by Eq. (3.55) with φ_1 equal to 825,000. The choice of the initial and final states as well as the value of φ_1 are arbitrary. The optimal initial values for the costates to four significant figures are given by Eq. (3.56). The optimal trajectory is shown in polar coordinates in Figures 3.2 and 3.3, while Figure 3.4 shows the optimal path in Cartesian coordinates. The time evolution of the covariance associated with the theta-theta direction is shown in Figure 3.5. The integral of the thrust acceleration squared shown in Figure 3.6 illustrates the early period of high thrust followed by the long period of near coast and the two final periods of high thrust.

$$\mathbf{Y}(t_0) = \begin{pmatrix} 1.41 & 3.24 & -.201 & .120 \end{pmatrix}^T \tag{3.54}$$

$$\mathbf{Y}(t_f) = \begin{pmatrix} 5.000 & .2569 & 3.200 & -.1000 \end{pmatrix}^T \tag{3.55}$$

$$\bar{\boldsymbol{\lambda}}(t_0) \begin{pmatrix} -44150 \\ -9308 \\ -11340 \\ -3753 \\ -1.000 \\ -27.33 \\ 451.0 \\ -338.7 \\ 1539 \\ -1860 \\ 2794 \\ -12700 \\ -1049 \\ 9537 \\ -21670 \end{pmatrix} \tag{3.56}$$

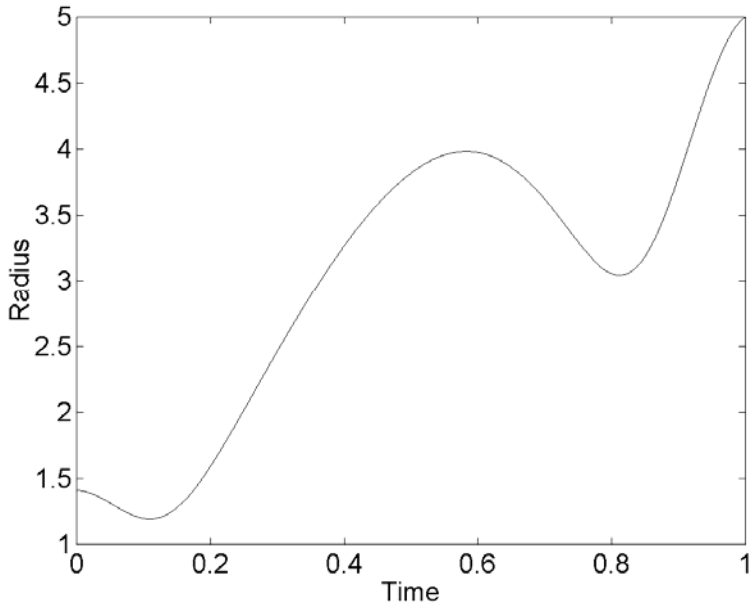

Figure 3.2 Radius vs Time

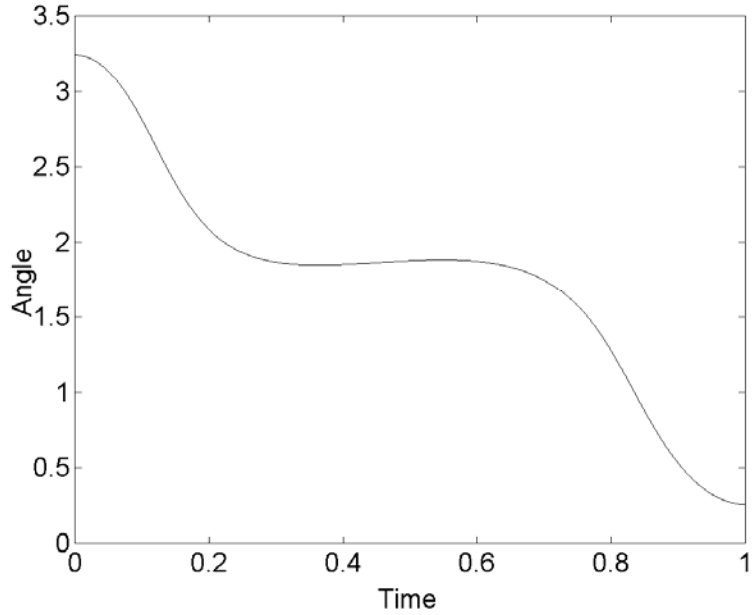

Figure 3.3 Polar Angle vs Time

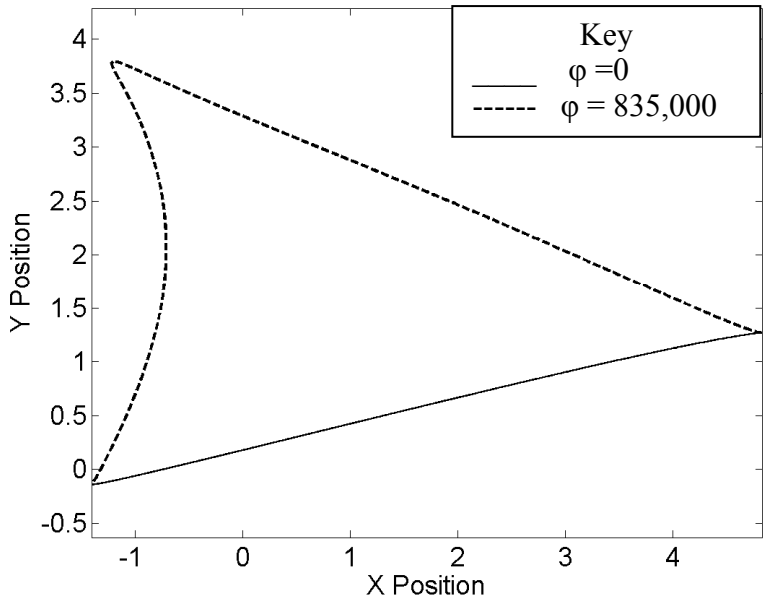

Figure 3.4 Optimal Trajectory

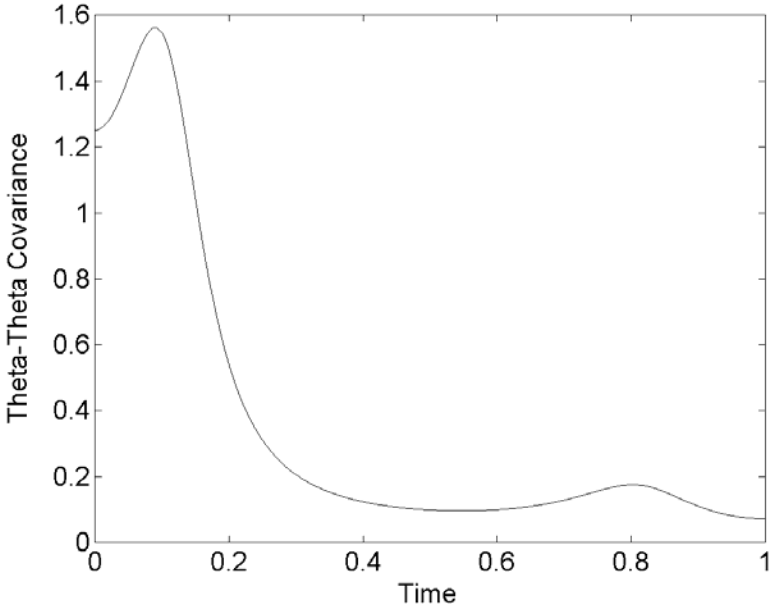

Figure 3.5 $P_{\theta\theta}$ vs Time

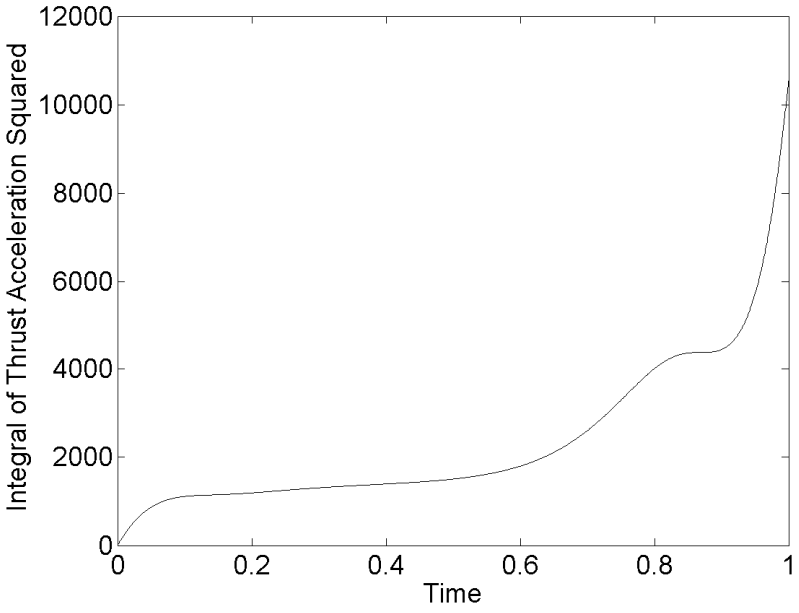

Figure3.6 Integral of Thrust Acceleration Squared vs Time

Alternatively, one could express the entire problem in Cartesian coordinates with the state defined as in Eq. (3.57). The **Y** state can be written as a function of the **X** state according to Eq. (3.58). The derivative of **Y** with respect to **X** is given in Eq. (3.59). Utilizing Eq. (3.3), the cost function, Eq. (3.39), can be rewritten as Eq. (3.60).

$$\mathbf{X} = \begin{pmatrix} x \\ y \\ \dot{x} \\ \dot{y} \end{pmatrix} \tag{3.57}$$

$$\mathbf{Y} = \mathbf{s}(\mathbf{X}) = \begin{pmatrix} \sqrt{x^2 + y^2} \\ \tan^{-1}\dfrac{y}{x} \\ \dfrac{x\dot{x}+y\dot{y}}{\sqrt{x^2 + y^2}} \\ \dfrac{x\dot{y}-y\dot{x}}{x^2 + y^2} \end{pmatrix} \tag{3.58}$$

$$\mathbf{A} = \begin{pmatrix} \dfrac{x}{\sqrt{x^2 + y^2}} & \dfrac{y}{\sqrt{x^2 + y^2}} & 0 & 0 \\ \dfrac{-y}{x^2 + y^2} & \dfrac{x}{x^2 + y^2} & 0 & 0 \\ \dfrac{y^2\dot{x} - xy\dot{y}}{\left(x^2 + y^2\right)^{3/2}} & \dfrac{x^2\dot{y} - xy\dot{x}}{\left(x^2 + y^2\right)^{3/2}} & \dfrac{x}{\sqrt{x^2 + y^2}} & \dfrac{y}{\sqrt{x^2 + y^2}} \\ \dfrac{y^2\dot{y} + 2xy\dot{x} - x^2\dot{y}}{\left(x^2 + y^2\right)^2} & \dfrac{y^2\dot{x} - 2xy\dot{y} - x^2\dot{x}}{\left(x^2 + y^2\right)^2} & \dfrac{-y}{x^2 + y^2} & \dfrac{x}{x^2 + y^2} \end{pmatrix} \tag{3.59}$$

$$W = J(t_f) + \phi_1 \frac{y^2 P_{xx} - 2xyP_{xy} + x^2 P_{yy}}{x^2 + y^2} \tag{3.60}$$

Again, the state must be augmented to include the covariance terms in order to use the calculus of variations to minimize the cost function. In this formulation the covariance that must be added to the state is the Cartesian covariance as shown by Eqs. (3.61) and (3.62). The costates associated with the augmented state are given by Eq. (3.63). The time derivative of the **X** state is shown in Eq. (3.64) where u_x and u_y are the accelerations provided by the control in the principle Cartesian directions. As before, no gravitational accelerations affect the spacecraft. The time derivative of the **X** covariance is given by Eq. (3.10). The expressions needed for this time derivative are expressed by

Eqs. (3.67) to (3.69) which can be determined from Eqs. (3.14) to (3.16) and (3.66). The complete expression for the Hamiltonian can be determined from Eq. (3.70).

$$\tilde{\mathbf{X}} = \begin{pmatrix} x & y & \dot{x} & \dot{y} & J & P_1 & P_2 & P_3 & P_4 & P_5 & P_6 & P_7 & P_8 & P_9 & P_{10} \end{pmatrix}^T \tag{3.61}$$

$$\mathbf{P}_X \equiv \begin{pmatrix} P_{xx} & P_{xy} & P_{x\dot{x}} & P_{x\dot{y}} \\ P_{xy} & P_{yy} & P_{y\dot{x}} & P_{y\dot{y}} \\ P_{x\dot{x}} & P_{y\dot{x}} & P_{\dot{x}\dot{x}} & P_{\dot{x}\dot{y}} \\ P_{x\dot{y}} & P_{y\dot{y}} & P_{\dot{x}\dot{y}} & P_{\dot{y}\dot{y}} \end{pmatrix} \equiv \begin{pmatrix} P_1 & P_2 & P_3 & P_4 \\ P_2 & P_5 & P_6 & P_7 \\ P_3 & P_6 & P_8 & P_9 \\ P_4 & P_7 & P_9 & P_{10} \end{pmatrix} \tag{3.62}$$

$$\boldsymbol{\lambda} = \begin{pmatrix} \lambda_x & \lambda_y & \lambda_{\dot{x}} & \lambda_y & \lambda_J & \lambda_1 & \lambda_2 & \lambda_3 & \lambda_4 & \lambda_5 & \lambda_6 & \lambda_7 & \lambda_8 & \lambda_9 & \lambda_{10} \end{pmatrix}^T \tag{3.63}$$

$$\dot{\mathbf{X}} = \begin{pmatrix} \dot{x} \\ \dot{y} \\ u_x \\ u_y \end{pmatrix} \tag{3.64}$$

$$J(t) = \int_{t_0}^{t} \frac{u_x^2 + u_y^2}{2} dt \tag{3.65}$$

$$\dot{A}(i,j) = \frac{\partial A(i,j)}{\partial x}\dot{x} + \frac{\partial A(i,j)}{\partial y}\dot{y} + \frac{\partial A(i,j)}{\partial \dot{x}}\ddot{x} + \frac{\partial A(i,j)}{\partial \dot{y}}\ddot{y} \tag{3.66}$$

$$\mathbf{H}_x = \frac{\partial \sqrt{x^2 + y^2}}{\partial \mathbf{X}} = \begin{pmatrix} \dfrac{x}{\sqrt{x^2 + y^2}} & \dfrac{y}{\sqrt{x^2 + y^2}} & 0 & 0 \end{pmatrix}^T \tag{3.67}$$

$$\mathbf{Q}_x = \begin{pmatrix} 0 & 0 & 0 & 0 \\ 0 & 0 & 0 & 0 \\ 0 & 0 & \dfrac{q_3 x^2}{x^2 + y^2} + q_4 y^2 & \dfrac{q_3 xy}{x^2 + y^2} - q_4 xy \\ 0 & 0 & \dfrac{q_3 xy}{x^2 + y^2} - q_4 xy & \dfrac{q_3 y^2}{x^2 + y^2} + q_4 x^2 \end{pmatrix} \tag{3.68}$$

$$\mathbf{F} = \begin{pmatrix} 0 & 0 & 1 & 0 \\ 0 & 0 & 0 & 1 \\ 0 & 0 & 0 & 0 \\ 0 & 0 & 0 & 0 \end{pmatrix} \tag{3.69}$$

$$H_a = \boldsymbol{\lambda}^T \dot{\tilde{\mathbf{X}}} \tag{3.70}$$

Again, using the calculus of variations, the optimal controls can be determined from Eqs. (3.71) and (3.72). The optimal time derivatives of the costates are again determined by the calculus of variations and are expressed in Eq. (3.73). The optimal values for the costates at the final time are given by Eq. (3.74) where the superscript * indicates the final value is free. A TPBVP can be set up to minimize Eq. (3.60). The unknowns are the values of the initial costates, and the constraints are given by Eq. (3.74) and the final specified state, $\mathbf{X}(t_f)$.

$$\frac{\partial H_a}{\partial u_x} = 0 \Rightarrow u_x = -\frac{\lambda_{\dot{x}}}{\lambda_J} \tag{3.71}$$

$$\frac{\partial H_a}{\partial u_y} = 0 \Rightarrow u_y = -\frac{\lambda_{\dot{y}}}{\lambda_J} \tag{3.72}$$

$$\dot{\boldsymbol{\lambda}} = \frac{-\partial H_a}{\partial \tilde{\mathbf{X}}} \tag{3.73}$$

$$\boldsymbol{\lambda}(t_f) = \begin{pmatrix} * & * & * & * & -1 & \dfrac{-\phi_1 y^2}{\left(x^2+y^2\right)^2} & \dfrac{2\phi_1 xy}{\left(x^2+y^2\right)^2} & 0 & 0 & \dfrac{-\phi_1 x^2}{\left(x^2+y^2\right)^2} & 0 & 0 & 0 & 0 & 0 \end{pmatrix}^T \tag{3.74}$$

The same transfer problem from the initial state, specified by Eq. (3.54), to the final state, specified by Eq. (3.55), is solved in Cartesian coordinates. The optimal value

of the initial Cartesian costates is given by Eq. (3.75). The optimal control is the same whether the optimal control problem is formulated in the polar or Cartesian frame. The optimal control also does not depend on the frame in which the covariance is propagated. The optimal trajectory, time evolution of the covariance associated with the theta-theta direction, and integral of thrust acceleration squared along the optimal path are identical to those shown by Figures 3.2 to 3.6.

$$\boldsymbol{\lambda}(t_0) = \begin{pmatrix} 696.5 \\ 1136 \\ 73.09 \\ 145.4 \\ -1.000 \\ -473.4 \\ 1725 \\ -1849 \\ 4383 \\ -1571 \\ 3369 \\ -7985 \\ -1806 \\ 8560 \\ -10150 \end{pmatrix} \tag{3.75}$$

Reducing Semimajor Axis Covariance

The transformation in Eq. (3.3) can be employed to minimize the covariance associated with the spacecraft semimajor axis. The example used to illustrate this technique is a 20,000 second transfer from an initial LEO with eccentricity equal to .05, semimajor axis equal to 7,500 kilometers, and argument of perigee equal to zero, to a

near GEO with eccentricity equal to .1, semimajor axis equal to 42,200 kilometers, and argument of perigee equal to zero. Unless specified, all distance units are kilometers and all time units are seconds. The Earth is the central gravity body and all third body effects are ignored. The state can be expressed as Eq. (3.57), and the time derivative of the state is given by Eq. (3.76). The time derivative of the covariance is given by Eq. (3.10). The observations are scalar range measurements from the center of the Earth in this example. The spectral density matrices and the initial value of the covariance for this example are expressed in the Cartesian frame and given by Eqs. (3.77) to (3.79). The cost function seeks to minimize the thrust acceleration provided by the engine and the covariance associated with the semimajor axis as shown by Eq. (3.80). It is important to note that minimizing J is equivalent to maximizing final mass for a power limited propulsion engine.[21] The mass can be recovered from J at any time using Eq. (2.3).

$$\dot{\mathbf{X}} = \begin{pmatrix} \dot{x} \\ \dot{y} \\ u_x - \dfrac{\mu x}{r^3} \\ u_y - \dfrac{\mu y}{r^3} \end{pmatrix} \tag{3.76}$$

$$\mathbf{P}_{\mathbf{X}}(t_0) = \begin{pmatrix} 10^{-5} & 0 & 0 & 0 \\ 0 & 10^{-5} & 0 & 0 \\ 0 & 0 & 10^{-8} & 0 \\ 0 & 0 & 0 & 10^{-8} \end{pmatrix} \tag{3.77}$$

$$\mathbf{Q} = \begin{pmatrix} 0 & 0 & 0 & 0 \\ 0 & 0 & 0 & 0 \\ 0 & 0 & 10^{-16} & 0 \\ 0 & 0 & 0 & 10^{-16} \end{pmatrix} \tag{3.78}$$

$$\mathbf{R} = 10^{-1} \tag{3.79}$$

$$W = J(t_f) + \phi_1 P_{aa}(t_f) = J(t_f) + \phi_1 \frac{\partial a}{\mathbf{X}} \mathbf{P}_{\mathbf{X}}(t_f) \left(\frac{\partial a}{\mathbf{X}} \right)^T \tag{3.80}$$

In order to solve the optimal control problem, an augmented state and costate, given by Eqs. (3.61) and (3.63), must be formed that include the covariance elements. A TPBVP can be formulated to solve the optimal control problem. The 17 unknowns are the true anomalies in the initial and final orbits and the initial value of the costates specified by Eq. (3.63). Four constraints require the spacecraft to match the state, $\mathbf{X}(t_f)$, specified by the final orbit and the final true anomaly. The final 13 constraints are provided by the fact that the initial and final position and velocity costates must satisfy Eq. (3.81), the final value of λ_J must be negative one, and the final value of the covariance costates must be given by Eq. (3.82).

$$\begin{aligned} \boldsymbol{\lambda}_{\mathbf{r}}^T(t_0) \frac{\partial \mathbf{r}(t_0)}{\partial \kappa_0} + \boldsymbol{\lambda}_{\mathbf{v}}^T(t_0) \frac{\partial \mathbf{v}(t_0)}{\partial \kappa_0} = 0 \\ \boldsymbol{\lambda}_{\mathbf{r}}^T(t_f) \frac{\partial \mathbf{r}(t_f)}{\partial \kappa_f} + \boldsymbol{\lambda}_{\mathbf{v}}^T(t_f) \frac{\partial \mathbf{v}(t_f)}{\partial \kappa_f} = 0 \end{aligned} \tag{3.81}$$

$$\lambda_i(t_f) = \frac{\partial}{\partial P_i} \left[\phi_1 \frac{\partial a}{\mathbf{X}} \mathbf{P}_{\mathbf{X}}(t_f) \left(\frac{\partial a}{\mathbf{X}} \right)^T \right] \tag{3.82}$$

The simplest way to solve this TPBVP is to set φ_1 to zero and determine a mass optimal solution. For this case, the unknowns can be reduced to the initial position and

velocity costates as well as the initial and final true anomalies. The constraints are given by Eq. (3.81), and the final position and velocity must match the position and velocity of an object at the final true anomaly in the target orbit. This solution with the covariance costates set to zero is a good initial guess for a solution with a small value of φ_1. The value of φ_1 can be increased until a solution that weights the final covariance in the desired manner is found.

The initial and final orbits as well as the mass optimal transfer and the transfer with φ_1 set to one-half are shown in Figure 3.7. Figures 3.8 and 3.9 show the covariance associated with the semimajor axis for both the mass optimal transfer and the transfer with φ_1 set to one-half. Clearly the trajectory that emphasizes the final value of the semimajor axis covariance does not have a lower value for the semimajor axis covariance throughout the trajectory. Figure 3.9 shows the semimajor axis covariance at the end of the trajectory is significantly reduced. Figures 3.10 and 3.11 show the differences in the thrust acceleration along each trajectory. The integral of the thrust acceleration squared and the final value of the semimajor axis covariance are shown in Table 3.1 for a variety of values of φ_1. The covariance associated with the semimajor axis at the final time can be reduced by over ten percent with less than a one-half percent increase in the integral of the thrust acceleration squared. As φ_1 is increased, the increased thrust acceleration required to further reduce the semimajor axis covariance increases dramatically.

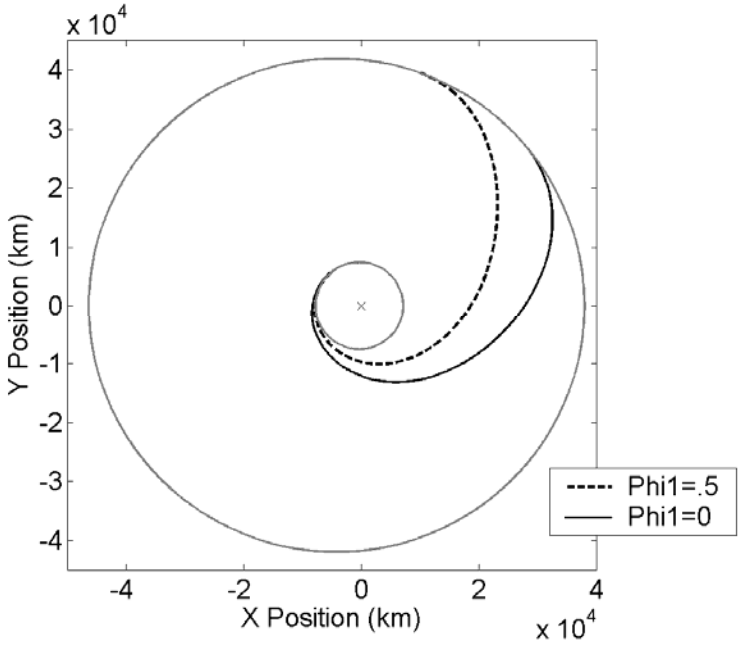

Figure 3.7 Optimal Transfer Trajectories

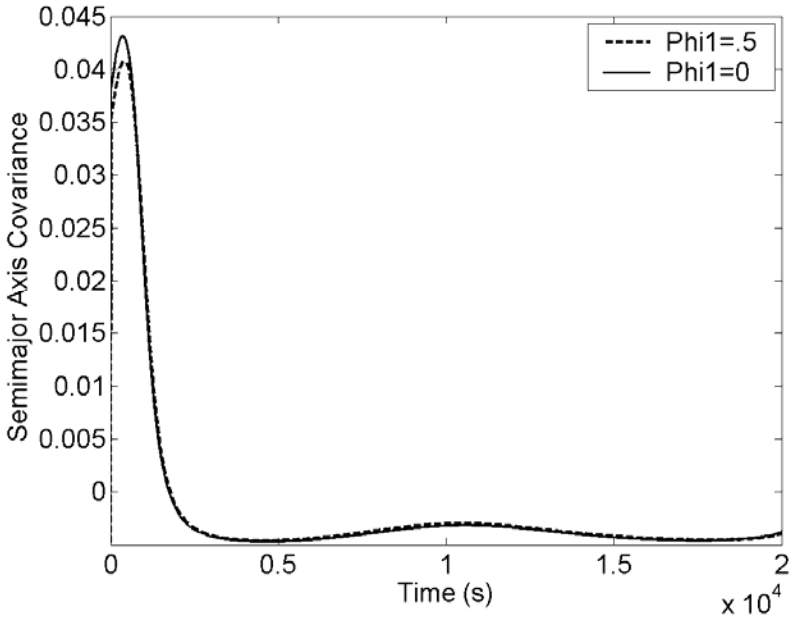

Figure 3.8 Semimajor Axis Covariance vs Time

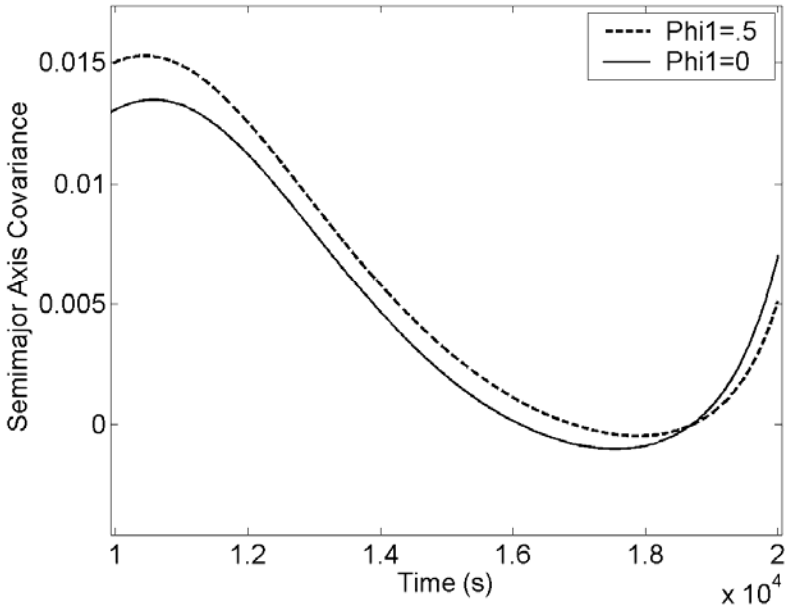

Figure 3.9 Semimajor Axis Covariance vs Time (Final Time Magnified)

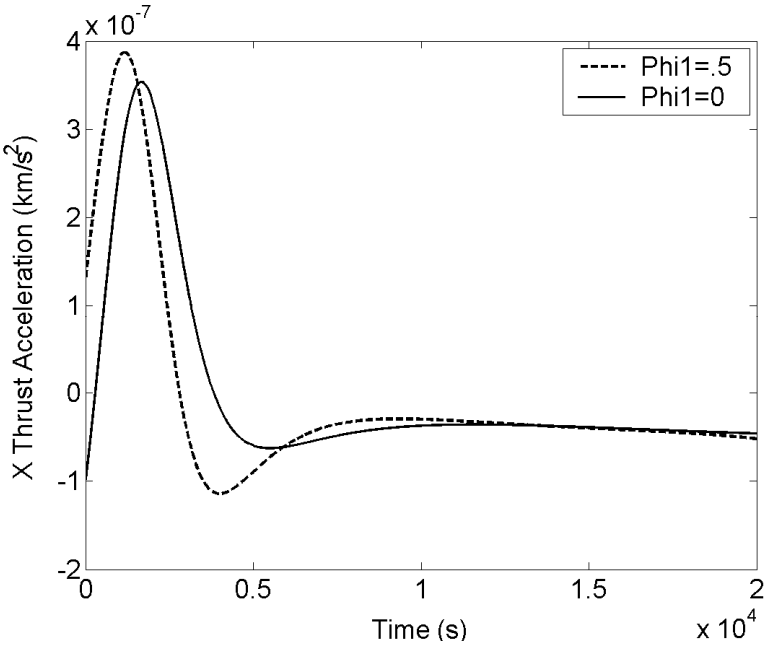

Figure 3.10 Thrust Acceleration in X-Direction vs Time

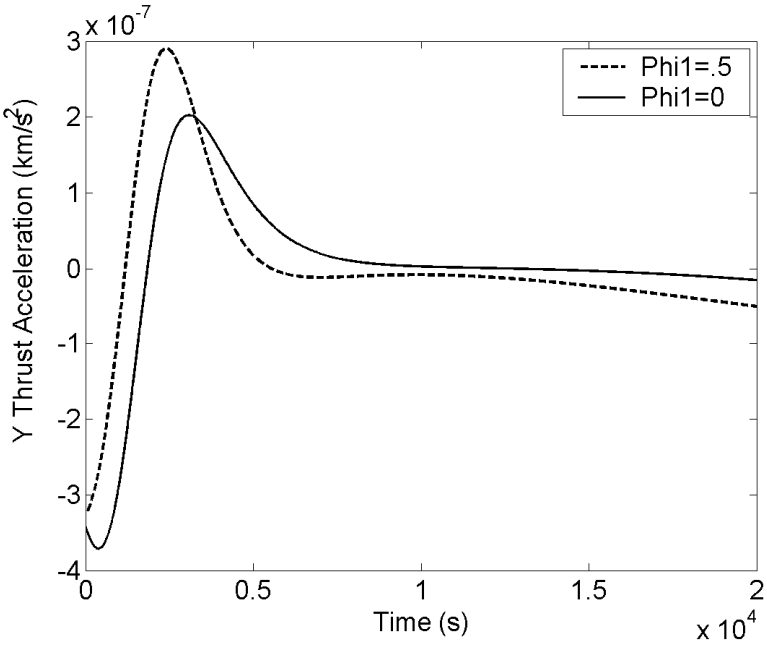

Figure 3.11 Thrust Acceleration in Y-Direction vs Time

Table 3.1 Comparison Of Semimajor Axis Covariance To The Integral Of The Thrust Acceleration Squared

φ_1	Integral of Thrust Acceleration Squared $*10^{-4}$	Change in Integral of Thrust Acceleration Squared $*10^{-10}$	Semimajor Axis Covariance at Final Time	Change in Semimajor Axis Covariance $*10^{-3}$	$\frac{\Delta P_{aa}}{\Delta J}$
.000	14.95407	N/A	1.2054	N/A	N/A
.001	14.95412	44	1.2009	-4.5	102.25
.005	14.95502	950	1.1855	-19.9	17
.010	14.95730	3224	1.1701	-35.3	6.75
.050	14.98811	34038	1.1110	-94.4	1.9
.100	15.02717	73100	1.0837	-121.7	0.7
.500	15.42040	466322	1.0133	-192.1	0.2

Chapter Conclusions

This chapter demonstrates that the covariance associated with a non-Cartesian frame can be minimized without deriving the optimality conditions or equations of motion for either the spacecraft or the covariance in a non-Cartesian frame. The method presented in this chapter produces equivalent results to formulating the problem in the non-Cartesian frame. The example problems demonstrate that the covariance associated with the semimajor axis can be reduced significantly without a significant increase in the integral of the thrust acceleration squared. A transfer trajectory that decreases the semimajor axis covariance should allow one to more accurately propagate the spacecraft state on the target orbit. Future applications of this method include minimizing a cost function that includes covariance terms from multiple frames and minimizing the covariance associated with flight path angle and other functions of the state which must be accurately predicted for precision landing.

CHAPTER 4 REDUCING UNCERTAINTY IN COMPLEX TRANSFERS

Chapter Summary

The purpose of this chapter is to extend the results from the previous chapters to more complicated models for the covariance propagation and gravitational fields. In the first extension, the observer is located on the surface of the Earth and rotates with the Earth. The same LEO to GEO transfer as in chapter 2 is used to demonstrate this technique so that the results can be compared with the results from the previous chapter where the observer is fixed at the center of the Earth. In the second extension, the changes in the optimal control needed to allow the noise in the equations of motion to depend on the amount of thrust provided by the engine are presented. The conditions on the optimal control are presented for two separate formulations of the modeled error in the thrust. The first formulation assumes three independent engines provide thrust in each of the coordinate directions; consequently, the noise in the equations in each coordinate direction is uncorrelated. The second formulation assumes a single engine provides thrust causing the noise in the coordinate directions to be coupled. The third extension is a transfer from Earth orbit to lunar orbit. The gravitational effects of both bodies affect the spacecraft throughout the transfer. A significant decrease in the covariance associated with the semimajor axis of the target orbit relative to the moon is demonstrated for a slight increase in the propellant.

Observer in Motion

The example transfer is a 20,000 second transfer from an initial orbit with eccentricity equal to .05, semimajor axis equal to 7,000 kilometers, and argument of perigee equal to zero to an orbit with eccentricity equal to 0.1, semimajor axis equal to 42,200 kilometers, and argument of perigee equal to zero. The cost function for this transfer is given by Eq. (4.1).

$$W = \phi\left[P_{xx}(t_f) + P_{yy}(t_f) + P_{\dot{x}\dot{x}}(t_f) + P_{\dot{y}\dot{y}}(t_f)\right] + J(t_f) + \phi_6 q(t_f) \tag{4.1}$$

In this example the observer's location can be any function of time that is known a priori. For this example, the observer's position relative to the Earth is given by Eq. (4.2) which approximates an observer on the Earth's surface with no occultation. The measurements will again be scalar range measurements taken continuously throughout the trajectory. Notice that none of the unknowns or constraints associated with the TPBVP change when the observer's position is a function of time. The equations of motion are now an explicit function of time, but no changes must be made to an optimization code, except **p**(t) must be calculated at each integration time instead of once at the beginning of the trajectory.

$$\mathbf{p}(t) = 6378\begin{bmatrix} \cos\left(\dfrac{2\pi t}{86400}\right) \\ \sin\left(\dfrac{2\pi t}{86400}\right) \end{bmatrix} \tag{4.2}$$

Table 4.1 shows a summary of the fuel consumption and observability along four trajectories that increasingly weight the trace of the covariance at the final time in the cost function. In this situation the trace of the covariance at the final time can be reduced

by 12.5 percent with a 0.6 percent increase in the integral of the thrust acceleration squared. For this example, the integral of the trace of the covariance **increases** by nearly 12 percent as well. Figures 4.1, 4.2, and 4.3 illustrate how the trace of the covariance behaves on these trajectories. Figure 4.2 is a magnified view of the peak in Figure 4.1, and Figure 4.3 is a magnified view of the trace of the covariance near the end of the trajectory. As the trace of the covariance at the final time is decreased, the peak value of the trace of the covariance increases. This increase at the peak causes the integral of the trace of the covariance to increase as the trace of the covariance at the final time is emphasized.

Table 4.1 Observability And Fuel Usage For Trajectories Minimizing The Trace Of The Covariance At The Final Time With Moving Observer

φ	Integral of Thrust Acceleration Squared $*10^{-4}$	Change in Integral of Thrust Acceleration Squared $*10^{-7}$	Integral of Trace of Covariance	Change in Integral of Trace of Covariance	Trace of Covariance at Final Time $*10^{-4}$	Change in Final Trace $*10^{-5}$
0	16.9774	N/A	69.2307	N/A	2.9845	N/A
.01	16.9920	14.6	71.6360	2.4053	2.8317	-1.528
.02	17.0284	51.0	74.4250	5.1943	2.7093	-2.752
.03	17.0778	100.4	77.4509	8.2202	2.6097	-3.748

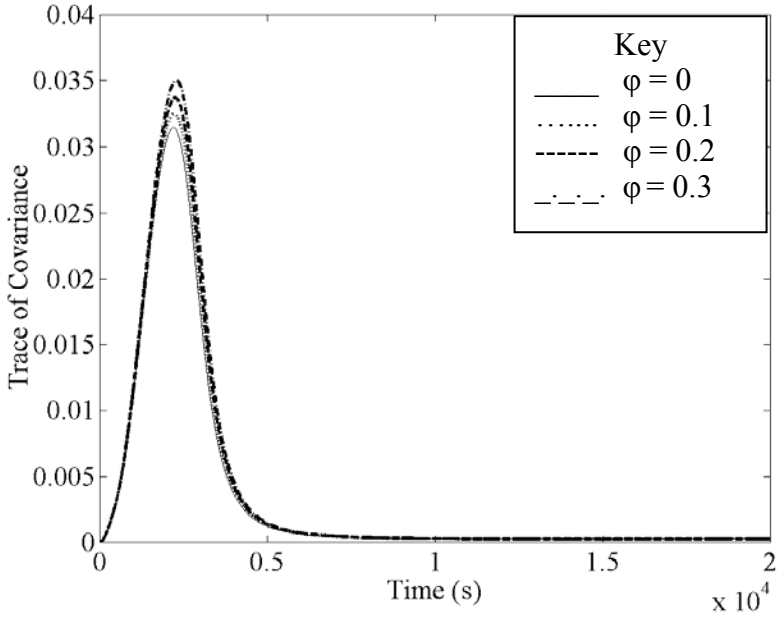

Figure 4.1 Trace of Covariance vs Time

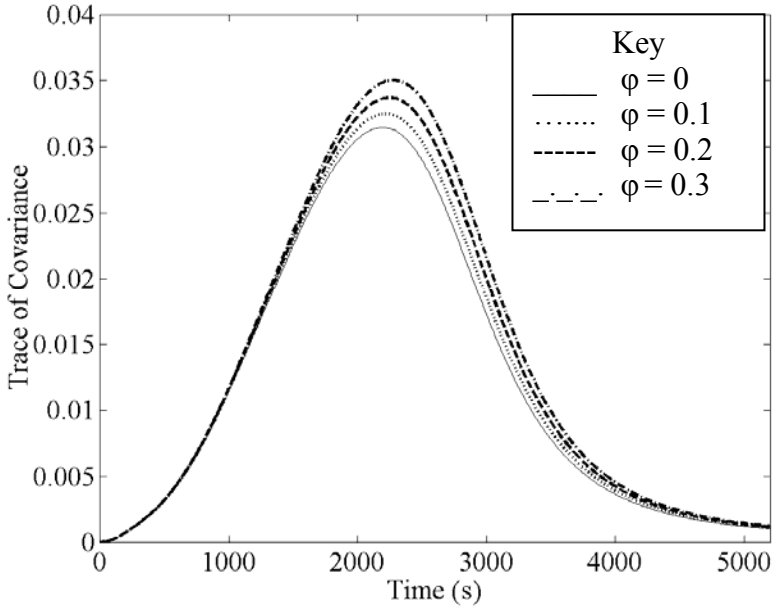

Figure 4.2 Trace of Covariance vs Time (Magnified)

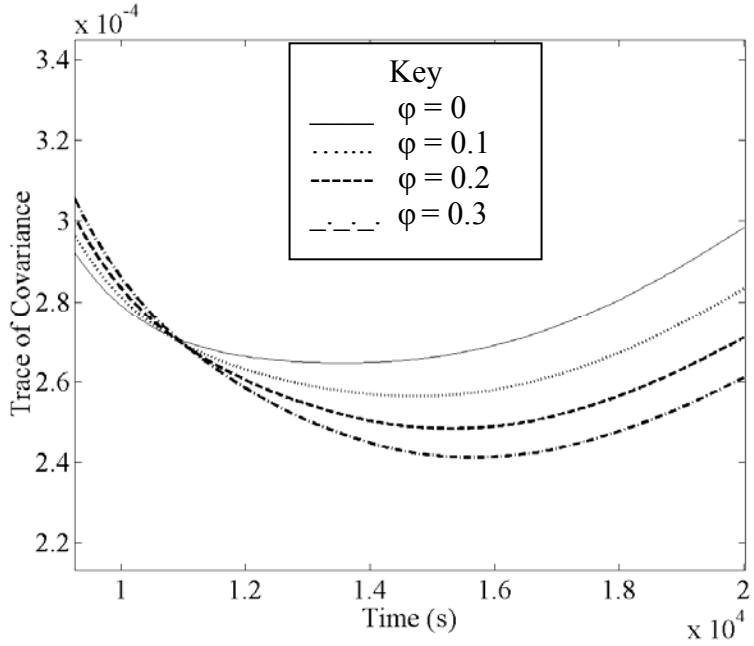

Figure 4.3 Trace of Covariance vs Time (Magnified)

Table 4.2 shows a summary of the fuel consumption and observability along four trajectories that increasingly weight the integral of the trace of the covariance in the cost function. Again, the integral of the trace of the covariance can be significantly decreased with only a slight increase in fuel consumption. The trace of the covariance at the final time increases slightly as the integral of the trace of the covariance is emphasized to a greater degree. Figure 4.4 illustrates the relationship between the integral of the thrust acceleration squared and the integral of the trace of the covariance. It is relatively inexpensive to decrease the covariance of the mass optimal solution slightly, but it becomes more expensive to further reduce the covariance. Figures 4.5 to 4.7 show significant differences between the trajectories and the thrust acceleration when φ_6 is changed from zero to $405*10^{-9}$.

Table 4.2 Observability And Fuel Usage For Trajectories Minimizing The Integral Of The Trace Of The Covariance With Moving Observer

φ_6 $*10^{-9}$	Integral of Thrust Acceleration Squared $*10^{-4}$	Change in Integral of Thrust Acceleration Squared $*10^{-8}$	Integral of Trace of Covariance	Change in Integral of Trace of Covariance	Trace of Covariance at Final Time $*10^{-4}$	Change in Final Trace $*10^{-7}$
0	16.9774	N/A	69.2307	N/A	2.9845	N/A
4.5	16.9776	2	66.9539	-2.277	2.9858	1.3
9	16.9778	4	64.9643	-4.266	2.9874	2.9
13.5	16.9782	8	63.2031	-6.028	2.9894	4.9
18	16.9786	12	61.6273	-7.603	2.9916	7.1
22.5	16.9792	18	60.2047	-9.026	2.9940	9.5
27	16.9798	24	58.9106	-10.320	2.9965	12.0
36.5	16.9814	40	56.5188	-12.712	3.0023	17.8
79.8	16.9896	122	49.1148	-20.116	3.0316	47.1
280	17.0308	534	36.1351	-33.096	3.1699	185.4
405	17.0542	768	32.6701	-36.561	3.2492	264.7

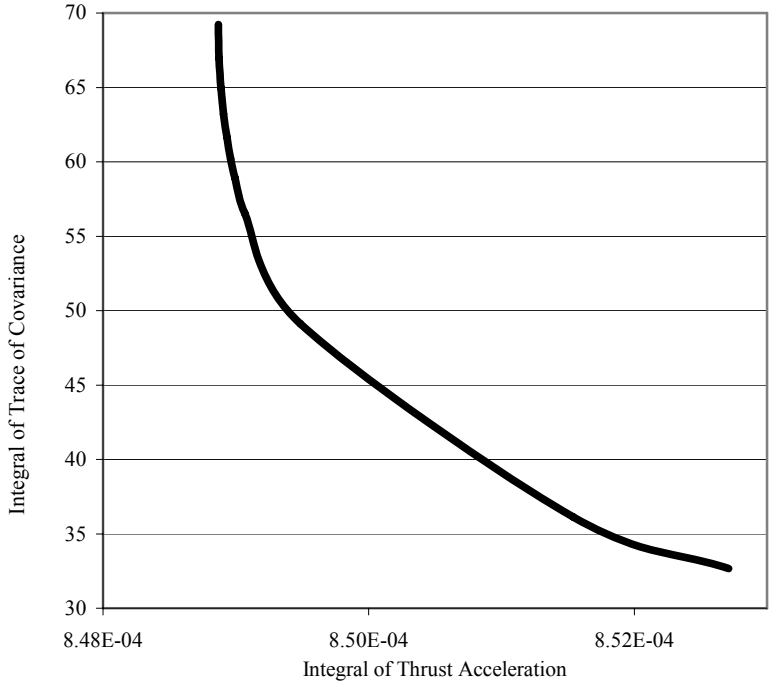

Figure 4.4 Integral of Trace of Covariance vs Integral of Thrust Acceleration Squared

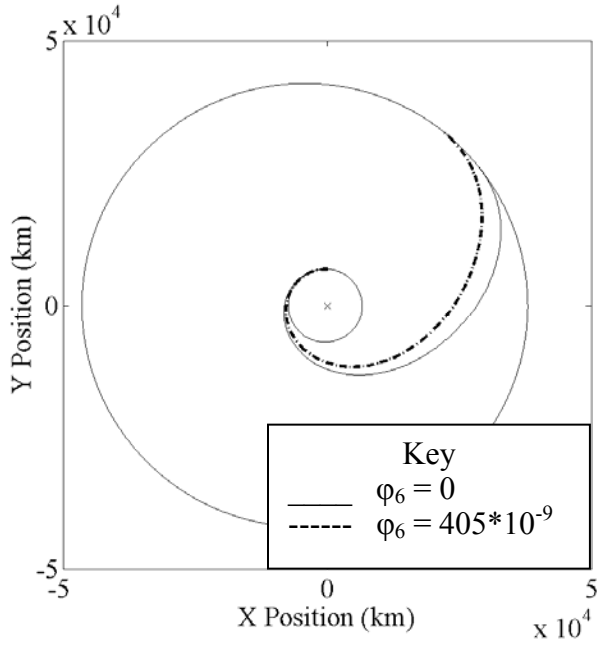

Figure 4.5 Optimal Trajectories with Moving Observer

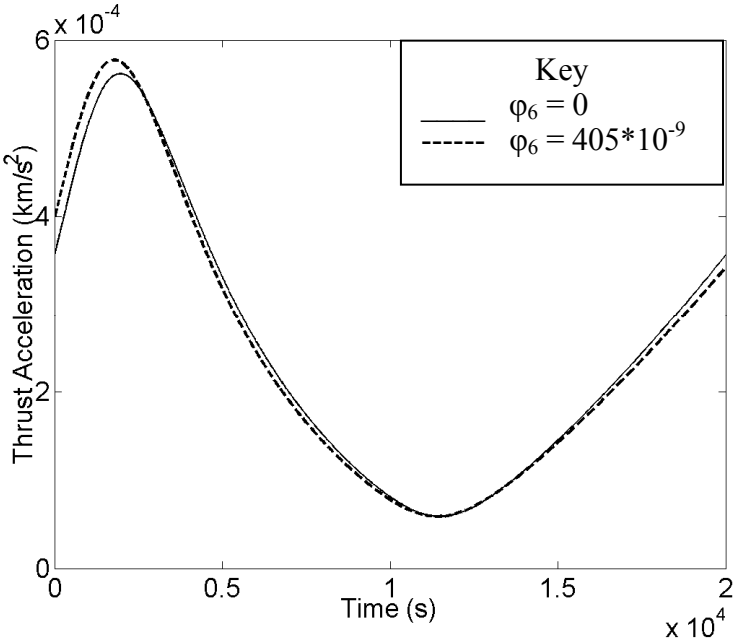

Figure 4.6 Thrust Acceleration Magnitude vs Time

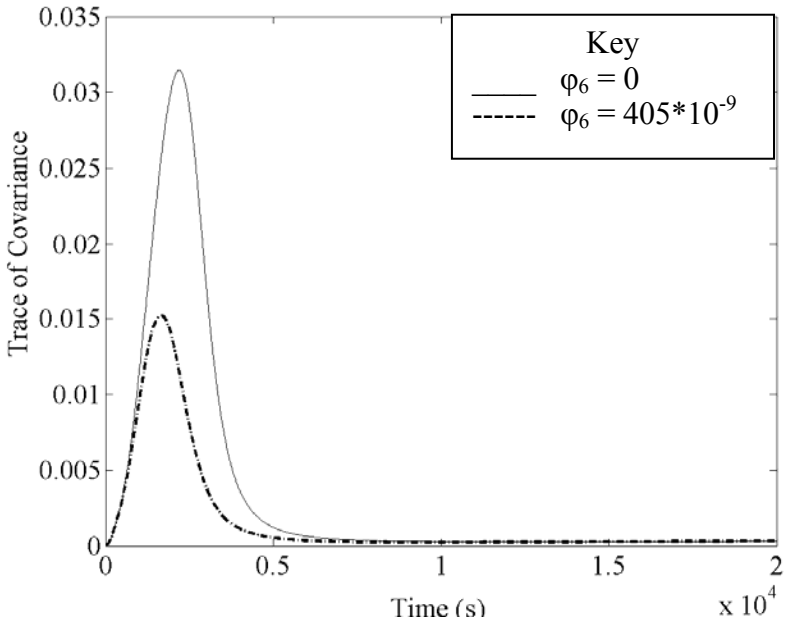

Figure 4.7 Trace of Covariance vs Time

Dynamic Errors Based on Thrust

The examples in chapter 2 assume that the error in the dynamic equations of motion is independent of the controls. One obvious shortcoming of that formulation is that errors in the thrust magnitude and direction contribute significantly to the errors in the dynamic equations of motion. These engine thrust errors are more significant when the engine is providing more thrust. This application allows the spectral density of the errors in the dynamics, **w** from Eq. (2.9), to be functions of the thrust magnitude and direction. The resulting optimal control depends on whether the controls are modeled as separate engines, each of which provides thrust acceleration in one of the coordinate directions, or as a single engine and two angles which provide the overall three dimensional thrust.

In the former case, the errors in the thrust magnitudes for each engine are assumed to be independent. As a result, **w** can be written as in Eq. (4.3) where ω_x, ω_y, and ω_z account for the errors in the dynamic equations due to gravitational terms, solar winds, and other forces which are not modeled. They have zero-mean, are independent, and have spectral density ω_1^2. The errors in the thrust acceleration, T_1, T_2, and T_3, are also zero-mean and independent of each other and ω. These errors are modeled as dependent on the magnitude of the thrust acceleration provided by each engine with spectral density specified by Eqs. (4.4) to (4.6). The spectral density, **Q,** can now be written as Eq. (4.7).

$$\mathbf{w}(t) = \begin{pmatrix} \omega_x \\ \omega_y \\ \omega_z \end{pmatrix} + \begin{pmatrix} T_1 \\ T_2 \\ T_3 \end{pmatrix} \tag{4.3}$$

$$\frac{E[T_1(t)T_1(\tau)]}{\delta(t-\tau)} = \frac{\Gamma_x^2}{\xi_1} \tag{4.4}$$

$$\frac{E[T_2(t)T_2(\tau)]}{\delta(t-\tau)} = \frac{\Gamma_y^2}{\xi_2} \tag{4.5}$$

$$\frac{E[T_3(t)T_3(\tau)]}{\delta(t-\tau)} = \frac{\Gamma_z^2}{\xi_3} \tag{4.6}$$

$$\mathbf{Q}(t)=\frac{E[\mathbf{w}(t)\mathbf{w}^{T}(\tau)]}{\delta(t-\tau)}=\begin{pmatrix} 0 & 0 & 0 & 0 & 0 & 0 \\ 0 & 0 & 0 & 0 & 0 & 0 \\ 0 & 0 & 0 & 0 & 0 & 0 \\ 0 & 0 & 0 & w_1^2+\frac{\Gamma_x^2}{\xi_1} & 0 & 0 \\ 0 & 0 & 0 & 0 & w_1^2+\frac{\Gamma_y^2}{\xi_2} & 0 \\ 0 & 0 & 0 & 0 & 0 & w_1^2+\frac{\Gamma_z^2}{\xi_3} \end{pmatrix} \tag{4.7}$$

The first order optimality conditions require that the derivative of the Hamiltonian with respect to Γ_x, Γ_y, and Γ_z be zero. The terms in the Hamiltonian involving Γ_x, Γ_y, and Γ_z are given by Eq. (4.8). The thrust acceleration along the optimal trajectory is then given by Eq. (4.9). Notice the similarity between Eqs. (2.29) and (2.30) and Eq. (4.9). If the error in the dynamic equations is not related to the magnitude of the thrust acceleration, then ζ_1, ζ_2, and ζ_3 would be infinite and the thrust acceleration terms in Eq. (4.9) would be unchanged from the values in Eqs. (2.29) and (2.30).

$$H_a=\lambda_{vx}\Gamma_x+\lambda_{vy}\Gamma_y+\lambda_{vz}\Gamma_z+\lambda_J\frac{\Gamma_x^2+\Gamma_y^2+\Gamma_z^2}{2}+\lambda_{16}\frac{\Gamma_x^2}{\xi_1}+\lambda_{19}\frac{\Gamma_y^2}{\xi_2}+\lambda_{21}\frac{\Gamma_z^2}{\xi_3}+\text{ non }\Gamma\text{ terms} \tag{4.8}$$

$$\Gamma_x=\frac{-\lambda_{vx}}{\lambda_J+\frac{2\lambda_{16}}{\xi_1}}\quad \Gamma_y=\frac{-\lambda_{vy}}{\lambda_J+\frac{2\lambda_{19}}{\xi_2}}\quad \Gamma_z=\frac{-\lambda_{vz}}{\lambda_J+\frac{2\lambda_{21}}{\xi_3}} \tag{4.9}$$

In most applications, separate engines are not used to create thrust in the three coordinate axes. In these cases, the errors in the dynamic equations of motion will be based on the difference between the actual thrust acceleration magnitude and the desired thrust acceleration magnitude as well as errors in the direction of the thrust acceleration. Consider a two dimensional example where the controls are the magnitude of the thrust

acceleration, Γ, and the thrust direction measured from the x-axis, α. The difference between the actual thrust acceleration magnitude and direction and the prescribed value is given by Eq. (4.11) where both T_1 and α_1 are zero-mean and independent with spectral density given by Eq. (4.12). Because both T_1 and α_1 are small, terms involving T_1 multiplied by α_1 or α_1^2 are ignored. As a result, Eq. (4.10) can be simplified as Eq. (4.13) by using a Taylor Series expansion. The spectral density, **Q,** can now be written as in Eq. (4.14). Note that the expected error in the thrust acceleration in the coordinate directions is coupled in this formulation unlike the previous formulation that assumed separate engines in the component directions.

$$\mathbf{w}(t) = \begin{pmatrix} \omega_x \\ \omega_y \end{pmatrix} + \Gamma^* \begin{bmatrix} \cos(\alpha^*) \\ \sin(\alpha^*) \end{bmatrix} - \Gamma^{\&} \begin{bmatrix} \cos(\alpha^{\&}) \\ \sin(\alpha^{\&}) \end{bmatrix} \tag{4.10}$$

$$\begin{aligned} \Gamma^* &= \Gamma^{\&} + T_1 \\ \alpha^* &= \alpha^{\&} + \alpha_1 \end{aligned} \tag{4.11}$$

$$\frac{E[T_1(t)T_1(\tau)]}{\delta(t-\tau)} = \frac{\left(\Gamma^{\&}\right)^2}{\xi_1} \qquad \frac{E[\alpha_1(t)\alpha_1(\tau)]}{\delta(t-\tau)} = \frac{1}{\xi_2} \tag{4.12}$$

$$\mathbf{w}(t) = \begin{pmatrix} \omega_x \\ \omega_y \end{pmatrix} + \frac{T_1}{\Gamma^*} \begin{pmatrix} \Gamma_x \\ \Gamma_y \end{pmatrix} + \alpha_1 \begin{pmatrix} -\Gamma_y \\ \Gamma_x \end{pmatrix} \tag{4.13}$$

$$\mathbf{Q}(t) = \frac{E[\mathbf{w}(t)\mathbf{w}^T(\tau)]}{\delta(t-\tau)} = \begin{pmatrix} 0 & 0 & 0 & 0 \\ 0 & 0 & 0 & 0 \\ 0 & 0 & w_1^2 + \frac{\Gamma_x^2}{\xi_1} + \frac{\Gamma_y^2}{\xi_2} & \Gamma_x\Gamma_y\left(\frac{1}{\xi_1} - \frac{1}{\xi_2}\right) \\ 0 & 0 & \Gamma_x\Gamma_y\left(\frac{1}{\xi_1} - \frac{1}{\xi_2}\right) & w_1^2 + \frac{\Gamma_x^2}{\xi_2} + \frac{\Gamma_y^2}{\xi_1} \end{pmatrix} \tag{4.14}$$

The terms in the Hamiltonian involving Γ_x and Γ_y are given by Eq. (4.15). The first order optimality conditions again require that the derivative of the Hamiltonian with respect to Γ_x and Γ_y be zero. The optimal thrust acceleration is then given by Eq. (4.16). Again, Eq. (4.16) reduces to Eqs. (2.29) and (2.30) when the error in the thrust acceleration is independent of the thrust magnitude and direction.

$$H_a = \lambda_{vx}\Gamma_x + \lambda_{vy}\Gamma_y + \lambda_J \frac{\Gamma_x^2 + \Gamma_y^2}{2} + \lambda_8\left(\frac{\Gamma_x^2}{\xi_1} + \frac{\Gamma_y^2}{\xi_2}\right) + \lambda_9\Gamma_x\Gamma_y\left(\frac{1}{\xi_1} - \frac{1}{\xi_2}\right) + \lambda_{10}\left(\frac{\Gamma_x^2}{\xi_2} + \frac{\Gamma_y^2}{\xi_1}\right) \quad (4.15)$$

$$\Gamma_y = -\frac{\lambda_{vy} - \lambda_9\lambda_{vx}d\left(\frac{1}{\xi_1} - \frac{1}{\xi_2}\right)}{\lambda_J + 2\left(\frac{\lambda_{10}}{\xi_1} + \frac{\lambda_8}{\xi_2}\right) - \lambda_9^2 d\left(\frac{1}{\xi_1} - \frac{1}{\xi_2}\right)^2}$$

$$\Gamma_x = -d\left[\lambda_{vx} + \lambda_9\Gamma_y\left(\frac{1}{\xi_1} - \frac{1}{\xi_2}\right)\right] \quad (4.16)$$

$$d = \left[\lambda_J + 2\left(\frac{\lambda_8}{\xi_1} + \frac{\lambda_{10}}{\xi_2}\right)\right]^{-1}$$

The same planar transfer from LEO to near GEO is used to illustrate the effect of allowing the error in the dynamic equations to be a function of the controls. The observer is fixed at the center of the Earth taking continuous scalar range measurements of the spacecraft position throughout the trajectory. Because it more accurately reflects the operation of an engine, the second formulation, in which the controls are thrust acceleration magnitude and direction, is used to illustrate this example. The constant term in the spectral density matrix for the error in the dynamic equations, w_1^2 given by Eq. (2.53) is reduced to one-half its value in the previous examples. The constants ξ_1 and ξ_2 are set to $1.1*10^8$ and 10^8, respectively. These values were chosen so errors in the

engine thrust magnitude and direction and errors due to dynamics that were not modeled would be of approximately the same magnitude. ξ_1 and ξ_2 have different values so the spectral density matrix, **Q**, is not diagonal.

Table 4.3 summarizes the effect that placing an increasing emphasis on the trace of the covariance at the final time has on the required thrust acceleration and the covariance. Again, a relatively large decrease in the trace of the covariance at the final time can be obtained for a small increase in the thrust acceleration. As the covariance at the final time is reduced, it becomes more expensive to reduce the final covariance. Following the trajectory that minimizes the trace of the covariance at the final time has nearly no affect on the trace of the covariance during the initial portion of the transfer but does significantly reduce the trace of the covariance at the final time.

Table 4.3 Observability And Fuel Usage For Trajectories Minimizing The Trace Of The Covariance At The Final Time With Variable Errors In The Dynamics

φ $*10^{-3}$	Integral of Thrust Acceleration Squared $*10^{-4}$	Change in Integral of Thrust Acceleration Squared $*10^{-8}$	Integral of Trace of Covariance	Change in Integral of Trace of Covariance $*10^{-1}$	Trace of Covariance at Final Time $*10^{-3}$	Change in Final Trace $*10^{-4}$
0.000	16.9774	N/A	58.8494	N/A	4.1586	N/A
0.002	16.9802	28	57.9147	-9.347	4.0164	-1.422
0.004	16.9878	104	57.0755	-17.739	3.8897	-2.689
0.006	16.9990	216	56.3185	-25.309	3.7762	-3.824
0.008	17.0134	360	55.6321	-32.173	3.6740	-4.846
0.010	17.0300	526	55.0065	-38.429	3.5815	-5.771

Table 4.4 shows the effect of placing an increasing emphasis on the integral of the trace of the covariance instead of the trace of the covariance at the final time. In this case, the integral of the trace of the covariance can be reduced by over eight percent with

less than a one-half percent increase in the integral of the thrust acceleration squared. Again, the ratio of the percentage decrease in the integral of the trace of the covariance to the percentage increase in the integral of the thrust acceleration squared decreases significantly as maximizing observability is emphasized. Figures 4.8 and 4.9 illustrate the effect of modeling the error in the dynamic equations as a function of the thrust magnitude. As the integral of the trace of the covariance is weighted more heavily in the optimization process, the maximum value for the thrust acceleration magnitude decreases, thus introducing less uncertainty into the equations of motion.

Table 4.4 Observability And Fuel Usage For Trajectories Minimizing The Integral Of The Trace Of The Covariance With Variable Errors In The Dynamics

φ_6 $*10^{-7}$	Integral of Thrust Acceleration Squared $*10^{-4}$	Change in Integral of Thrust Acceleration Squared $*10^{-8}$	Integral of Trace of Covariance	Change in Integral of Trace of Covariance $*10^{-1}$	Trace of Covariance at Final Time $*10^{-3}$	Change in Final Trace $*10^{-4}$
0	16.97740	N/A	58.8494	N/A	4.159	N/A
3.83	16.98224	48.4	57.5619	-1.2875	3.981	-1.78
15.4	17.04062	632.2	54.4267	-4.4227	3.563	-5.96
17.9	17.05930	819	53.8654	-4.9840	3.491	-6.68

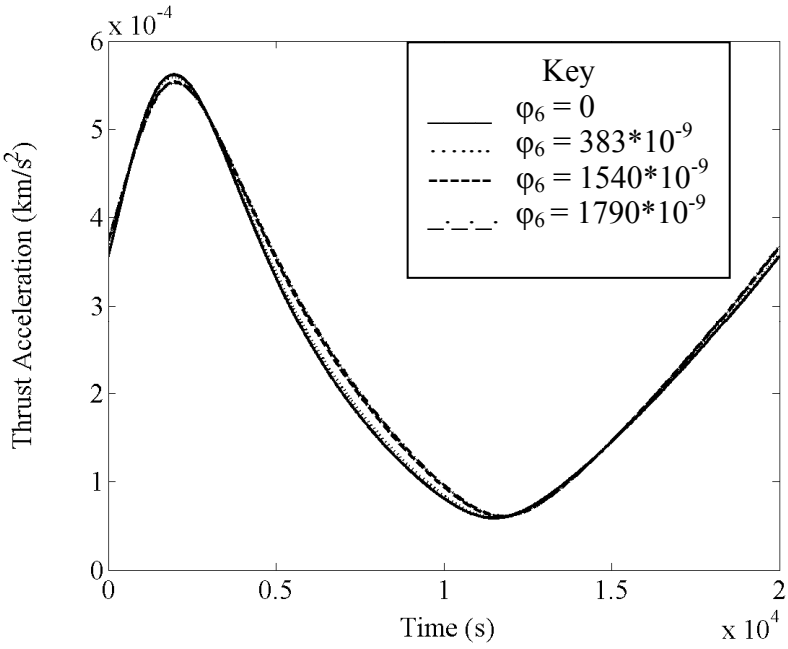

Figure 4.8 Thrust Acceleration Magnitude vs Time

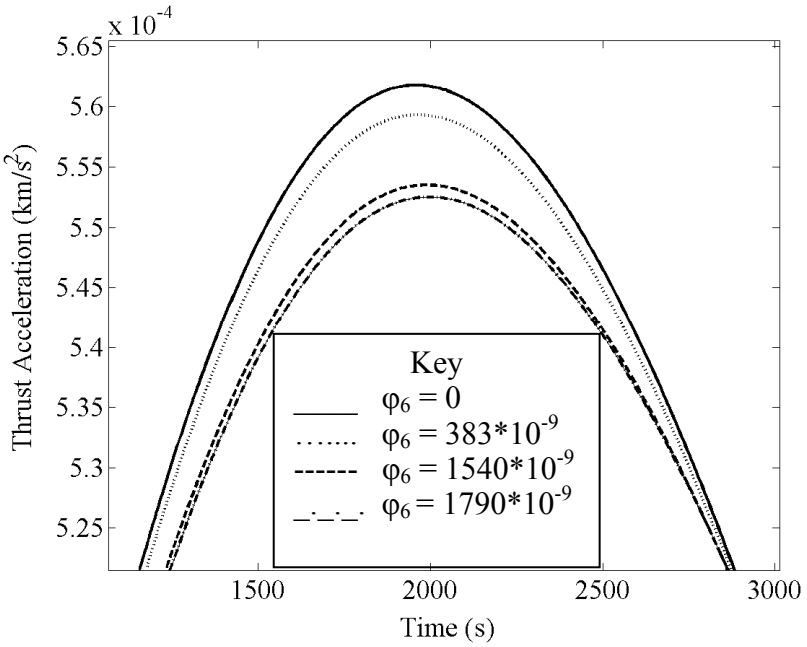

Figure 4.9 Maximum Thrust Acceleration Magnitude vs Time

Multiple Gravitational Bodies

The techniques presented in the previous sections and chapters do not theoretically require any significant modification in order to accommodate a transfer between multiple gravitational bodies. The equations of motions and partial derivatives which depend on them must be modified in order to include the gravitational effects of the additional bodies. As the following Earth orbit to lunar orbit transfer demonstrates, numerical difficulties require some modifications to the technique.

Earth Orbit to Lunar Orbit

A 36 hour planar transfer from an initial Earth orbit with eccentricity equal to 0.05, semimajor axis equal to 42,000 kilometers, and argument of perigee equal to zero to a lunar orbit with eccentricity equal to 0.1, semimajor axis equal to 3,476 kilometers (two moon radii), and argument of perigee equal to zero is employed to demonstrate this application. Throughout the trajectory, the gravitational effects from both the Earth and the moon affect the spacecraft. The moon is modeled as traveling in a circular orbit around the Earth at a distance of 384,400 km. At the beginning of the example transfer, the moon has a specified mean anomaly which is set to 190 degrees. This effect of the initial mean anomaly on the optimal solution can be studied parametrically, or one could add this value to the list of free variables with only slight modifications to the optimality conditions.

During the transfer, a series of scalar range measurements of the spacecraft state are taken. The observers are located at three locations on the surface of the Earth which are separated by 120 degrees. The locations of these observers are expressed as a function of time in Eq. (4.17). These observations are modeled as alternating periods of continuous measurements and no measurements with each period lasting for one hour

until the final two hours of the transfer during which continuous observations are made. The measurements are taken by the observer who views the spacecraft with the highest elevation at the beginning of the measurement period. Consequently, none of the measurements are occulted by the Earth. The cost function is again the sum of the integral of the thrust acceleration squared and the covariance associated with the semimajor axis of the spacecraft with respect to the moon at the end of the transfer as specified by Eq. (4.18).

$$\begin{aligned}
\mathbf{p}_1(t) &= 6378\begin{bmatrix}\cos\left(\frac{2\pi t}{86400}\right)\\ \sin\left(\frac{2\pi t}{86400}\right)\end{bmatrix}\\
\mathbf{p}_2(t) &= 6378\begin{bmatrix}\cos\left(\frac{2\pi t}{86400}+\frac{2\pi}{3}\right)\\ \sin\left(\frac{2\pi t}{86400}+\frac{2\pi}{3}\right)\end{bmatrix}\\
\mathbf{p}_3(t) &= 6378\begin{bmatrix}\cos\left(\frac{2\pi t}{86400}+\frac{4\pi}{3}\right)\\ \sin\left(\frac{2\pi t}{86400}+\frac{4\pi}{3}\right)\end{bmatrix}
\end{aligned} \tag{4.17}$$

$$W = J(t_f) + \phi P_{aa}(t_f) = J(t_f) + \phi \frac{\partial a}{\mathbf{X}} \mathbf{P}_{\mathbf{X}}(t_f)\left(\frac{\partial a}{\mathbf{X}}\right) \tag{4.18}$$

Numerical Considerations

One might think that this optimal transfer can be determined by solving the same TPBVP that was solved in the second chapter with the unknowns specified by Eq. (2.49) and the constraints specified by Eqs. (2.23), (2.26), and (2.43). While these unknowns and constraints are a valid set of unknowns and constraints to determine a first order

extremal solution, numerical convergence issues make the implementation difficult. In order to solve the TPBVP, one must determine the derivative of each of the constraints with respect to each of the unknown parameters from Eq. (2.49). A small perturbation to any of these parameters can cause large changes in the spacecraft state and the constraints at the final time, making finite difference derivatives difficult to calculate. Even with the use of state transition matrix derivatives (See Appendix A), numerical integration errors make these derivatives difficult to calculate and cause the search for solutions to the TPBVP to be extremely sensitive.

In order to overcome the numerical sensitivity of the solution process, the costates are reset at an intermediate point in the trajectory. The set of unknowns is now a 28 dimensional vector specified by Eq. (4.19). Ten additional constraints require that the covariance costates are continuous at the time they are reset as specified by Eq. (4.20). These new parameters and new constraints do not alter the optimal solution or cause any changes in the control. They simply allow one to prevent numerical integration error from growing over the longer integration times.

$$\boldsymbol{\alpha}^{\mathrm{T}} = \left(\boldsymbol{\lambda}_{\mathbf{r}}^{\mathrm{T}}(\mathrm{t}_0)\ \boldsymbol{\lambda}_{\mathbf{v}}^{\mathrm{T}}(\mathrm{t}_0)\ \lambda_{\mathrm{J}}(\mathrm{t}_0)\ \lambda_1(\mathrm{t}_0)\ \ldots\ \lambda_{10}(\mathrm{t}_0)\ \lambda_{\mathrm{q}}\ \kappa_0\ \kappa_{\mathrm{f}}\ \lambda_1(\mathrm{t}_1)\ \ldots\ \lambda_{10}(\mathrm{t}_1)\right) \tag{4.19}$$

$$\lambda_i(t_{1+}) = \lambda_i(t_{1-}) \tag{4.20}$$

Another numerical consideration that arises during this optimization process is the frame in which to integrate the equations of motion. Theoretically, one could place either the Earth or the moon at the center of the integration frame and treat the other body as a perturbing body without altering the solution. In practice, numerical error is larger when the spacecraft is not in the sphere of influence of the body that is treated as the center of the integration frame. In this study, the Earth is the center of the integration frame at the

beginning of the trajectory, and the moon is the center at the end of the integration. At an intermediate point in the trajectory, the spacecraft position and velocity are shifted to reflect this change in frames. The optimal location for this shift is at the edge of the moon's sphere of influence. Because the difference in integration error is not sensitive to the exact location of this shift of frames, the frames are shifted after 90 percent of the transfer time.

Optimization Results

The results from this optimization indicate that the covariance associated with the semimajor axis of the target lunar orbit can be reduced significantly with only a slight increase in thrust acceleration. Table 4.5 documents the integral of the thrust acceleration squared and the covariance associated with the target orbit semimajor axis for several trajectories that increasingly weight the covariance in the cost function. The covariance associated with the semimajor axis of the target orbit can be reduced by over 75 percent with an increase in the integral of the thrust acceleration squared of only slightly more than three-quarters of one percent.

Table 4.5 Semimajor Axis Covariance and Thrust Acceleration for Near GEO to Lunar Orbit Transfers

φ $*10^{-4}$	Integral of Thrust Acceleration Squared $*10^{-1}$	Change in Integral of Thrust Acceleration Squared $*10^{-5}$	Semimajor Axis Covariance at Final Time $*10^{-3}$	Change in Semimajor Axis Covariance $*10^{-3}$
0	4.2646	N/A	32.82	N/A
3	4.2668	22	25.32	-7.50
6	4.2728	82	18.56	-14.26
9	4.2802	156	13.53	-19.29
12	4.2870	224	12.72	-20.10
15	4.2928	282	8.14	-24.68
18	4.2976	330	6.68	-26.14

The mass optimal transfer with φ equal to zero and the transfer with φ equal to $1.8*10^{-4}$ that optimizes for fuel consumption and observability are shown in Figure 4.10 and Figure 4.11. Despite the fact that the covariance associated with the semimajor axis is reduced significantly, the transfer trajectory is not altered significantly.

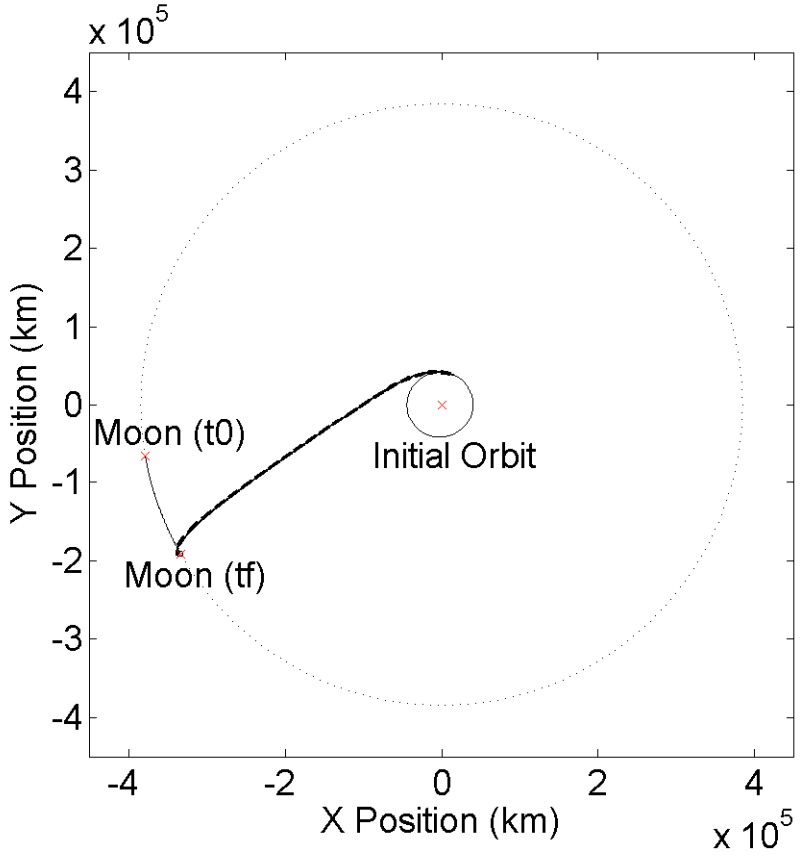

Figure 4.10 Earth Orbit to Lunar Orbit Transfer

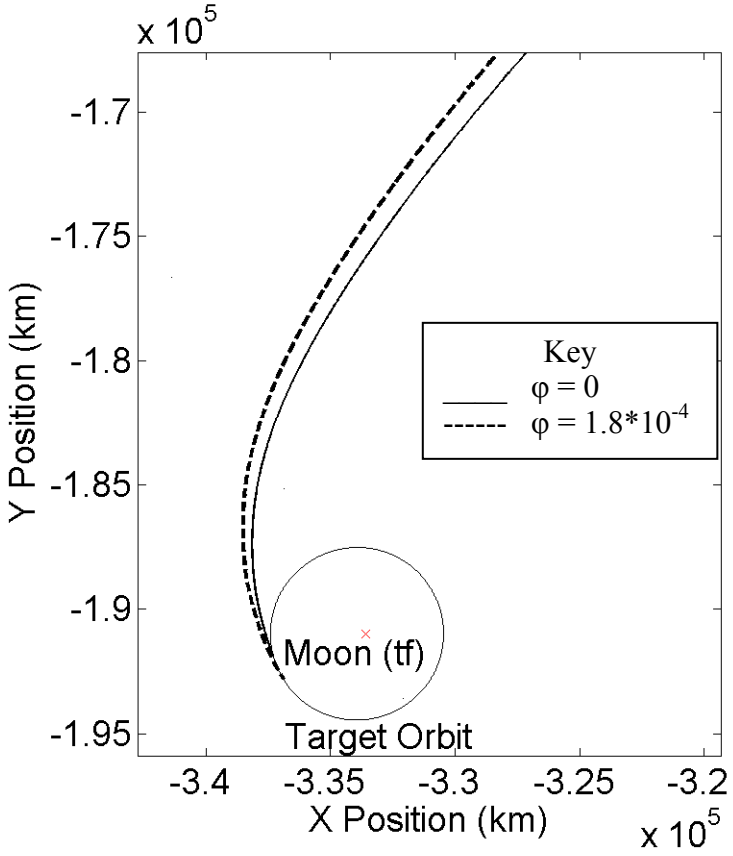

Figure 4.11 Earth Orbit to Lunar Orbit Transfer (Magnified)

Figure 4.12 shows the magnitude of the thrust acceleration for the mass optimal transfer. Figures 4.13 and 4.14 show the change in the thrust acceleration magnitude and the thrust direction when φ changes from 0 to $1.8*10^{-4}$. Notice that the thrust acceleration magnitude is altered by between one-tenth of one percent and 10 percent during different periods of the transfer.

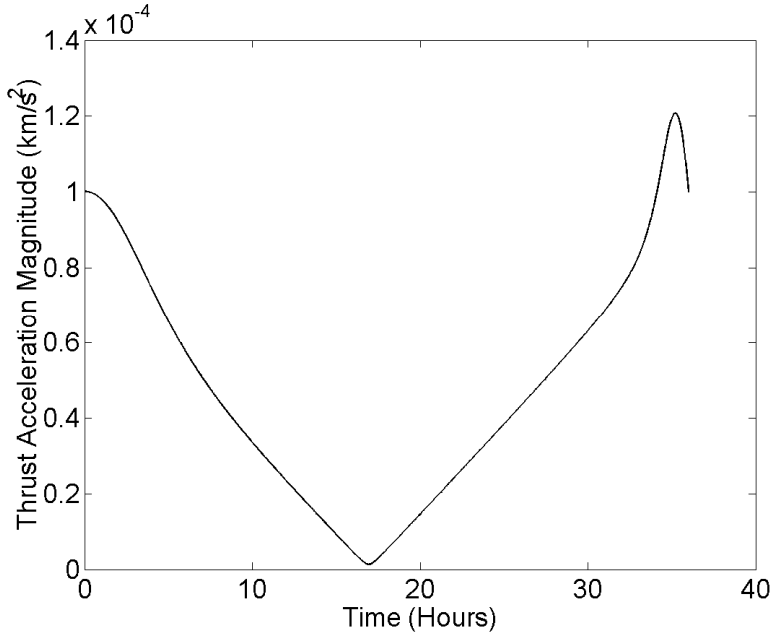

Figure 4.12 Thrust Acceleration Magnitude on Mass Optimal Transfer vs Time

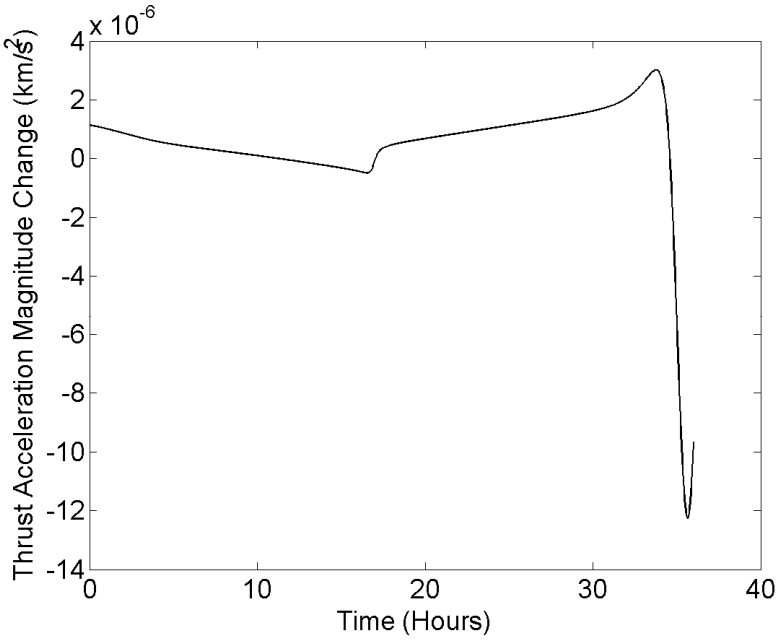

Figure 4.13 Change in Thrust Acceleration Magnitude Between Transfer with φ=.00018 and Mass Optimal Transfer vs Time

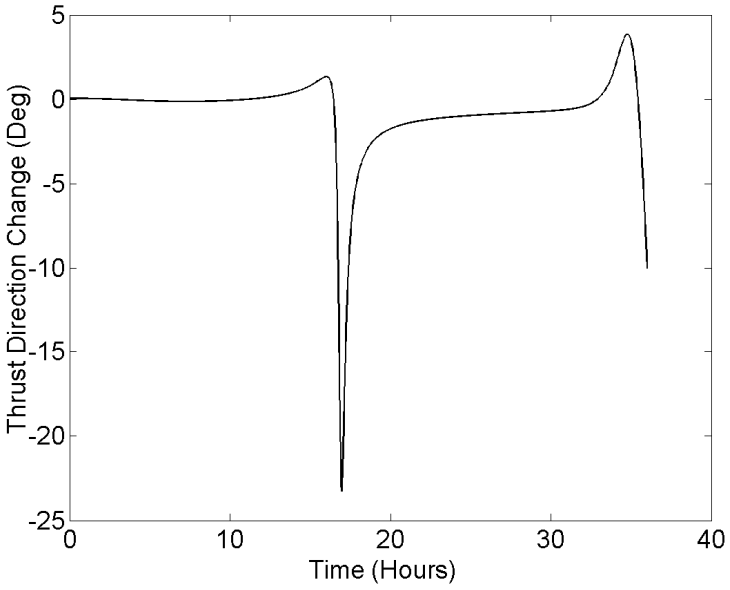

Figure 4.14 Change in Thrust Direction Between Transfer with φ=.00018 and Mass Optimal Transfer vs Time

The covariance associated with the spacecraft semimajor axis with respect to the moon along these two trajectories is shown in Figure 4.15. This covariance is only plotted near the end of the trajectory because the spacecraft semimajor axis relative to the moon does not have a significant meaning until the spacecraft approaches the moon.

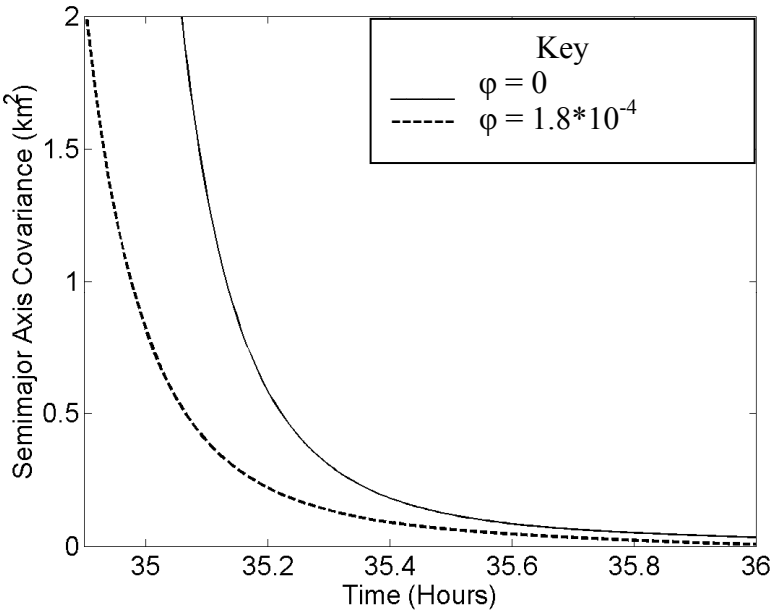

Figure 4.15 Covariance Associated with the Semimajor Axis of the Target Lunar Orbit vs Time

The costate associated with P_{yy} is plotted in Figure 4.16. Notice how this costate is largely unchanged during the early part of the trajectory and then changes a great deal as the spacecraft approaches the moon. These large changes near the end of the trajectory make it difficult to determine the initial value of these covariance costates because a very small change in the initial value of the costate or numerical integration error during the long portion of the trajectory where the costate remains nearly constant can cause a large violation of the constraint on these costates at the final time. These difficulties can be significantly reduced by including the value of the costate at an intermediate time in the unknown parameter list and constraining the value of the costate before and after this intermediate time as specified by Eqs. (4.19) and (4.20). Figure 4.17 shows the costate associated with P_{yy} near the end of the transfer for various values of φ. Notice that for

this transfer from Earth orbit to lunar orbit, the covariance costates do not exhibit the same phase and amplitude behavior as they exhibited in previous transfers. The covariance costates do not simply increase in amplitude as the observability terms are weighted more heavily in the cost function. The cause of this behavior is unknown.

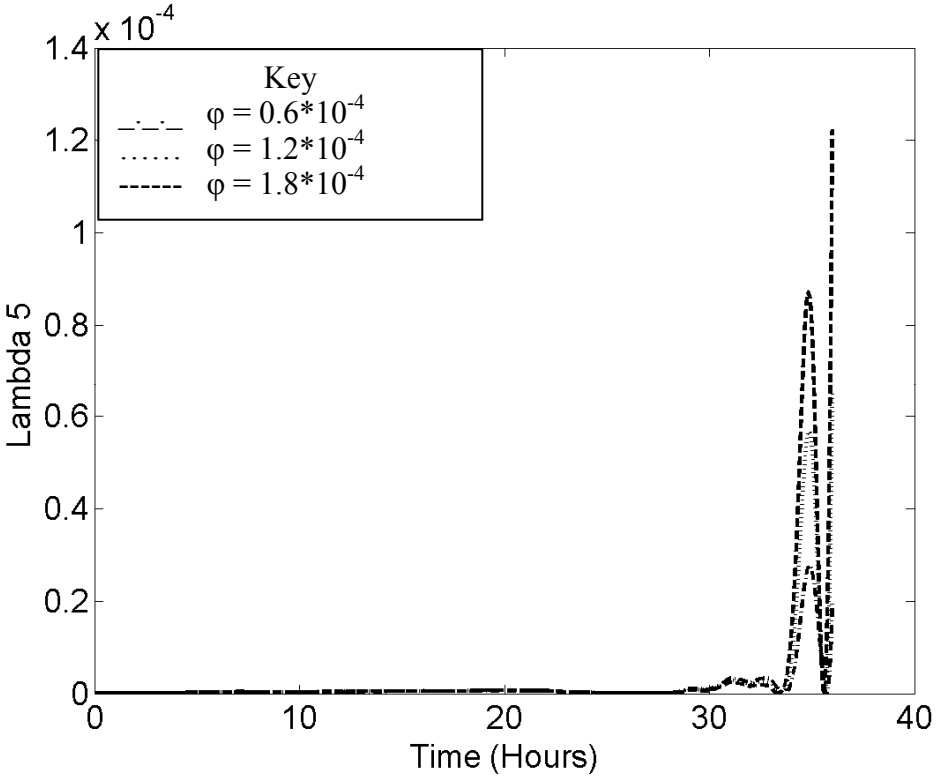

Figure 4.16 Covariance Costate Associated with P_{yy} vs Time

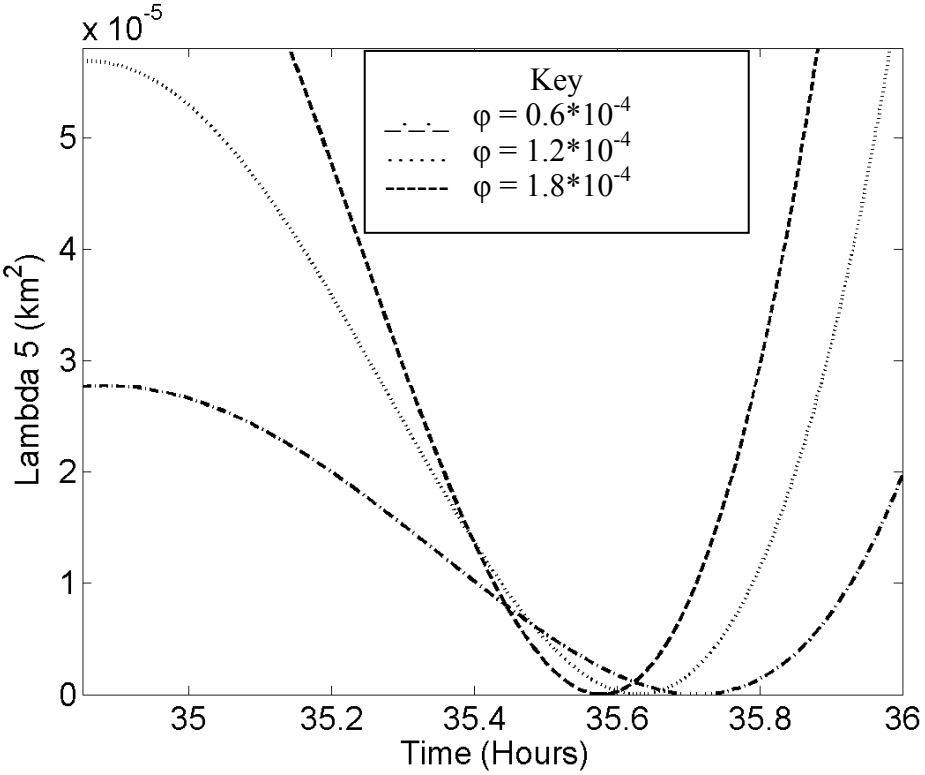

Figure 4.17 Covariance Costate Associated with P_{yy} vs Time (Magnified)

Chapter Conclusions

The effects of allowing the observer's location to vary with time and assuming the errors in the dynamics will be a function of the thrust magnitude and direction are not intuitive for the LEO to GEO transfer studied in this chapter. For the case of continuous scalar range observations from a stationary observer at the center of the Earth, the trace of the covariance at the end of the mass optimal transfer can be decreased 12 percent for a one-half of one percent increase in the integral of the thrust acceleration squared while the integral of the trace of the covariance can be reduced 31 percent for a 0.6 percent increase in the integral of the thrust acceleration squared. For this case, reducing either

the trace of the covariance at the final time or the integral of the trace of the covariance does not cause the other to increase.

For the moving observer example in this chapter, the trace of the covariance at the final time can be reduced 12.5 percent for a 0.6 percent increase in the integral of the thrust acceleration squared while the integral of the trace of the covariance can be decreased 47 percent for a 0.3 percent increase in the integral of the thrust acceleration squared. Modeling the observer as moving on the surface of the Earth has little effect on the cost of reducing the final value of the trace of the covariance but makes it much less costly to reduce the integral of the trace of the covariance. For the moving observer case, decreasing the final value of the covariance causes the integral of the trace of the covariance to increase while decreasing the integral of the trace of the covariance causes the final value of the trace to increase. The cause of this phenomenon is unknown.

The final value of the trace of the covariance can be reduced by 13.9 percent for a 0.3 percent increase in the integral of the thrust acceleration squared while the integral of the trace of the covariance can be reduced by 8 percent for a 0.5 percent increase in the integral of the thrust acceleration squared for the case of dynamic errors based on the thrust. The fact that it is more difficult to reduce the integral of the trace of the covariance by changing the thrust profile should be expected. When the engine thrusts more in an effort to place the spacecraft on a trajectory that is more observable, this process introduces more error into the equations of motion (because the model for dynamic error assumes that the error is proportional to thrust magnitude), thus causing the covariance to increase. The reason that it is less expensive in terms of thrust acceleration to reduce the final value of the trace of the covariance is unclear.

The transfer from Earth orbit to lunar orbit demonstrates that this technique can be applied to more complicated models for the dynamics and multiple observers without a great deal of difficulty. Some numerical convergence issues require slight modifications to the optimization procedure.

The results from this section indicate that covariance can be reduced for a small fuel penalty regardless of whether the observer is stationary or moving and regardless of whether the errors in the dynamics are modeled as a function of the thrust magnitude. Properly modeling the observer and the errors in the dynamics will allow one to most accurately determine the cost of reducing the covariance. Furthermore, the results from the moving observer case indicate that the analyst must know when in the trajectory it is important for the covariance to be minimized. Choosing to minimize the integral of the trace of the covariance instead of the trace of the covariance at the final time or vice-versa could result in a trajectory that is less observable for its mission.

CHAPTER 5 CONCLUSION

Summary of Dissertation Results

This dissertation provides a foundation upon which trajectory optimization can be accomplished with observability included as part of the cost function. In chapter 2, the calculus of variations is used to develop the necessary theory and derive the optimality conditions for a spacecraft to transfer from a set of initial conditions to a set of final conditions while minimizing a combination of fuel consumption and a function of the covariance matrix associated with the spacecraft's Cartesian position and velocity components. The theory is developed in a general manner that allows for multiple observers, moving observers, any observation type, multiple gravity bodies, discrete observations, and uncertainties in the spacecraft equations of motion based on the engine's thrusting status. In that chapter, a series of example planar transfers from LEO to near GEO demonstrate that the integral of the trace of the Cartesian covariance and the Cartesian covariance at the end of the mass optimal transfer can both be reduced significantly for only a small fuel consumption penalty. For the transfer with continuous scalar range measurements, the integral of the trace of the covariance on the mass optimal transfer is reduced by 12 percent for only a one-half percent increase in the integral of the thrust acceleration squared. The trace of the covariance at the end of the same transfer can be reduced by 31 percent for a one-half percent increase in integral of the thrust acceleration squared. This chapter also demonstrates that the results are not significantly

altered if there are periods without observations or if the observations are modeled as discrete.

The third chapter extends the theory of chapter 2 to allow one to minimize the uncertainty of the spacecraft state in a frame other than the one in which the spacecraft equations of motion and covariance are expressed. The technique allows one to minimize the uncertainty in any function of the spacecraft state without developing the equations of motion for the spacecraft or covariance in a non-Cartesian frame. The results of this technique are shown to be equivalent to solving the entire problem in the non-Cartesian frame. An example transfer demonstrates that the covariance associated with the semimajor axis at the end of a mass optimal transfer can be reduced by over ten percent with only a one-half percent increase in the integral of the thrust acceleration squared.

The fourth chapter again extends the results of the previous two chapters to solve more difficult transfers with more complicated models for the propagation of the covariance matrix. A method is developed in this chapter to allow the noise in the equations of motion to be a function of the thrust magnitude and direction. By applying this technique to the same LEO to near GEO planar transfer from chapters 2 and 3, the trace of the Cartesian covariance at the end of the mass optimal transfer can be reduced by 14 percent for about a one-third percent increase in the integral of the thrust acceleration squared.

The first appendix provides a method of using the state transition matrix to determine the derivatives of a function of the spacecraft state at the final time with respect to parameters that determine the spacecraft state at an earlier time. This technique provides an original method that allows the derivatives to be calculated even

when the spacecraft states or equations of motion are discontinuous at a finite number of intermediate locations. These derivatives are accurate to the order of the integrator used to propagate the spacecraft equations of motion. These derivatives are also shown to be able to converge to the optimal solution more quickly and more robustly than finite difference derivatives. These derivatives are employed throughout the examples in this dissertation in order to converge to optimal solutions.

The second appendix provides a summary of the adjoint control transformation which is used to determine the initial value of the position and velocity costates. The third appendix illustrates the patched conic gravity assist model that is employed in the first appendix.

General Conclusions

The results throughout this dissertation indicate that adding either the trace of the covariance at discrete times or the integral of the trace of the covariance to the cost function allows one to determine trajectories with significantly improved observability with very little additional propellant required. This general trend applies to all of the transfer problems and models studied. The amount of fuel required to improve the observability along a trajectory by a given percentage will depend on numerous factors including the initial and final orbits as well as the transfer time. This research has not attempted to determine which trajectories require less propellant to improve observability.

One should not overlook the significance of the results for the moving observer in chapter 4. In this transfer, if the cost function is the integral of the thrust acceleration

squared plus the trace of the covariance at the end of the transfer, the integral of the trace of the covariance increases. If instead one minimizes the integral of the trace of the covariance and the thrust acceleration, the trace of the covariance at the final time increases. These results demonstrate the importance of the analyst determining the function of the covariance matrix to minimize. Minimizing some function of the covariance matrix at a particular time may cause other functions of the covariance matrix to increase either at that time or at other times.

Another significant finding of this dissertation is the results indicate that the cost of further improving the observability increases as observability is improved. It appears to be quite inexpensive to slightly reduce the covariance associated with a mass optimal transfer. It becomes quite expensive in a relative sense to further reduce the covariance.

The differences between the optimal trajectories for continuous measurements throughout the trajectory, alternating periods of continuous measurements and no measurements, and discrete measurements are insignificant for the example transfer from LEO to GEO. The optimal control histories and optimal costates are similar for these three types of measurements. The results indicate that the exact times of the observations do not need to be known a priori in order to determine the fuel cost of decreasing the covariance by a given amount using this technique, but the results do indicate that one must know the quality and quantity of the measurements that will be taken. Additionally, this study only examined trajectories where the temporal spacing of the observations was equal. Further study is necessary to determine the affect of different measurement spacing.

The similarity between the results using discrete observations and the results using continuous observations indicate the continuous model is sufficient to determine optimal trajectories including observability. While one could theoretically use the method presented in this paper to solve an optimization problem with any number of discrete observations, difficulties limit the practical application of this method. In order to solve the TPBVP, one must compute the derivatives of the states and costates at the final time with respect to the costates at the initial time. As the number of observations increases, the number of jumps in the augmented state increases as well. These jumps in the state elements and the corresponding jumps in the costate elements make it difficult to compute these derivatives with enough accuracy to determine optimal trajectories with thousands of discrete measurements.

Future Work

The most obvious area of future work would be to apply this technique to a three dimensional transfer. All of the necessary theory for this application is presented in chapter 2 of this dissertation. The process of coding the equations for the three dimensional transfer would be time consuming, but not theoretically difficult. Another area of future research would be to account for the times when the line of sight from the observer to the spacecraft is occulted by either the Earth or some other celestial body. Again, all of the theory for such a formulation has been presented in chapter 2. One could also investigate how observability could be reduced on much longer missions such as spiral escape trajectories. An interesting study that could be conducted with the techniques of this dissertation would be to determine the number of measurements that

could be removed during the transfer without increasing the covariance at the end of the transfer for a given amount of additional propellant. This dissertation has demonstrated that the covariance after the transfer can be reduced significantly for a small fuel penalty. If instead of reducing the covariance, one wanted to reduce the number of measurements, the trajectory could be modified. A much more difficult area of further study would be adding the capability to account for optical measurements. One would need to quantify the quality of information in an optical measurement based on the spacecraft state at the time of the measurement.

APPENDIX A STATE TRANSITION MATRIX DERIVATIVES

Appendix Summary

This appendix provides a tool to calculate derivatives of the cost and constraint functions with respect to the free parameters in a trajectory optimization problem. This section demonstrates the use of this tool for trajectory optimization problems where the spacecraft state and the spacecraft equations of motion are discontinuous. These derivatives are shown to be more accurate than finite difference derivatives and their use is shown to make trajectory optimization algorithms more robust. Gravity assist trajectories using impulsive thrust, constant specific impulse, and variable specific impulse engines are used to demonstrate some of the applications of this technique. The method is completely general and can be used to compute derivatives for any state with respect to the parameters that affect the state at an arbitrary time. These state transition matrix derivatives are used throughout this dissertation wherever derivatives are necessary.

Nomenclature

c	specific impulse
C	constraint function
e	unit vector for adjoint control transformation
g	gravitational acceleration acting on spacecraft
h	orbital angular momentum of spacecraft

$\mathbf{I}$	identity matrix
J	cost function
m	spacecraft mass
P	power available for propulsion system
q	number of gravity assists
$\mathbf{r}$	spacecraft position
$\mathbf{R}$	transformation matrix for adjoint control transformation
$\mathbf{R}_{fb}$	transformation matrix used to express the flyby $\Delta\mathbf{v}$ in an inertial frame
r_m	periapse on hyperbolic flyby trajectory
S	switching function
T	thrust magnitude
t	time
$\mathbf{u}$	thrust direction unit vector
$\mathbf{v}$	velocity
v_∞	velocity of spacecraft relative to flyby planet
$\mathbf{X}$	augmented spacecraft state (position, velocity, mass, and costates)
$\mathbf{x}$	perturbation of true state from nominal state
y	position
$\mathbf{Z}$	spacecraft state in orbital elements
α	adjoint control parameter
β	flyby angle
γ	adjoint control parameter

$\boldsymbol{\Gamma}$	thrust acceleration vector
δ_{fb}	flyby turn angle
δ	time free variation
$\tilde{\delta}$	time fixed variation
Δv_{pow}	impulsive velocity change made by the engine at periapse of the hyperbolic flyby
$\Delta \mathbf{v}$	impulsive velocity change
ζ	relaxation parameter
κ	parameter that affects spacecraft state
λ_J	spacecraft thrust acceleration costate
λ_m	spacecraft mass costate
$\boldsymbol{\lambda}_\mathbf{r}$	spacecraft position costate
$\boldsymbol{\lambda}_\mathbf{v}$	spacecraft velocity costate
$\lambda_{v_{fb-}}^{\perp}$	component of velocity costate at t_{fb-} that is perpendicular to $v_{\infty i}$
$\lambda_{v_{fb+}}^{\perp}$	component of velocity costate at t_{fb+} that is perpendicular to $v_{\infty o}$
$\lambda_{v_{fb-}}^{\parallel}$	component of velocity costate at t_{fb-} that is parallel to $v_{\infty i}$
$\lambda_{v_{fb+}}^{\parallel}$	component of velocity costate at t_{fb+} that is parallel to $v_{\infty o}$
μ_{fb}	gravitational parameter of gravity assist planet
υ	Lagrange multiplier
$\boldsymbol{\xi}$	Lagrange multiplier
$\boldsymbol{\rho}$	Lagrange multiplier
$\boldsymbol{\sigma}$	Lagrange multiplier

$\mathbf{\Phi}$	state transition matrix for spacecraft state described by $\mathbf{X}$
$\mathbf{\Phi}_{\alpha}$	state transition matrix with orbital elements

Subscripts

-	immediately before
+	immediately after
0	initial
A0	immediately after a flyby that occurs at t_{fb}
B0	at t_{fb} where no flyby occurs at t_{fb}
B1	immediately before a flyby that occurs at $t_{fb}+\Delta t_{fb}$
C0	state spacecraft must have at t_{fb} in order to pass through $\mathbf{X}_{C1}$
C1	immediately after a flyby that occurs at $t_{fb}+\Delta t_{fb}$
f	final
fb	flyby
i	inbound
max	maximum
min	minimum
o	outbound
p	flyby planet
s	switching
t	target planet

Superscripts

*	nominal
-	perturbed backward
+	perturbed forward
&	denotes a partial derivative mapped to a common time

Introduction

Most techniques to determine optimal low-thrust spacecraft trajectories require derivatives of the cost and/or constraint functions with respect to the free parameters. Usually these derivatives are calculated using finite differences because of the ease of calculating them. Some researchers have used the state transition matrix to calculate derivatives in a limited class of problems (impulsive maneuvers). D'Amario et. al.[23] and Sauer[24] used the state transition matrix to calculate partial derivatives that are used to optimize an impulsive $\Delta\mathbf{v}$ multiple flyby trajectory. Mirfakhraie and Conway[25] used the state transition matrix to calculate the necessary derivatives for a cooperative time-fixed impulsive rendezvous. The state transition matrix in these previous studies only applied to the position and velocity of the spacecraft. Ocampo and Rosborough[26] used the state transition matrix applied to the full spacecraft state and costates to find optimal finite duration thrust trajectories. This appendix will present a method to use the state transition matrix applied to the full spacecraft state and costates to find optimal trajectories where the spacecraft state is discontinuous. This section also presents a method for calculating the necessary derivatives for a constant specific impulse (CSI)

gravity assist trajectory using the state transition matrix where both the spacecraft state and the spacecraft equations of motion may be discontinuous during the trajectory.

The optimization process in this section will be accomplished using two different methods in order to show that the state transition matrix derivatives work in both cases. The first method is an indirect method where calculus of variations is used to derive the optimality conditions resulting in a two-point boundary-value problem (TPBVP). The second method is a hybrid method that uses a continuous control and searches for optimal values of the initial costates. The kinematic boundary conditions are satisfied through the use of equality constraints, and the transversality conditions are satisfied by minimizing the cost function using a sequential quadratic programming code. These methods both require the derivatives of the cost and constraint functions with respect to all of the free parameters. The accuracy with which the optimal trajectory can be found depends on the accuracy of these derivatives. The derivatives calculated using the state transition matrix will be shown to be exact to the accuracy of the integrator used to propagate the equations of motion and the state transition matrix. Optimal transfers from the Earth to Saturn with intermediate patched-conic gravity assists are used to demonstrate the benefits of this method compared to the use of finite difference derivatives.

Finite Difference Partial Derivatives

The fundamental definition of the derivative of the state at time t_1 with respect to a parameter κ that affects the state at t_0 is given by Eq. (A.1) where the definitions of $\mathbf{X}^+$ and $\mathbf{X}^-$ are given in Figure A.1. Alternate methods of computing this derivative are necessary because, in general, the solution to Eq. (A.1) is unknown. One way to

calculate partial derivatives in a trajectory optimization algorithm is to use a finite difference method. Eq. (A.2) provides a first- and second-order method to calculate the finite difference derivatives of the state at time t_1 with respect to a parameter, κ, that affects the state at t_0.

$$\frac{\partial \mathbf{X}(t_1)}{\partial \kappa} = \lim_{\Delta\kappa \to 0} \frac{\mathbf{X}^+(t_1) - \mathbf{X}(t_1)}{\Delta\kappa} \tag{A.1}$$

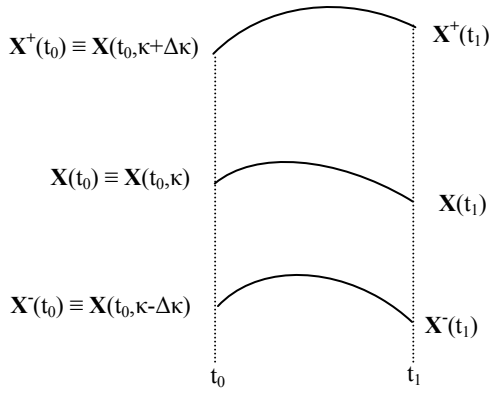

Figure A.1 Finite Difference Derivatives

$$\begin{aligned}
\frac{\partial \mathbf{X}(t_1)}{\partial \kappa} &= \frac{\left(\mathbf{X}^+(t_0, \kappa + \Delta\kappa) + \int_{t_0}^{t_1} \dot{\mathbf{X}}(\mathbf{X}^+(t), t)dt\right) - \left(\mathbf{X}(t_0, \kappa) + \int_{t_0}^{t_1} \dot{\mathbf{X}}(\mathbf{X}(t), t)dt\right)}{\Delta\kappa} \\
\frac{\partial \mathbf{X}(t_1)}{\partial \kappa} &= \frac{\left(\mathbf{X}^+(t_0, \kappa + \Delta\kappa) + \int_{t_0}^{t_1} \dot{\mathbf{X}}(\mathbf{X}^+(t), t)dt\right) - \left(\mathbf{X}^-(t_0, \kappa - \Delta\kappa) + \int_{t_0}^{t_1} \dot{\mathbf{X}}(\mathbf{X}^-(t), t)dt\right)}{2\Delta\kappa}
\end{aligned} \tag{A.2}$$

Error will be introduced into the derivative because, in general, $\mathbf{X}(t_1)$ will be corrupted by error associated with numerically integrating $\mathbf{X}$ from t_0 to t_1. In addition to

this error source, the choice of $\Delta\kappa$ will introduce error as well. If $\Delta\kappa$ is too large, truncation error will be large; if $\Delta\kappa$ is too small, the derivatives will be corrupted by round-off error. If the proper perturbation size is used, a good estimate of the accuracy of a derivative of a function with respect to a parameter is one half the accurate digits to which the function is known[27]. For this case it would be one half of the accurate digits to which $\mathbf{X}(t_1)$ could be determined. Attempts to find the optimal perturbation size are complicated by the fact that the optimal value for the perturbation will be different not only for each derivative but for each derivative on each iteration. It is important to compute each derivative accurately because the convergence of any parameter optimization algorithm will be limited by the accuracy of the worst derivative[28].

Partial Derivatives with the State Transition Matrix

The state transition matrix, which can be determined from Eqs. (A.3) and (A.4), provides an alternative method to calculate partial derivatives. It is a tool that maps the first order perturbations in the complete augmented spacecraft state (including costates) from one time to another without any error if the state transition matrix can be computed analytically. In general, the state transition matrix must be determined through numerical integration which will introduce error into the mapping of these first order perturbations. The state transition matrix can only map perturbations between two times where the spacecraft state and spacecraft equations of motion are continuous. Figure A.2 shows a mapping of a perturbation at time t_0 to the time t_1. The perturbed trajectory is defined to have initial condition $\mathbf{X}^+(t_0) = \mathbf{X}(t_0, \kappa+\Delta\kappa)$, and the nominal trajectory is defined to have initial condition $\mathbf{X}^*(t_0) = \mathbf{X}(t_0, \kappa)$. Because the derivative of $\mathbf{X}(t_0)$ with respect to κ is

known, one can write Eq. (A.5) using a Taylor series. Using the state transition matrix, the value of the perturbation at time t_1 can then be written as in Eq. (A.6). Eq. (A.7) is written from Eq. (A.6) and the fundamental definition of a derivative expressed in Eq. (A.1). Eq. (A.7) requires the equations of motion and the spacecraft state to be continuous between t_0 and t_1 and the partial derivative of the spacecraft state at t_0 with respect to κ to be known analytically.

$$\dot{\mathbf{\Phi}}(t,t_0) = \frac{\partial \dot{\mathbf{X}}}{\partial \mathbf{X}} \mathbf{\Phi}(t,t_0) \tag{A.3}$$

$$\mathbf{\Phi}(t_0,t_0) = \mathbf{I} \tag{A.4}$$

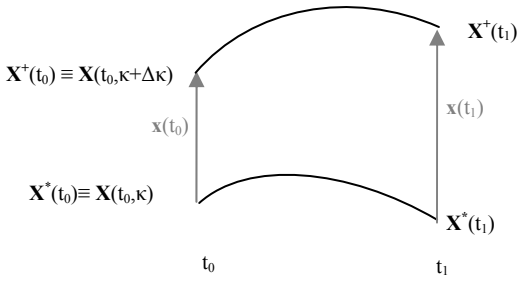

Figure A.2 State Transition Matrix Derivative Mappings

$$\mathbf{X}^{+}(t_0) - \mathbf{X}^{*}(t_0) \equiv \mathbf{x}(t_0) = \Delta\kappa \frac{\partial \mathbf{X}(t_0)}{\partial \kappa} + O(\Delta\kappa^2) \tag{A.5}$$

$$\mathbf{X}^{+}(t_1) - \mathbf{X}^{*}(t_1) \equiv \mathbf{x}(t_1) = \mathbf{\Phi}(t_1,t_0) \frac{\partial \mathbf{X}(t_0)}{\partial \kappa} \Delta\kappa + O\left(\Delta\kappa^2\right) \tag{A.6}$$

$$\frac{\partial \mathbf{X}(t_1)}{\partial \kappa} = \mathbf{\Phi}(t_1,t_0) \frac{\partial \mathbf{X}(t_0)}{\partial \kappa} \tag{A.7}$$

In general, these state transition matrix derivatives will not be exact because the state transition matrix will be numerically integrated, but these derivatives will be more accurate than the finite difference derivatives. Truncation and round-off error from $\Delta\kappa$ will not be introduced into the derivatives using this method because the derivatives are taken in the limit as $\Delta\kappa$ goes to zero and no difference is computed as in the finite difference case.

Discontinuities in the Spacecraft State

Eq. (A.7) can be used to determine the derivative of the spacecraft state just before a discontinuity in the state with respect to a parameter, κ, that affects the spacecraft state at an earlier time. The partial derivative of the spacecraft state and costate after the discontinuity with respect to the spacecraft state before the discontinuity must be known analytically so that the chain rule can be used to compute the derivative of the spacecraft state after the discontinuity with respect to κ. Using the chain rule and Eq. (A.7) allows the computation of the partial derivative of the spacecraft state at any time with respect to a parameter κ that affects the spacecraft state at any other time. For example, if κ affects the spacecraft state at t_3 and the spacecraft state is discontinuous at t_4, then the derivative of the spacecraft state at t_5 with respect to κ is determined from Eq. (A.8). Eq. (A.8) is valid only if the equations of motion are continuous between t_3 and t_{4-} and between t_{4+} and t_5, and the partial derivative of the spacecraft state at t_{4+} with respect to the state at t_{4-} is known analytically. Eq. (A.8) is valid for any discontinuity where the partial derivative of the state after the discontinuity with respect to the state before the discontinuity is known.

$$\frac{\partial \mathbf{X}(t_5)}{\partial \kappa} = \mathbf{\Phi}(t_5, t_{4+}) \frac{\partial \mathbf{X}(t_{4+})}{\partial \mathbf{X}(t_{4-})} \mathbf{\Phi}(t_{4-}, t_3) \frac{\partial \mathbf{X}(t_3)}{\partial \kappa} \tag{A.8}$$

Eq. (A.8) and the chain rule can be used to determine the partial derivative of any cost or constraint function, C, that is a function of only the state at a particular time and the time. The derivative provided in Eq. (A.9) is accurate to the accuracy of the integrator used to integrate the equations of motion of the state vector and the state transition matrix.

$$\frac{\partial C(\mathbf{X}(t), t)}{\partial \kappa} = \left(\frac{\partial C}{\partial \mathbf{X}} \right)_{\mathbf{X}=\mathbf{X}^*(t)} \frac{\partial \mathbf{X}(t)}{\partial \kappa} \tag{A.9}$$

Partial Derivatives with Respect to Time Parameters

If the parameter with which the partial derivatives is desired is the time of a state discontinuity or the initial time, a slightly different method must be used because the state transition matrix can map only perturbations that occur at a common time. Although the example used to illustrate this state discontinuity is a patched conic gravity assist (See Appendix C), a similar analysis will apply to any state discontinuity. In order to use this method, one must determine the value of the state at t_{fb+} if the flyby occurs at the nominal value of t_{fb} and what the value of the spacecraft state would be at t_{fb+} if the flyby occurs at $t_{fb}+\Delta t_{fb}$ in the limit as Δt_{fb} goes to zero. Note that t_{fb+} is the time immediately following a patched conic flyby on the nominal trajectory. The value of this difference is used in Eq. (A.10) to determine the partial derivative $\left[\partial / \partial t_{fb}(\mathbf{X}(t_{fb}))\right]_{\&}$ mapped to the common time, t_{fb}. In Figure A.3, subscript 0 denotes t_{fb} and subscript 1 denotes $t_{fb}+\Delta t_{fb}$. $\mathbf{X}_{A0}$ is the nominal value of the spacecraft state after a flyby occurring at t_{fb}. $\mathbf{X}_B$ denotes the path

the spacecraft would traverse if the flyby did not occur until $t_{fb}+\Delta t_{fb}$. $\mathbf{X}_{C1}$ is what the spacecraft state would be immediately after a flyby if the flyby occurred at $t_{fb}+\Delta t_{fb}$. $\mathbf{X}_{C0}$ is the value the spacecraft state would have at t_{fb} if the spacecraft state equations of motion were integrated backward in time from $\mathbf{X}_{C1}$ at $t_{fb}+\Delta t_{fb}$ to t_{fb}.

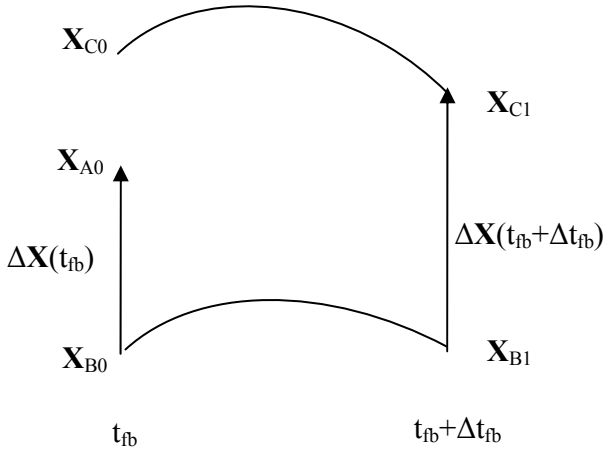

Figure A.3 Derivatives with Respect to Time

$$\left(\frac{\partial \mathbf{X}(t_{fb})}{\partial t_{fb}}\right)_{\&} = \lim_{\Delta t_{fb}\to 0} \frac{\mathbf{X}_{C0} - \mathbf{X}_{A0}}{\Delta t_{fb}} \tag{A.10}$$

The spacecraft position and the cost function are continuous across a flyby and the velocity of the spacecraft is changed only by the $\Delta\mathbf{v}$ from the flyby which is a function of the time of the flyby because the velocity of the planet providing the gravity assist varies with time.

$$\mathbf{r}_{B0} = \mathbf{r}_{A0} \tag{A.11}$$

$$\mathbf{v}_{B0} = \mathbf{v}_{A0} - \Delta\mathbf{v}(t_{fb}) \tag{A.12}$$

$$J_{B0} = J_{A0} \tag{A.13}$$

Using a Taylor series expansion about the time of the flyby, $\mathbf{X}_{B1}$ can be written as

$$\mathbf{X}_{B1} = \mathbf{X}_{B0} + \dot{\mathbf{X}}_{B0}\Delta t_{fb} + O(\Delta t_{fb}{}^2) \tag{A.14}$$

By definition,

$$\mathbf{r}_{C1} = \mathbf{r}_{B1} \tag{A.15}$$

$$\mathbf{v}_{C1} = \mathbf{v}_{B1} + \Delta\mathbf{v}(t_{fb}+\Delta t_{fb}) \tag{A.16}$$

$$J_{C1} = J_{B1} \tag{A.17}$$

Again using a Taylor series expansion,

$$\Delta\mathbf{v}(t_{fb}+\Delta t_{fb})=\Delta\mathbf{v}(t_{fb}) + \frac{d\,\Delta\mathbf{v}(t_{fb})}{dt}\Delta t_{fb} + O(\Delta t_{fb}{}^2) \tag{A.18}$$

It is noted that $\boldsymbol{\lambda}$ is discontinuous across the flyby with the parameters α, γ, $\dot{\alpha}$, $\dot{\gamma}$, $\lambda_v(t_{fb+})$, and $\dot{\lambda}_v(t_{fb+})$ held fixed in the computation of the partial derivative because they are not a function of the time of the flyby. See Appendix B for an explanation of the adjoint control transformation that utilizes these parameters. As a result, using another Taylor series expansion, this time about the position and velocity of the spacecraft on the nominal trajectory at the time of the flyby, one obtains the value of the costates in Eq. (A.19). Note that the higher-order terms in Eqs. (A.19) and (A.20) are $O(\Delta t_{fb}{}^2)$ because $\mathbf{X}_{C1}$ - $\mathbf{X}_{A0}$ is $O(\Delta t_{fb})$. The partial derivatives in Eqs. (A.19), (A.20), and (A.25) are evaluated at $\mathbf{X}=\mathbf{X}_{A0}$.

$$\boldsymbol{\lambda}_{C1} = \boldsymbol{\lambda}_{A0} + \left(\frac{\partial\boldsymbol{\lambda}}{\partial\mathbf{r}}\right)_{\mathbf{X}=\mathbf{X}_{A0}}(\mathbf{r}_{C1}-\mathbf{r}_{A0}) + \left(\frac{\partial\boldsymbol{\lambda}}{\partial\mathbf{v}}\right)_{\mathbf{X}=\mathbf{X}_{A0}}(\mathbf{v}_{C1}-\mathbf{v}_{A0}) + O(\Delta t_{fb}{}^2) \tag{A.19}$$

$$\dot{\mathbf{X}}_{C1} = \dot{\mathbf{X}}_{A0} + \left(\frac{\partial\dot{\mathbf{X}}}{\partial\mathbf{X}}\right)_{\mathbf{X}=\mathbf{X}_{A0}}(\mathbf{X}_{C1}-\mathbf{X}_{A0}) + O(\Delta t_{fb}{}^2) \tag{A.20}$$

$$\mathbf{X}_{C0} = \mathbf{X}_{C1} - \dot{\mathbf{X}}_{C1}\Delta t_{fb} + O(\Delta t_{fb}{}^2) \tag{A.21}$$

Eqs. (A.11) to (A.21) can be used to determine $\mathbf{X}_{C0,}$

$$\mathbf{r}_{C0} = \mathbf{r}_{A0} + O(\Delta t_{fb}{}^2) \tag{A.22}$$

$$\mathbf{v}_{C0} = \mathbf{v}_{A0} + (\frac{d\,\Delta\mathbf{v}(t_{fb})}{dt} + \dot{\mathbf{v}}_{B0} - \dot{\mathbf{v}}_{A0})\Delta t_{fb} + O(\Delta t_{fb}{}^2) \tag{A.23}$$

$$J_{C0} = J_{A0} - \dot{J}_{A0}\Delta t_{fb} + O(\Delta t_{fb}{}^2) \tag{A.24}$$

$$\boldsymbol{\lambda}_{C0} = \boldsymbol{\lambda}_{A0} + \left[\left(\frac{\partial \boldsymbol{\lambda}}{\partial \mathbf{r}}\right)_{\mathbf{X}=\mathbf{X}_{A0}} \mathbf{v}_{B0} + \left(\frac{\partial \boldsymbol{\lambda}}{\partial \mathbf{v}}\right)_{\mathbf{X}=\mathbf{X}_{A0}} \dot{\mathbf{v}}_{B0} - \dot{\boldsymbol{\lambda}}_{A0}\right]\Delta t_{fb} + O(\Delta t_{fb}{}^2) \tag{A.25}$$

Combining Eqs. (A.10) and (A.22) with (A.25) yields the partial derivative mapped to the time of the flyby. These partial derivatives in Eq. (A.26) can be used to compute the partial derivative of the state at any time with respect to the time of the flyby by using Eq. (A.8). Note that Eq. (A.26) should only be used if the state transition matrix will be used to map the derivative from the time of the flyby to a future common time. For example, Eq. (A.27) could be used to calculate the derivative of the spacecraft state at the final time with respect to the time of the flyby. If the partial derivative of the spacecraft state at the time of the flyby with respect to the time of the flyby is desired, one can use the normal method of calculating a partial derivative and obtain Eq. (A.28). The method to obtain the partial derivative of the state with respect to the initial time can be computed in the same way.

$$\left(\frac{\partial \mathbf{X}(t_{fb+})}{\partial t_{fb}}\right)_{\&} = \begin{pmatrix} \mathbf{0} \\ \frac{d\,\Delta\mathbf{v}(t_{fb})}{dt} + \dot{\mathbf{v}}_{B0} - \dot{\mathbf{v}}_{A0} \\ \dot{\mathbf{J}}_{B0} - \dot{\mathbf{J}}_{A0} \\ \left(\frac{\partial \boldsymbol{\lambda}_{\mathbf{r}}}{\partial \mathbf{r}}\right)_{\mathbf{X}=\mathbf{X}_{A0}} \mathbf{v}_{B0} + \left(\frac{\partial \boldsymbol{\lambda}_{\mathbf{r}}}{\partial \mathbf{v}}\right)_{\mathbf{X}=\mathbf{X}_{A0}} \dot{\mathbf{v}}_{B0} - \dot{\boldsymbol{\lambda}}_{\mathbf{r}_{A0}} \\ \left(\frac{\partial \boldsymbol{\lambda}_{\mathbf{v}}}{\partial \mathbf{r}}\right)_{\mathbf{X}=\mathbf{X}_{A0}} \mathbf{v}_{B0} + \left(\frac{\partial \boldsymbol{\lambda}_{\mathbf{v}}}{\partial \mathbf{v}}\right)_{\mathbf{X}=\mathbf{X}_{A0}} \dot{\mathbf{v}}_{B0} - \dot{\boldsymbol{\lambda}}_{\mathbf{v}_{A0}} \\ 0 \end{pmatrix} \tag{A.26}$$

$$\frac{\partial \mathbf{X}(t_f)}{\partial t_{fb}} = \boldsymbol{\Phi}(t_f, t_{fb+}) \left(\frac{\partial \mathbf{X}(t_{fb+})}{\partial t_{fb}}\right)_{\&} \tag{A.27}$$

$$\frac{\partial \mathbf{X}(t_{fb})}{\partial t_{fb}} = \lim_{\Delta t_{fb} \to 0} \frac{\mathbf{X}_{C1} - \mathbf{X}_{A0}}{\Delta t_{fb}} = \begin{pmatrix} \mathbf{v}_{B0} \\ \frac{d\,\Delta\mathbf{v}(t_{fb})}{dt} + \dot{\mathbf{v}}_{B0} \\ \dot{\mathbf{J}}_{B0} \\ \left(\frac{\partial \boldsymbol{\lambda}_{\mathbf{r}}}{\partial \mathbf{r}}\right)_{\mathbf{X}=\mathbf{X}_{A0}} \mathbf{v}_{B0} + \left(\frac{\partial \boldsymbol{\lambda}_{\mathbf{r}}}{\partial \mathbf{v}}\right)_{\mathbf{X}=\mathbf{X}_{A0}} \dot{\mathbf{v}}_{B0} \\ \left(\frac{\partial \boldsymbol{\lambda}_{\mathbf{v}}}{\partial \mathbf{r}}\right)_{\mathbf{X}=\mathbf{X}_{A0}} \mathbf{v}_{B0} + \left(\frac{\partial \boldsymbol{\lambda}_{\mathbf{v}}}{\partial \mathbf{v}}\right)_{\mathbf{X}=\mathbf{X}_{A0}} \dot{\mathbf{v}}_{B0} \\ 0 \end{pmatrix} \tag{A.28}$$

Discontinuities in the Equations of Motion

If there are discontinuities in the equations of motion, modifications must be made to the state transition matrix in order to map the first order perturbations in the state. In order to use this method, the discontinuities in the equations of motion must be finite in number and based on the sign of a switching function that is a function of the spacecraft state and possibly the time. Again, the nominal trajectory is defined to have initial condition $\mathbf{X}^*(t_0) = \mathbf{X}(t_0, \kappa)$, and the perturbed trajectory has initial condition $\mathbf{X}^+(t_0)$

= $\mathbf{X}(t_0, \kappa+\Delta\kappa)$. The equations of motion on the nominal trajectory are discontinuous when the switching function, S(X), goes through zero at time t_s^*, and the equations of motion on the perturbed trajectory are discontinuous at time t_s as seen in Figure A.4. The equations of motion on the perturbed and nominal trajectories are not discontinuous at the same time because the perturbation will cause the switching function to change sign at a slightly different time as shown in Figure A.5. This time difference is exaggerated significantly in Figures A.4 and A.5.

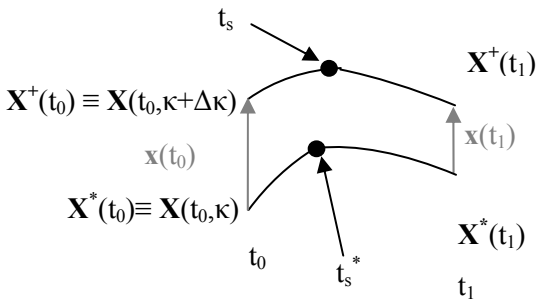

Figure A.4 State Transition Matrix Derivative Mappings

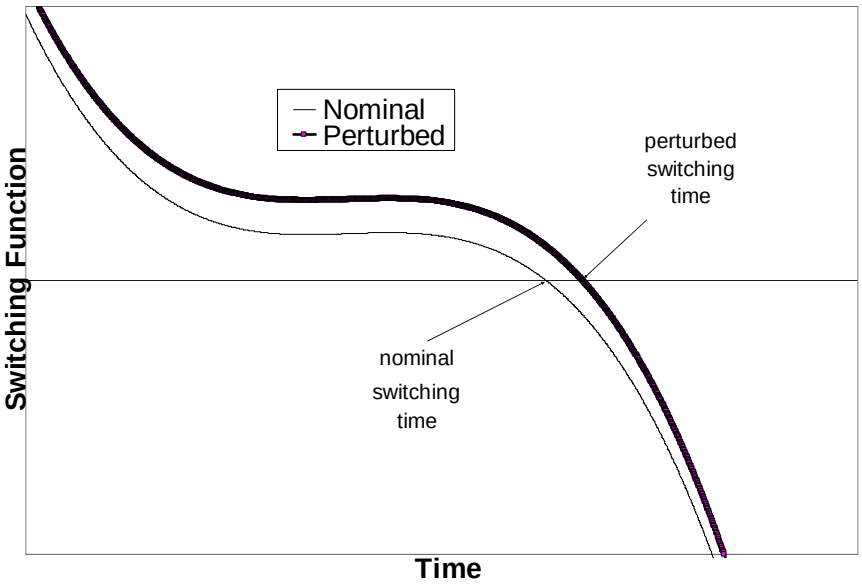

Figure A.5 Change in Switching Time

The time-fixed perturbation in the switching function value at the nominal switching time is the difference between the value of the switching function on the perturbed solution and the value of the switching function on the nominal trajectory at the nominal switching time. The time fixed perturbation can be calculated exactly by using Eq. (A.29). In Eq. (A.29), $\Delta\kappa$ is the perturbation to the parameter, κ. Multiplying $\Delta\kappa$ by the partial derivative of the initial state with respect to κ yields the perturbation in the initial state due to the change in κ. The state transition matrix between the initial time and just before the switching time maps the perturbation in the state to the nominal switching time. Since the switching function depends only on the state and the time, and this is the time-fixed perturbation, multiplying by the derivative of the switching function with respect to the spacecraft state yields the perturbation in the switching function due to the perturbation in κ.

$$\tilde{\delta}S = \frac{\partial S}{\partial \mathbf{X}} \mathbf{\Phi}(t_{s-}, t_0) \frac{\partial \mathbf{X}(t_0)}{\partial \kappa} \Delta\kappa \tag{A.29}$$

The fact that the switching function must equal zero when the equations of motion are discontinuous on the perturbed trajectory requires that the time free perturbation in the switching function must be zero. The time free perturbation in the switching function is the time fixed perturbation in the switching function given by Eq. (A.29) plus the derivative of the switching function with respect to time multiplied by the perturbation in the switching time given by Eq. (A.30). Eq. (A.30) allows one to determine the first-order change in the switching time because of the perturbation introduced in the state by the change in κ. The change in the switching time is proportional to Δκ.

$$\delta S = \tilde{\delta} S + \left(\frac{\partial S}{\partial \mathbf{X}} \dot{\mathbf{X}}(t_{s-}) + \frac{\partial S}{\partial t} \right) \delta t_s = 0 \tag{A.30}$$

In order to determine the derivative of the spacecraft state immediately after the nominal switching time with respect to the parameter κ, one must determine both the derivative of the spacecraft immediately before the switching time with respect to κ as well as the change in the spacecraft state because the switching time changes. The first portion of Eq. (A.31) accounts for the change in the state at t_s that occurs because of the change in the initial state caused by varying κ. The second portion of Eq. (A.31) accounts for the change that occurs because varying κ changes the time where the equations of motion switch. The derivatives in Eqs. (A.31) and (A.32) are mapped to a common time which is necessary in order to use state transition matrix derivatives. Eq.

(A.32) demonstrates how to map this forward to a time when the derivative of the spacecraft state with respect to κ is desired.

$$\left(\frac{\partial \mathbf{X}(t_{s+})}{\partial \kappa}\right)_{\&} = \mathbf{\Phi}(t_{s-},t_0)\frac{\partial \mathbf{X}(t_0)}{\partial \kappa} + \frac{\left(\dot{\mathbf{X}}(t_{s-}) - \dot{\mathbf{X}}(t_{s+})\right)\delta t_s}{\Delta \kappa} \tag{A.31}$$

$$\frac{\partial \mathbf{X}(t_1)}{\partial \kappa} = \mathbf{\Phi}(t_1,t_{s+})\left(\frac{\partial \mathbf{X}(t_{s+})}{\partial \kappa}\right)_{\&} \tag{A.32}$$

Analytic Solution for Discontinuous Equations of Motion

In order to verify the results of the previous section, consider a system that begins at t_0=0 with the initial conditions and equations of motion defined in Eq. (A.33). The final time, t_f, is specified to be 3. For this problem, $\ddot{y}$ will instantaneously change from +20 to -20 at t=2. The partial derivatives of the final state with respect to the initial state are desired. They can be determined analytically using an expansion about the nominal as shown in Eq. (A.34).

$$\begin{aligned} y(0) &= 0 \\ \dot{y}(0) &= 0 \end{aligned} \qquad \ddot{y} = \begin{cases} -20 \text{ if } y > 40 \\ 20 \text{ if } y <= 40 \end{cases} \tag{A.33}$$

$$\begin{aligned} \frac{\partial y_f}{\partial y_0} &= 0 \\ \frac{\partial y_f}{\partial \dot{y}_0} &= 1 \\ \frac{\partial \dot{y}_f}{\partial y_0} &= -1 \\ \frac{\partial \dot{y}_f}{\partial \dot{y}_0} &= -1 \end{aligned} \tag{A.34}$$

The state transition matrix for this problem can be determined analytically from t_0 until t=2 and from t=2 until t=3.

$$\begin{aligned}\boldsymbol{\Phi}(2,0) &= \begin{pmatrix} 1 & 2 \\ 0 & 1 \end{pmatrix} \\ \boldsymbol{\Phi}(3,2) &= \begin{pmatrix} 1 & 1 \\ 0 & 1 \end{pmatrix}\end{aligned} \tag{A.35}$$

Using these analytic values for the state transition matrix and Eqs. (A.29) and (A.30), the change in the switching time, δt, when y_0 is increased by $\Delta\kappa$ is $-\Delta\kappa/40$. Similarly, δt when $\dot{y}_0$ is increased by $\Delta\kappa$ is $-\Delta\kappa/20$. Using this information in Eq. (A.32) yields the same values for the partial derivatives as Eq. (A.34). Because the state transition matrix could be integrated analytically, there is no approximation in the derivatives computed using the state transition matrix method. If the state transition matrix could not be integrated analytically, numerical integration errors would be introduced into the solution.

Example Transfers Employing State Transition Matrix Derivatives

A series of example problems is used to demonstrate the benefits of state transition matrix derivatives. The first transfer is an impulsive $\Delta\mathbf{v}$ gravity assist trajectory that shows the benefits of state transition derivatives for impulsive transfers with discontinuities in the state. The next example is a transfer employing a variable specific impulse engine that demonstrates the advantage of using these derivatives for finite thrust transfers with state discontinuities. In both of these examples, the state transition matrix derivatives are able to satisfy the trajectory constraints to orders of magnitude greater

accuracy than the central difference derivatives. The state transition matrix method also requires less computational time to find an optimal trajectory.

The third example is a CSI trajectory that includes a patched conic gravity assist which is optimized using the indirect method. In this third example, both the spacecraft state and the spacecraft equations of motion are discontinuous. The discontinuities in the spacecraft state are caused by gravity assists, and the discontinuities in the equations of motion are caused by the spacecraft thrust being discontinuous. Because the spacecraft equations of motion and state transition matrix must be integrated numerically, no analytic value for the gradients is available. Both the finite difference derivatives and the analytic derivatives are used to find an optimal interplanetary gravity assist trajectory. A comparison is made on the robustness of convergence to an optimal solution using both methods and the same initial guess for the free parameters. The final example problem is a CSI trajectory that is optimized using the hybrid method. Again, the equations of motion are discontinuous and no analytical derivatives are available. Consequently, the finite difference derivatives and state transition matrix method derivatives are both used to find an optimal trajectory. In this example, state transition matrix derivatives converge to the optimal trajectory which has a different thrusting structure than the initial guess while the central difference derivatives do not converge to the optimal trajectory.

Impulsive ΔV Model

For the impulsive $\Delta\mathbf{v}$ model, the trajectory begins with the spacecraft on an Earth escape trajectory with a hyperbolic excess velocity vector. The magnitude and direction of this hyperbolic excess velocity are free parameters which are optimized. The

spacecraft then coasts until the time of the first flyby which is modeled as an instantaneous velocity change as discussed in Appendix C. An impulsive Δv may be made parallel to the velocity of the spacecraft with respect to the flyby planet at periapse of the flyby. After the first flyby, the spacecraft coasts until it makes an impulsive post-flyby $\Delta\mathbf{v}$ maneuver and then coasts until it makes its next flyby. The spacecraft can repeat the previous step for any number of gravity assists. Following its final flyby, the spacecraft coasts until it makes a final impulsive $\Delta\mathbf{v}$ maneuver after which it coasts until the final time when it must intercept the target. The number of gravity assists and the planet providing each gravity assist must be determined a priori. This method determines only a locally optimal trajectory for a given sequence of gravity assists. The free parameters for this case are the initial time, final time, flyby times, post-flyby maneuver times, flyby radii, flyby angles, magnitude and direction of the initial hyperbolic excess velocity, magnitude and direction of each impulsive $\Delta\mathbf{v}$, and magnitude of the impulsive Δv provided by the engine at periapse of each flyby. The cost is the sum of the impulsive Δvs plus the initial hyperbolic excess velocity. The constraints require the spacecraft to have the same position as the planet providing each gravity assist at the time of the gravity assist. The spacecraft must also intercept the target planet at the final time.

The spacecraft state is numerically integrated using DLSODE[29] on each trajectory segment. DLSODE uses predictor-corrector methods for nonstiff ordinary differential equations and backward-differentiation formula methods for stiff differential equations. The JPL DE405[30] ephemerides are used to determine the position of the Sun and the planets. The gravity model used to propagate the equations of motion treats the Sun as the center of an inertial frame and the only gravitational body that affects the motion of

the spacecraft except for the zero sphere of influence patched conic $\Delta\mathbf{v}$s which are obtained from the gravity assists.

Impulsive ΔV Model Example

It is desired to compute the minimum fuel trajectory from Earth to Saturn using three Venus gravity assists and the impulsive $\Delta\mathbf{v}$ model. The optimal trajectory is shown in Figure A.8. There are 12 equality constraints requiring the spacecraft to intercept Venus at the time of each flyby and Saturn at the final time and three inequality constraints requiring the flyby periapse to be greater than or equal to 6,400 kilometers for each of the gravity assist maneuvers. The partial derivatives (a total of 377) of the cost and equality constraints with respect to each of the 29 free parameters are needed in order to determine the optimal values of these parameters. The derivatives of the inequality constraints with respect to the free parameters are trivial and can be calculated analytically.

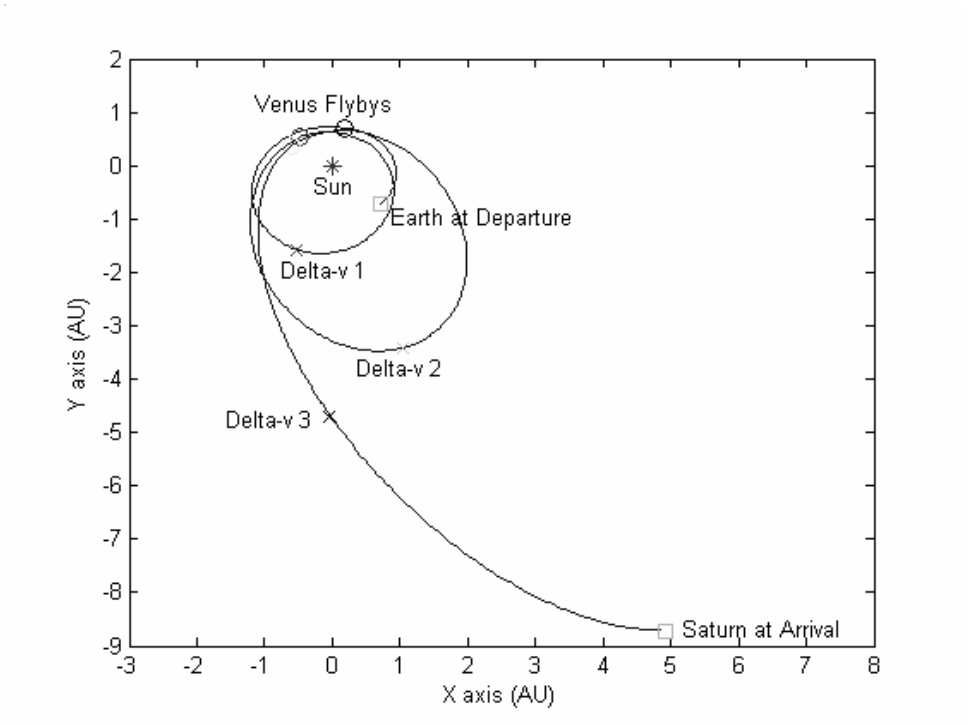

Figure A.8 Impulsive Δv Earth-Venus-Venus-Venus-Saturn Trajectory

Table A.1 provides a sample of the partial derivatives of the constraints with respect to the free parameters. The analytic solution is obtained by propagating the orbit using Kepler's equation. The state transition matrix for the orbital elements of a spacecraft in a central body force field is available analytically from Eq. (A.36). The analytic state transition matrix for the spacecraft state can be obtained from Eq. (A.37) where **Z** is the spacecraft state in orbital elements. CD^{*} are central difference derivatives with a perturbation of 10^{-4}; FD^{**} are forward difference derivatives with a perturbation of 10^{-6}; CD^{***} are central difference derivatives calculated using the optimal perturbation size given by Hull.[28] The state transition matrix derivatives agree with the analytic derivatives to at least six digits while the derivatives obtained using the optimal

perturbation step agree only to at least four digits. The central difference and forward difference derivatives calculated using a perturbation step size of 10^{-4} and 10^{-6} respectively do not all agree with the analytic solution to more than one significant figure. As a result, one must tune the step sizes using either Hull's method or another technique in order to use finite difference derivatives. The state transition matrix derivatives do not require any tuning.

$$\mathbf{\Phi}_{\alpha}(t,t_0) = \begin{pmatrix} 1 & 0 & 0 & 0 & 0 & 0 \\ 0 & 1 & 0 & 0 & 0 & 0 \\ 0 & 0 & 1 & 0 & 0 & 0 \\ 0 & 0 & 0 & 1 & 0 & 0 \\ 0 & 0 & 0 & 0 & 1 & 0 \\ -\dfrac{3\sqrt{\mu}(t-t_0)}{2a^{2.5}} & 0 & 0 & 0 & 0 & 1 \end{pmatrix} \tag{A.36}$$

$$\mathbf{\Phi}(t,t_0) = \frac{\partial \mathbf{X}(t)}{\partial \mathbf{Z}(t)} \mathbf{\Phi}_{\alpha}(t,t_0) \frac{\partial \mathbf{Z}(t_0)}{\partial \mathbf{X}(t_0)} \tag{A.37}$$

Table A.1 Accuracy Of State Transition Matrix and Finite Difference Partial Derivatives For The Impulsive Transfer

	$\frac{\partial y_f}{\partial \alpha_{pfb1}}$ (AU)	$\frac{\partial x_{fb3}}{\partial r_{m1}}$ (AU/km)	$\frac{\partial x_f}{\partial r_{m1}}$ (AU/km)	$\frac{\partial x_{fb1}}{\partial \Delta v_0}$ (Days)	$\frac{\partial y_f}{\partial \Delta v_0}$ (Days)
Analytic Solution	14.01651	$-1.248655*10^{-3}$	$1.11043871*10^{-2}$	-187.41078837	11746.297
STM	14.01649	$-1.248648*10^{-3}$	$1.11043892*10^{-2}$	-187.41078844	11746.305
STM Accurate Digits	6	6	7	10	6
CD*	14.01839	$-1.243751*10^{-3}$	$1.103744*10^{-2}$	-187.4135	4738.943
CD* Accurate Digits	4	3	2	5	0
FD**	14.01537	$-1.137700*10^{-3}$	$8.662536*10^{-3}$	-187.4205	5186.494
FD Accurate Digits**	4	1	1	4	1
CD***	14.01846	$-1.248639*10^{-3}$	$1.110478*10^{-2}$	-187.4107	11746.69
CD* Accurate Digits**	4	5	5	6	5
CD* Perturbations**	$1.87*10^{-4}$	$7.81*10^{-1}$	$3.00*10^{-3}$	$3.53*10^{-7}$	$8.83*10^{-10}$

CD* are central difference derivatives with a perturbation size of 10^{-4}
FD** are forward difference derivatives with a perturbation size of 10^{-6}
CD*** are central difference derivatives with the perturbation size given by Hull's method [28]

The central difference derivatives require one to determine the optimal perturbation step size for each constraint with respect to each parameter. Note in Table A1 that the optimal perturbation step size for Δv_0 to compute the derivative of the spacecraft's x position at the time of the first flyby with respect to Δv_0 is three orders of magnitude smaller than the optimal Δv_0 perturbation to calculate the derivative of the spacecraft's final y position with respect to Δv_0. Because the computational time necessary to perturb the free parameters and integrate the trajectory 754 times (twice for each required derivative) is large, a single perturbation size for each parameter must be determined that will allow the derivatives of all constraints with respect to that parameter to be calculated as accurately as possible.

The state transition matrix derivatives require significantly less computational time than the central difference derivatives for this example. The state transition matrix

derivatives are faster because they require the trajectory to be integrated only one time using 42 equations. The central difference derivatives require 6 equations to be integrated 59 times each for a total of 354 equation integrations. The time required to use the central difference derivatives can be reduced slightly through the use of nodes in the calculation of the central difference derivatives.

Table A.2 provides the optimized values for each of the free parameters obtained using a sequential quadratic programming algorithm[31]. The same initial estimate of the free parameters was used to optimize the parameters using both a central difference derivative method with derivatives tuned using Hull's method[28] and a state transition matrix method. The costs using both methods are within three hundredths of one percent. In order to determine which method could satisfy the constraints to a greater accuracy, the convergence criteria was made increasingly stringent until the method failed to converge. The state transition method was able to satisfy the constraints to four orders of magnitude more than the central difference method. The central difference method also took over 17 times more computational time than the state transition matrix method. All computational times were determined on a 2.4 GHz Pentium 4® processor.

Table A.2 Initial Estimate and Optimal Values of the Free Parameters For The Impulsive ΔV Transfer

Parameters	Units	Initial Estimate	Converged Central Difference Values	Converged State Transition Matrix Values
t_0	Julian Date	2455414.500	2455415.572	2455415.983
t_f	Julian Date	2459066.500	2459095.251	2459084.386
$v_{\infty 0}$	km/s	3.0932	3.0643	3.0657
α_0	radians	.02866	-0.00571	-0.01677
γ_0	radians	3.170370	3.15983	3.15856
t_{fb1}	Julian Date	2455522.500	2455523.153	2455523.226
r_{m1}	km	6400	6437.742	6400.000
β_1	radians	6.28	6.2433	6.2453
Δv_{pow1}	m/s	10	-0.002133	$2.1315*10^{-7}$
t_{pfb1}	Julian Date	2455735.500	2455740.630	2455742.318
Δv_{pfb1}	km/s	1.048949	.907019	.913924
α_{pfb1}	radians	2.80579	3.18473	3.15633
γ_{pfb1}	radians	-.08727	0.00228	0.00151
t_{fb2}	Julian Date	2456006.500	2456008.088	2456008.100
r_{m2}	km	6400	6400.000	6400.000
β_2	radians	6.28	6.2990	6.3385
Δv_{pow2}	m/s	10	9.149208	19.573638
t_{pfb2}	Julian Date	2456532.500	2456586.529	2456571.467
Δv_{pfb2}	km/s	.440677	.251181	.254642
α_{pfb2}	radians	2.570033	3.15411	3.20358
γ_{pfb2}	radians	-.00713	0.03142	0.10534
t_{fb3}	Julian Date	2457141.500	2457141.311	2457141.343
r_{m3}	km	6400	6400.000	6400.000
β_3	radians	6.28	6.7057	6.7079
Δv_{pow3}	m/s	10	0.00458442	$2.901430*10^{-7}$
t_{pfb3}	Julian Date	2457532.500	2457540.164	2457536.620
Δv_{pfb3}	km/s	2.562117	.188114	.167205
α_{pfb3}	radians	2.11001	-0.38073	-0.42447
γ_{pfb3}	radians	.20579	1.44400	1.43881
Cost	km/s	7.174943	4.419799	4.421049
Computational Time	s	N/A	489	28
$\lvert\mathbf{r}(t_{fb1}) - \mathbf{r}_{p1}(t_{fb1})\rvert$	m	N/A	1927.118	.25507
$\lvert\mathbf{r}(t_{fb2}) - \mathbf{r}_{p2}(t_{fb2})\rvert$	m	N/A	134230.175	13.66192
$\lvert\mathbf{r}(t_{fb3}) - \mathbf{r}_{p3}(t_{fb3})\rvert$	m	N/A	1239144.187	37.01409
$\lvert\mathbf{r}(t_f) - \mathbf{r}_{pf}(t_f)\rvert$	m	N/A	19937981.480	777.743842

Variable Specific Impulse Engines

The finite thrust trajectory consists of a number of segments equal to one plus the number of gravity assists. The first segment begins after the spacecraft has escaped the initial planet on a parabolic escape trajectory. On the first segment the spacecraft travels from the initial planet to the first flyby planet. On each subsequent segment the spacecraft travels from one flyby planet to the next except for the last segment when the spacecraft travels from the final gravity assist planet to the target. Figure A.9 shows a single gravity assist trajectory for the finite thrust engine. The number of gravity assists and the planet providing each gravity assist must be determined a priori. This method only determines a locally optimal trajectory for a given sequence of gravity assists.

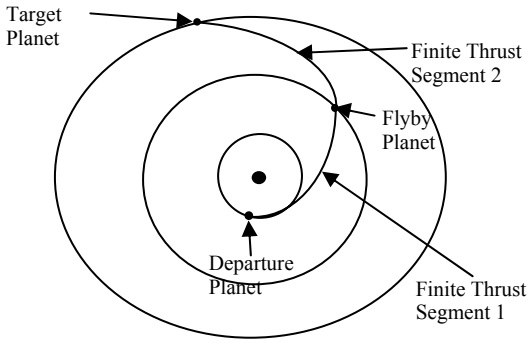

Figure A.9 Finite Thrust Single Flyby Trajectory

The optimal control problem is solved as a parameter optimization problem by treating the costate Lagrange multiplier vector as part of the parameter vector. The Euler-Lagrange equations are numerically integrated and the control satisfies the Pontryagin Maximum Principle. The free parameters for this case are the initial time, final time, flyby time(s), flyby radii, flyby angles, and the initial Lagrange multipliers for

each segment. The spacecraft is constrained to intercept each of the flyby planets at the time of each flyby and the target planet at the final time. The cost function is the total mass consumed.

In order to minimize the propellant consumed for a mission scenario using a power limited propulsion (PLP) engine, one can minimize the integral of the thrust acceleration squared which is defined by Eq. (A.38). The thrust acceleration vector must be the velocity costate vector in order to satisfy Pontryagin's Maximum Principle. Minimizing J instead of minimizing the propellant consumed allows one to determine the optimal trajectory without knowing the initial mass of the spacecraft or the power available to the propulsion system. This model assumes that the power is constant throughout the mission. The mass of the spacecraft at any time can be determined using Eq. (A.40).[21]

$$J \equiv \int_{t_0}^{t_f} \frac{\Gamma^2}{2}\, dt \tag{A.38}$$

$$\boldsymbol{\Gamma} = \boldsymbol{\lambda}_{\mathbf{v}} \tag{A.39}$$

$$m(t) = \frac{m(t_0)\, P_{max}}{P_{max} + m(t_0)\, J(t)} \tag{A.40}$$

The spacecraft state and its derivative with respect to time are defined to be

$$\mathbf{X} = \begin{pmatrix} \mathbf{r} \\ \mathbf{v} \\ J \\ \boldsymbol{\lambda}_{\mathbf{r}} \\ \boldsymbol{\lambda}_{\mathbf{v}} \\ \lambda_J \end{pmatrix} \tag{A.41}$$

$$\dot{\mathbf{X}} = \begin{pmatrix} \mathbf{v} \\ \mathbf{g}(\mathbf{r}) + \boldsymbol{\lambda}_{\mathbf{v}} \\ \frac{\lambda_v^{\,2}}{2} \\ -\frac{\partial \mathbf{g}}{\partial \mathbf{r}} \boldsymbol{\lambda}_{\mathbf{v}} \\ -\boldsymbol{\lambda}_{\mathbf{r}} \\ 0 \end{pmatrix} \tag{A.42}$$

The partial derivative of $\dot{\mathbf{X}}$ with respect to $\mathbf{X}$ for the PLP engine is given by Eq. (A.43).

$$\frac{\partial \dot{\mathbf{X}}}{\partial \mathbf{X}} = \begin{pmatrix} \mathbf{0}_{3x3} & \mathbf{I}_{3x3} & \mathbf{0}_{3x1} & \mathbf{0}_{3x3} & \mathbf{0}_{3x3} & \mathbf{0}_{3x1} \\ \frac{\partial \mathbf{g}}{\partial \mathbf{r}} & \mathbf{0}_{3x3} & \mathbf{0}_{3x1} & \mathbf{0}_{3x3} & \mathbf{I}_{3x3} & \mathbf{0}_{3x1} \\ \mathbf{0}_{1x3} & \mathbf{0}_{1x3} & 0 & \mathbf{0}_{1x3} & \boldsymbol{\lambda}_{\mathbf{v}}^{\mathrm{T}} & 0 \\ -\frac{\partial}{\partial \mathbf{r}} \frac{\partial \mathbf{g}}{\partial \mathbf{r}} \boldsymbol{\lambda}_{\mathbf{v}} & \mathbf{0}_{3x3} & \mathbf{0}_{3x1} & \mathbf{0}_{3x3} & -\frac{\partial \mathbf{g}}{\partial \mathbf{r}} & \mathbf{0}_{3x1} \\ \mathbf{0}_{3x3} & \mathbf{0}_{3x3} & \mathbf{0}_{3x1} & -\mathbf{I}_{3x3} & \mathbf{0}_{3x3} & \mathbf{0}_{3x1} \\ \mathbf{0}_{1x3} & \mathbf{0}_{1x3} & 0 & \mathbf{0}_{1x3} & \mathbf{0}_{1x3} & 0 \end{pmatrix} \tag{A.43}$$

For the VSI engine transfers, the costates are not continuous across the instantaneous gravity assist. The optimal value for the costates after an unpowered flyby can be determined from Eqs. (A.44) to (A.47) and the fact that the velocity costate vector immediately before and immediately after the flyby is in the plane defined by the incoming and outgoing hyperbolic excess velocity vectors.[32] ξ is a Lagrange multiplier whose value is determined by solving the optimal control problem. In Eq. (A.47), $\mathbf{g}(\mathbf{r}(t_{fb}))$ is defined to be the gravitational acceleration of the spacecraft at the time of the flyby. Note that since this is a zero sphere of influence patched conic approximation, the gravitational force due to the flyby planet is not included in $\mathbf{g}(\mathbf{r}(t_{fb}))$. Also note that

$\left\{\dot{\mathrm{v}}_{\mathrm{p}}(\mathrm{t}_{\mathrm{fb}}) - \mathbf{g}[\mathbf{r}(\mathrm{t}_{\mathrm{fb}})]\right\}$ would equal zero if the flyby planet had its equations of motion determined by integrating through the same gravity field that the spacecraft is traversing. If, however, the planet being flown by has its position and velocity determined by an ephemeris file that accounts for perturbations not included in the gravity field being used to determine the equations of motion of the spacecraft, this term may not equal zero.

$$\boldsymbol{\lambda}_{\mathbf{r}_{fb-}} = \boldsymbol{\lambda}_{\mathbf{r}_{fb+}} + \boldsymbol{\xi} \tag{A.44}$$

$$\lambda_{\mathrm{v}_{fb-}}{}^{\perp} = \left|\boldsymbol{\lambda}_{\mathbf{v}_{fb-}} \times \mathbf{v}_{\infty_i}\right| = \left|\boldsymbol{\lambda}_{\mathbf{v}_{fb+}} \times \mathbf{v}_{\infty_o}\right| = \lambda_{\mathrm{v}_{fb+}}{}^{\perp} \tag{A.45}$$

$$\lambda_{\mathrm{v}_{fb+}}{}^{\square} - \lambda_{\mathrm{v}_{fb-}}{}^{\square} = \frac{\lambda_{\mathrm{v}_{fb-}}{}^{\perp}}{\mathrm{v}_{\infty_i}\sin(\delta_{\mathrm{fb}})}\left(2\cos(\delta_{\mathrm{fb}}) + \frac{4\mathrm{r}_{\mathrm{m}}\sin^2\left(\frac{\delta_{\mathrm{fb}}}{2}\right)\sin(\delta_{\mathrm{fb}})\mathrm{v}_{\infty_i}{}^2}{\mu_{\mathrm{fb}}\left(1-\sin^2\left(\frac{\delta_{\mathrm{fb}}}{2}\right)\right)^{\frac{1}{2}}}\right) \tag{A.46}$$

$$\boldsymbol{\lambda}_{\mathbf{r}_{fb+}}{}^{\mathrm{T}}\mathbf{v}_{\infty_o} - \boldsymbol{\lambda}_{\mathbf{r}_{fb-}}{}^{\mathrm{T}}\mathbf{v}_{\infty_i} = \left(\boldsymbol{\lambda}_{\mathbf{v}_{fb+}} - \boldsymbol{\lambda}_{\mathbf{v}_{fb-}}\right)^{\mathrm{T}}\left[\left(\dot{\mathbf{v}}_{\mathrm{p}}(\mathrm{t}_{\mathrm{fb}})\right) - \mathbf{g}(\mathbf{r}(\mathrm{t}_{\mathrm{fb}})\right] \tag{A.47}$$

Instead of using Eqs. (A.44) to (A.47), the values of the costates immediately after the flyby can be added to the list of free parameters. The value of the costates on the minimum fuel transfer will satisfy these equations. Again, an adjoint control transformation is used and the optimal values of $\alpha, \dot{\alpha}, \gamma, \dot{\gamma}, \lambda_{\mathrm{v}}(\mathrm{t}_{\mathrm{fb}+})$, and $\dot{\lambda}_{\mathrm{v}}(\mathrm{t}_{\mathrm{fb}+})$ must be estimated. The costates immediately after the flyby are then defined according to Eqs. (B.4) and (B.5). As a result, these costates are a function of $\mathbf{r}(\mathrm{t}_{\mathrm{fb}+})$ and $\mathbf{v}(\mathrm{t}_{\mathrm{fb}+})$. Because $\mathbf{r}(\mathrm{t}_{\mathrm{fb}+})$ and $\mathbf{v}(\mathrm{t}_{\mathrm{fb}+})$ are a function of $\mathbf{r}(\mathrm{t}_{\mathrm{fb}-})$ and $\mathbf{v}(\mathrm{t}_{\mathrm{fb}-})$, the costates after the flyby are a function of $\mathbf{r}(\mathrm{t}_{\mathrm{fb}-})$ and $\mathbf{v}(\mathrm{t}_{\mathrm{fb}-})$; they are not however a function of $\boldsymbol{\lambda}_{\mathbf{r}}(\mathrm{t}_{\mathrm{fb}-})$ or $\boldsymbol{\lambda}_{\mathbf{v}}(\mathrm{t}_{\mathrm{fb}-})$.

Variable Specific Impulse Model Example

An optimal trajectory using PLP from Earth to Saturn with two gravity assists provided by Venus is used to demonstrate the accuracy of the state transition matrix derivatives for the finite thrust model. Table A.3 provides a sample of the derivatives of the costs and constraints with respect to the free parameters. Again, the state transition matrix derivatives agree closely with the optimal central difference derivatives without requiring any work to determine the optimal perturbation step sizes. In this case, there is no theoretical value for the derivatives, but the state transition matrix derivatives are accurate to the accuracy of the integrator's ability to integrate the equations of motion for the spacecraft state and the state transition matrix. Using the rule of thumb given by Gill, the central difference derivatives are accurate to one half the accurate digits determined by integrating the equations of motion of the spacecraft state[27]. As a result, the state transition matrix derivatives are considered to be the true solution when calculating the accurate digits in the finite difference derivatives. For this trajectory, using the central difference derivatives to compute the derivatives requires about 40 percent more computational time per iteration than the state transition matrix derivatives.

Table A.3 Accuracy Of Partial Derivatives For Earth-Venus-Venus-Saturn PLP Trajectory

	$\frac{\partial J}{\partial \dot{\gamma}_0}$ **(AU²/Day²)**	$\frac{\partial x_{fb1}}{\partial \dot{\lambda}_{v0}}$ **(Day³)**	$\frac{\partial z_f}{\partial \dot{\lambda}_{v0}}$ **(Day³)**	$\frac{\partial y_f}{\partial \alpha_0}$ **(AU)**	$\frac{\partial x_f}{\partial \dot{\alpha}_1}$ **(AU*Days)**
STM	$1.94263*10^{-4}$	$4.70782*10^{7}$	$7.36889*10^{10}$	38075.09	2243.230
CD*	$2.42869*10^{-4}$	$4.70795*10^{7}$	$7.36838*10^{10}$	36750.53	2271.388
CD* Accurate Digits	1	4	4	1	2
FD**	$1.97418*10^{-4}$	$4.72702*10^{7}$	$7.02872*10^{10}$	38057.03	2229.010
FD** Accurate Digits	2	2	1	3	2
CD***	$1.94270*10^{-4}$	$4.70782*10^{7}$	$7.36923*10^{10}$	38062.61	2243.490
CD*** Accurate Digits	4	6	4	3	4
CD*** Perturbations	$1.286*10^{-7}$	$7.437*10^{-12}$	$1.835*10^{-13}$	$9.946*10^{-8}$	$1.537*10^{-7}$

CD* are central difference derivatives with a perturbation size of 10^{-4}
FD** are forward difference derivatives with a perturbation size of 10^{-6}
CD*** are central difference derivatives with the perturbation size given by Hull's method [28]

In order to demonstrate the benefits of using the more accurate derivatives obtained from the state transition method, an optimal trajectory using PLP from Earth to Saturn with one Venus flyby is sought. The spacecraft must satisfy six equality constraints requiring it to intercept Venus at the time of the gravity assist and to intercept Saturn at the final time. The total mission time is constrained to be less than or equal to 2000 days and the flyby radius is constrained to be greater than or equal to 250 kilometers. This flyby radius is obviously a subsurface flyby which is not possible in an actual mission. The small flyby radius is used to create a single gravity assist trajectory that has a lower cost than a simple trajectory from Earth to Saturn with no flyby. Obviously, a flyby of Venus is not beneficial for a 2,000 day Earth to Saturn intercept mission using a PLP engine. The optimal trajectory is shown in Figure A.10. Table A.4 shows a comparison of the optimal trajectories computed using both central difference and state transition matrix derivatives. Like the impulsive $\Delta\mathbf{v}$ case, the cost is nearly the

same for both solutions but the state transition matrix derivatives are able to satisfy the constraints 100 times better and require significantly less computational time than the central difference derivatives.

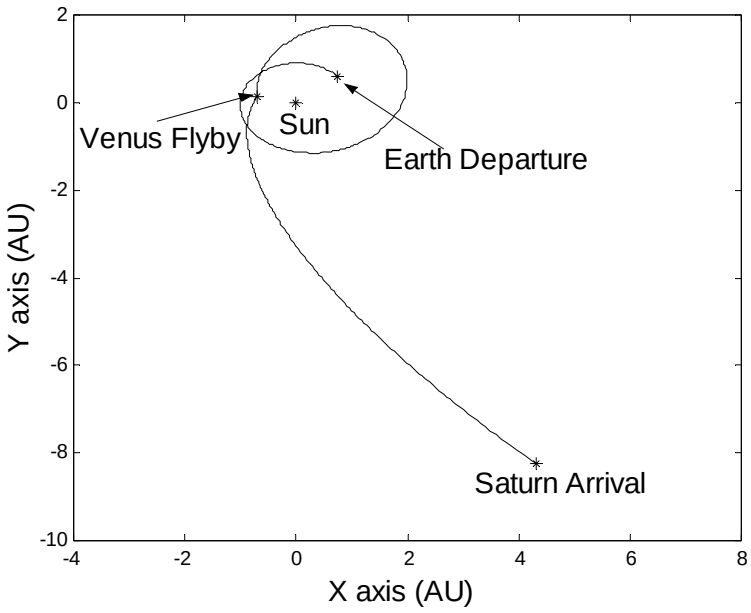

Figure A.10 Earth-Venus-Saturn PLP Trajectory

Table A.4 Optimal Values Of Free Parameters For Earth-Venus-Saturn PLP Trajectory

Parameters	Units	Initial Estimate	Converged Central Difference Values	Converged State Transition Matrix Values
t_0	Julian Date	2456967.358	2456964.820	2456965.025
t_f	Julian Date	2458967.360	2458964.622	2458964.714
α_0	radians	1.60231	1.60575	1.60181
γ_0	radians	0.51606	0.42259	0.53478
$\dot{\alpha}_0$	rad/s	-0.32021	-0.34486	-0.26348
$\dot{\gamma}_0$	rad/s	8.82879	8.83680	8.40122
λ_{v0}	AU/Day^2	$-9.04494*10^{-12}$	$8.33069*10^{-10}$	$1.87900*10^{-10}$
$\dot{\lambda}_{v0}$	AU/Day^3	$8.04304*10^{-8}$	$7.99615*10^{-8}$	$8.03277*10^{-8}$
t_{fb1}	Julian Date	2457828.632	2457826.184	2457826.269
r_{m1}	km	252.500	252.038	250.824
β_1	radians	6.08664	6.03326	6.02885
α_1	radians	2.78957	2.51727	1.82834
γ_1	radians	-0.306563	-0.96504	-0.16443
$\dot{\alpha}_1$	rad/s	-8.1872	-7.94359	-7.72772
$\dot{\gamma}_1$	rad/s	-3.33312	-3.56769	-4.02256
λ_{v1}	AU/Day^2	$1.00000*10^{-9}$	$-1.76753*10^{-11}$	$-8.29047*10^{-12}$
$\dot{\lambda}_{v1}$	AU/Day^3	0.00000	$-1.78137*10^{-10}$	$-1.78889*10^{-10}$
Cost	km^2/s^3	N/A	$1.3082*10^{-2}$	$1.3081*10^{-2}$
Computational Time	s	N/A	19	15
$\lvert\mathbf{r}(t_{fb1})- \mathbf{r}_{p1}(t_{fb1})\rvert$	km	$3.92124*10^6$	3.54656	.14097
$\lvert\mathbf{r}(t_f)- \mathbf{r}_{pf}(t_f)\rvert$	km	$3.70381*10^8$	9772.62944	88.82233

Constant Specific Impulse Engines

The CSI trajectory also consists of a number of segments equal to one plus the number of gravity assists. An example trajectory using one gravity assist is shown in Figure A.11. At the beginning of the first segment, the spacecraft has escaped the departure planet with no excess hyperbolic velocity. The spacecraft then travels on a finite thrust segment until it reaches the first flyby planet. In the example in Figure A.11, the spacecraft thrusts and then coasts during segment one. The flybys are modeled using a zero sphere of influence patched conic approximation discussed in Appendix C. Following the first flyby, the spacecraft travels on another finite thrust segment which

transports it to either the next gravity assist maneuver or the target planet. In the example in Figure A.11, segment 2 consists of a coasting period, followed by a thrusting period, and a final coasting period. The number of flybys is unlimited and the thrusting structure is free, but the number of gravity assists and the planet providing each gravity assist must be determined a priori. This method only determines a locally optimal trajectory for a given sequence of gravity assists. The free parameters are the initial time, final time, flyby times, flyby radii, flyby angles, and adjoint control parameters for each segment. The adjoint control parameters are discussed in Appendix B. The cost function is the total mass used by the engine.

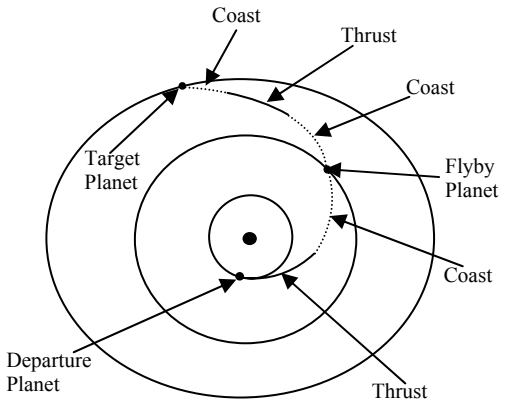

Figure A.11 Finite Thrust Single Flyby Trajectory

The spacecraft state, **X**, is defined to include the spacecraft position, velocity, and mass as well as their costates as shown in Eq. (A.48). The spacecraft engine has a constant specific impulse and the thrust is constrained to be less than a maximum value. The system Hamiltonian is given in Eq. (A.49). The constraints requiring the spacecraft

to intercept the gravity assist planets at the times of the flybys and the target planet at the final time as well as requiring a minimum flyby radius at each gravity assist are adjoined to the cost function using Lagrange multipliers to form the modified cost function given in Eq. (A.50). Applying Pontryagin's Maximum Principle and the first order necessary conditions for the optimal control problem yields the time derivative of **X** shown in Eq. (A.51). The thrust must be equal to T_{max} when the switching function defined in Eq. (A.52) is greater than zero, and it must be T_{min} when the switching function is negative. The switching function is only a function of the spacecraft state, and the spacecraft equations of motion will be discontinuous when the switching function crosses through a zero. The state transition matrix can be determined using Eqs. (A.3), (A.4), and (A.53).

$$\mathbf{X}^T \equiv \left(\mathbf{r}^T \ \mathbf{v}^T \ \mathrm{m} \ \boldsymbol{\lambda}_\mathbf{r}^T \ \boldsymbol{\lambda}_\mathbf{v}^T \ \lambda_\mathrm{m}\right)^T \tag{A.48}$$

$$\mathrm{H} = \boldsymbol{\lambda}_\mathrm{r}{}^T \mathbf{v} + \boldsymbol{\lambda}_\mathbf{v}{}^T \mathbf{g}(\mathbf{r}) + \frac{\mathrm{T}}{\mathrm{m}} \boldsymbol{\lambda}_\mathbf{v}{}^T \mathbf{u} - \frac{\mathrm{T}}{\mathrm{c}} \lambda_\mathrm{m} \tag{A.49}$$

$$\mathrm{W}' = -m_\mathrm{f} + \sum_\mathrm{i}^\mathrm{q} \{\mathbf{v}_\mathrm{i}{}^T [\mathbf{r}(\mathrm{t}_{\mathrm{fb}_\mathrm{i}}) - \mathbf{r}_{\mathrm{p}_\mathrm{i}}(\mathrm{t}_{\mathrm{fb}_\mathrm{i}})] + \rho_\mathrm{i}(\mathrm{r}_{\mathrm{m}_\mathrm{i}} - \mathrm{r}_{\mathrm{min}_\mathrm{i}})\} + \boldsymbol{\sigma}^T [\mathbf{r}(\mathrm{t}_\mathrm{f}) - \mathbf{r}_\mathrm{t}(\mathrm{t}_\mathrm{f})] \tag{A.50}$$

$$\dot{\mathbf{X}} \equiv \begin{pmatrix} \mathbf{v} \\ \mathbf{g}(\mathbf{r}) + \frac{\mathrm{T}}{\mathrm{m}} \boldsymbol{\lambda}_\mathrm{v} \\ -\frac{\mathrm{T}}{\mathrm{c}} \\ -\frac{\partial \mathbf{g}}{\partial \mathbf{r}} \boldsymbol{\lambda}_\mathrm{v} \\ -\boldsymbol{\lambda}_\mathrm{r} \\ \frac{\mathrm{T}\,\lambda_\mathrm{v}}{\mathrm{m}^2} \end{pmatrix} \tag{A.51}$$

$$S = \frac{\lambda_v}{m} - \frac{\lambda_m}{c} \tag{A.52}$$

$$\frac{\partial \dot{\mathbf{X}}}{\partial \mathbf{X}} = \begin{pmatrix} \mathbf{0}_{3x3} & \mathbf{I}_{3x3} & \mathbf{0}_{3x1} & \mathbf{0}_{3x3} & \mathbf{0}_{3x3} & \mathbf{0}_{3x1} \\ \frac{\partial \mathbf{g}}{\partial \mathbf{r}} & \mathbf{0}_{3x3} & -\frac{T\,\boldsymbol{\lambda}_v}{m^2 \lambda_v} & \mathbf{0}_{3x3} & \frac{T}{m}\left(\frac{\mathbf{I}_{3x3}}{\lambda_v} - \frac{\boldsymbol{\lambda}_v \boldsymbol{\lambda}_v^{\,T}}{\lambda_v^{\,3}}\right) & \mathbf{0}_{3x1} \\ \mathbf{0}_{1x3} & \mathbf{0}_{1x3} & 0 & \mathbf{0}_{1x3} & \mathbf{0}_{1x3} & 0 \\ -\frac{\partial}{\partial \mathbf{r}}\frac{\partial \mathbf{g}}{\partial \mathbf{r}}\boldsymbol{\lambda}_v & \mathbf{0}_{3x3} & \mathbf{0}_{3x1} & \mathbf{0}_{3x3} & -\frac{\partial \mathbf{g}}{\partial \mathbf{r}} & \mathbf{0}_{3x1} \\ \mathbf{0}_{3x3} & \mathbf{0}_{3x3} & \mathbf{0}_{3x1} & -\mathbf{I}_{3x3} & \mathbf{0}_{3x3} & \mathbf{0}_{3x1} \\ \mathbf{0}_{1x3} & \mathbf{0}_{1x3} & -\frac{2T\lambda_v}{m^3} & \mathbf{0}_{1x3} & \frac{T\,\boldsymbol{\lambda}_v}{m^2 \lambda_v} & 0 \end{pmatrix} \tag{A.53}$$

The optimal control problem is solved as a TPBVP with the constraints determined using variational calculus and taking the first variation of Eq. (A.50). An optimal trajectory must meet the constraints given by Eqs. (A.54) to (A.61) at each flyby.[32] In addition, Eqs. (A.62) to (A.64) must be satisfied for an optimal trajectory.

$$\mathbf{r}_{sc}(t_{fb}) - \mathbf{r}_p(t_{fb}) = \mathbf{0} \tag{A.54}$$

$$r_m - r_{min} + \rho^2 = 0 \tag{A.55}$$

$$\lambda_{v_{fb-}}^{\perp} \rho = 0 \tag{A.56}$$

$$\lambda_{v_{fb-}}^{\perp} = \left| \boldsymbol{\lambda}_{\mathbf{v}_{fb-}} \times \mathbf{v}_{\infty_i} \right| = \left| \boldsymbol{\lambda}_{\mathbf{v}_{fb+}} \times \mathbf{v}_{\infty_o} \right| = \lambda_{v_{fb+}}^{\perp} \tag{A.57}$$

$$\lambda_{v_{fb+}}^{\square} - \lambda_{v_{fb-}}^{\square} = \frac{\lambda_{v_{fb-}}^{\perp}}{v_{\infty_i} \sin(\delta_{fb})} \left(2\cos(\delta_{fb}) + \frac{4 r_m \sin^2\left(\frac{\delta_{fb}}{2}\right) \sin(\delta_{fb}) v_{\infty_i}^2}{\mu_{fb}\left(1 - \sin^2\left(\frac{\delta_{fb}}{2}\right)\right)^{\frac{1}{2}}} \right) \tag{A.58}$$

$$\boldsymbol{\lambda}_{\mathbf{r}_{fb+}}{}^{T} \mathbf{v}_{\infty_o} - \boldsymbol{\lambda}_{\mathbf{r}_{fb-}}{}^{T} \mathbf{v}_{\infty_i} = \left(\boldsymbol{\lambda}_{\mathbf{v}_{fb+}} - \boldsymbol{\lambda}_{\mathbf{v}_{fb-}} \right)^{T} \left[\frac{d}{dt}\left(\mathbf{v}_p(t_{fb}) \right) - \mathbf{g}(\mathbf{r}(t_{fb})) \right] \tag{A.59}$$

$$\left(\boldsymbol{\lambda}_{\mathrm{v}_{fb-}}^{\perp}\right)^{\mathrm{T}}\left(\mathbf{v}_{\infty_i}\times\mathbf{v}_{\infty_o}\right)=0 \tag{A.60}$$

$$\left(\boldsymbol{\lambda}_{\mathrm{v}_{fb+}}^{\perp}\right)^{\mathrm{T}}\left(\mathbf{v}_{\infty_i}\times\mathbf{v}_{\infty_o}\right)=0 \tag{A.61}$$

$$\mathbf{r}(\mathrm{t_f})-\mathbf{r}_{\mathrm{t}}(\mathrm{t_f})=\mathbf{0} \tag{A.62}$$

$$\boldsymbol{\lambda}_{\mathbf{v}}(\mathrm{t_f})=\mathbf{0} \tag{A.63}$$

$$\boldsymbol{\lambda}_{\mathbf{r}}(\mathrm{t_f})^{\mathrm{T}}\left(\mathbf{v}(\mathrm{t_f})-\mathbf{v}_{\mathrm{t}}(\mathrm{t_f})\right)=0 \tag{A.64}$$

The free parameters are the initial time, initial adjoint control parameters excluding $\lambda_{\mathrm{v}}(\mathrm{t}_0)$ (which is determined from the initial value of the switching function being zero), flyby times, flyby radii, flyby radii slack variables, flyby angles, adjoint control parameters after each flyby, and the final time. There are seven plus ten times the number of gravity assists free parameters and an equal number of constraints given by Eqs. (A.54) to (A.64).

Earth-Venus-Saturn Constant Specific Impulse Transfer

An Earth to Saturn intercept trajectory using a CSI engine with a gravity assist provided by Venus is used in order to demonstrate the benefits of using the state transition matrix to calculate derivatives. The trajectory consists of two segments: the Earth to Venus segment and the Venus to Saturn segment. During each segment, the spacecraft can have periods where the thrust is on and periods where the thrust is off. The number of times the engine may turn on or off during any segment is unlimited. The engine is capable of providing a maximum thrust of 20 Newtons, and has a specific

impulse of 3.2 million seconds. Clearly this value for the specific impulse is not realistic with current engines; it was selected to demonstrate the capabilities of the two different derivative methods on long duration trajectories. The spacecraft has an initial mass of 30,000 kg. The planets' locations and masses are determined using the JPL DE405[30] ephemerides, and the only gravitational body that affects the spacecraft between gravity assists is the Sun. Because the equations of motion are discontinuous, all integration was performed using DLSODAR[29], a solver for ordinary differential equations that integrates until a root in the switching function occurs. For this trajectory the minimum flyby radius is set to be zero in order to simplify the constraint equations. As a result, Eqs. (A.54) to (A.64) can be replaced by Eqs. (A.65) to (A.74). Consequently, the trajectory will not provide a feasible mission if the flyby radius converges to a value that is less than the radius of Venus. This problem has 16 free parameters: initial time, initial adjoint control parameters excluding $\lambda_v(t_0)$ (which is determined from the initial value of the switching function being zero due to the continuity of the Hamiltonian), flyby time, flyby radius, flyby angle, adjoint control parameters after the flyby, and the final time.

$$\mathbf{r}(t_{fb}) - \mathbf{r}_p(t_{fb}) = \mathbf{0} \tag{A.65}$$

$$\lambda_{v_{fb+}}^{\square} = \lambda_{v_{fb-}}^{\square} \tag{A.66}$$

$$\boldsymbol{\lambda}_{\mathbf{r}_{fb+}}{}^{T}\mathbf{v}_{\infty_o} - \boldsymbol{\lambda}_{\mathbf{r}_{fb-}}{}^{T}\mathbf{v}_{\infty_i} = \left(\boldsymbol{\lambda}_{\mathbf{v}_{fb+}} - \boldsymbol{\lambda}_{\mathbf{v}_{fb-}}\right)^{T}\left[\frac{d}{dt}\left(\mathbf{v}_p(t_{fb})\right) - \mathbf{g}(\mathbf{r}(t_{fb}))\right] \tag{A.67}$$

$$\left(\boldsymbol{\lambda}_{v_{fb-}}^{\perp}\right)^{T}\left(\mathbf{v}_{\infty_i} \times \mathbf{v}_{\infty_o}\right) = 0 \tag{A.68}$$

$$\left(\boldsymbol{\lambda}_{v_{fb-}}^{\perp}\right)^{T}\left[\left(\mathbf{v}_{\infty_i} \times \mathbf{v}_{\infty_o}\right) \times \mathbf{v}_{\infty_i}\right] = 0 \tag{A.69}$$

$$\left(\boldsymbol{\lambda}_{\mathbf{v}_{fb+}}^{\perp}\right)^{\mathrm{T}}\left(\mathbf{v}_{\infty_i}\times\mathbf{v}_{\infty_o}\right)=0 \tag{A.70}$$

$$\left(\boldsymbol{\lambda}_{\mathbf{v}_{fb+}}^{\perp}\right)^{\mathrm{T}}\left[\left(\mathbf{v}_{\infty_i}\times\mathbf{v}_{\infty_o}\right)\times\mathbf{v}_{\infty_i}\right]=0 \tag{A.71}$$

$$\mathbf{r}(\mathrm{t_f})-\mathbf{r}_{\mathrm{t}}(\mathrm{t_f})=\mathbf{0} \tag{A.72}$$

$$\boldsymbol{\lambda}_{\mathbf{v}}(\mathrm{t_f})=\mathbf{0} \tag{A.73}$$

$$\boldsymbol{\lambda}_{\mathbf{r}}(\mathrm{t_f})^{\mathrm{T}}\left(\mathbf{v}(\mathrm{t_f})-\mathbf{v}_{\mathrm{t}}(\mathrm{t_f})\right)=0 \tag{A.74}$$

Both state transition matrix derivatives and central difference derivatives were used in a Newton rootfinding method in order to find the optimal values for the free parameters. At each iteration, the new set of free parameters was determined from the previous estimate using Eq. (A.75). The relaxation parameter, ζ, was set to 10^{-3} when the estimate was far from the solution and increased to 10^{-2} and 10^{-1} as the system converged to the solution. The relaxation parameter could not be set to one using either the central difference or state transition matrix derivatives because it would cause the iterative scheme to overcorrect for errors and diverge from the solution.

$$\mathbf{x}_{\mathrm{k+1}}=\mathbf{x}_{\mathrm{k}}-\varsigma\left(\left.\frac{\partial\mathbf{C}}{\partial\mathbf{x}}\right|_{\mathbf{x}=\mathbf{x}_{\mathrm{k}}}\right)^{-1}\mathbf{C}(\mathbf{x}_{\mathrm{k}}) \tag{A.75}$$

The state transition matrix derivatives were able to begin at the initial estimate given in Table A.5 and converge to the solution given in the table using 13,000 iterations with ζ set to 10^{-3}, followed by 1,000 iterations with ζ set to 10^{-2}, and 200 iterations with ζ set to 10^{-1}. The number of iterations could be reduced by empirically finding the optimal value for ζ on each iteration, but that would require more analyst intervention and computational time than using a value of ζ that is not optimal. The locally optimal

trajectory shown in Figure A.12 consists of a thrust-coast-thrust-coast-thrust-coast-gravity assist-coast structure. Note that all figures are plotted in the ecliptic plane. Figure A.13 more clearly shows the trajectory before the gravity assist with the solid lines showing periods when the spacecraft is thrusting, and the dotted lines indicating coasting. Figure A.13 also clearly shows the discontinuity in the spacecraft velocity at the time of the gravity assist. The switching function can be seen in Figure A.14. The optimal trajectory is infeasible because the optimal value for the flyby radius is 458 kilometers which is below the surface of Venus. The purpose of this paper was not to find feasible gravity assist trajectories; it was to demonstrate whether state transition matrix derivatives can be beneficial to optimization algorithms when the spacecraft state and equations of motion are discontinuous. An optimal feasible solution can be found by employing Eqs. (A.54) to (A.64) instead of Eqs. (A.65) to (A.74), because Eqs. (A.54) to (A.64) are capable of enforcing a minimum flyby radius.

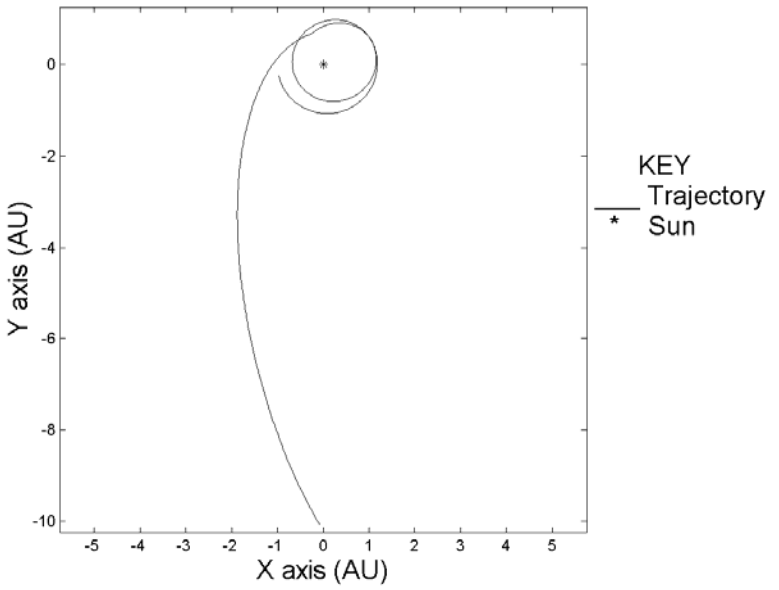

Figure A.12 Optimal Earth-Venus-Saturn Trajectory

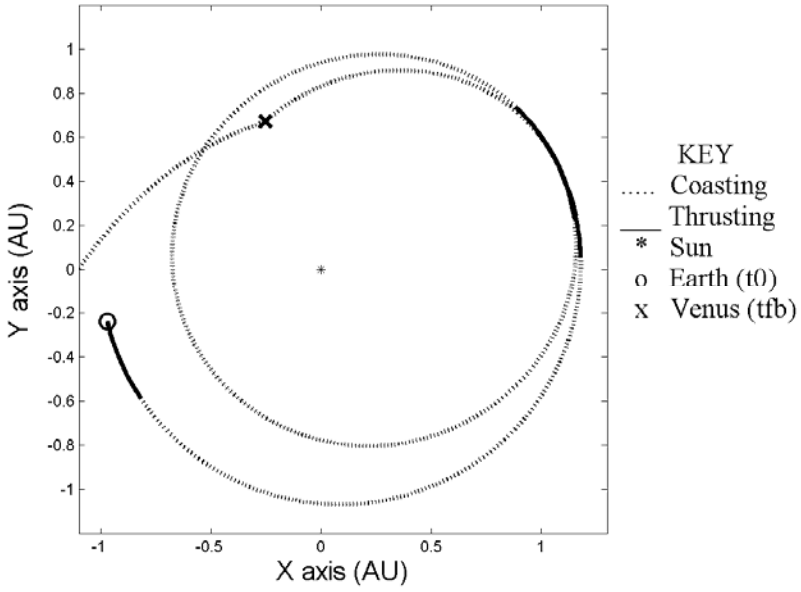

Figure A.13 Optimal Earth-Venus-Saturn Trajectory

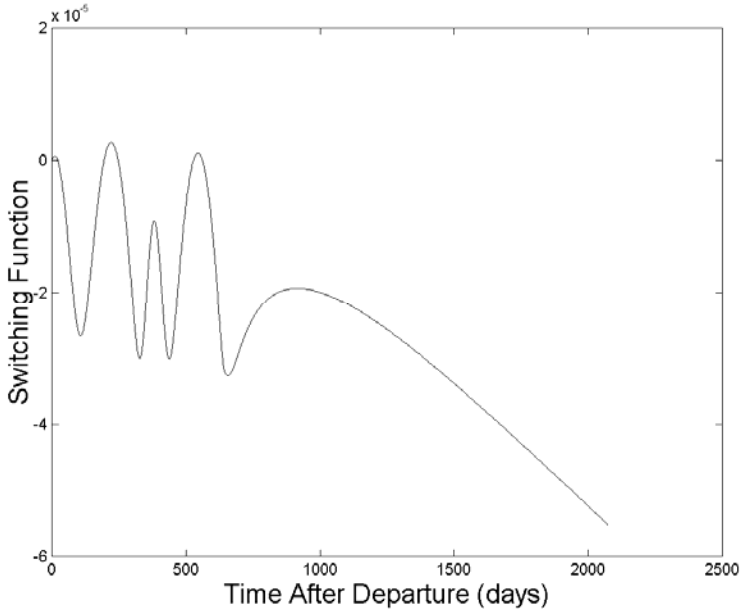

Figure A.14 Switching Structure for Optimal Earth-Venus-Saturn Trajectory

Starting from the same initial guess and using central difference derivatives tuned by using Hull's method[28] instead of the state transition matrix derivatives, the Newton iteration method is unable to converge to the optimal values. Instead it diverges after approximately 5,000 iterations with ζ set to 10^{-3} without approaching the optimal solution found by the state transition matrix method. An attempt was made to determine if the central difference derivatives would converge to the optimal solution from an initial estimate that was closer to the optimal solution than the initial estimate used by the state transition matrix derivative method. In order to obtain an initial estimate that was closer to the optimal solution, the state transition matrix derivatives were employed for a multiple of 1,000 iterations with the relaxation parameter set to 10^{-3}. After a multiple of

1,000 iterations with the state transition matrix derivatives, the process was continued using central difference derivatives.

Table A.5 Free Parameters For Earth-Venus-Saturn Constant Specific Impulse Trajectory

Parameters	Units	Initial Estimate State Transition Matrix	Initial Estimate Central Difference	Optimal Values
		Free Parameters		
t_0	Julian Date	2456020	2456038	2456021
t_f	Julian Date	2459323	2457474	2458094
α_0	radians	6.4015	6.4106	6.3932
γ_0	radians	-0.1167	-0.1182	-0.1233
$\dot{\alpha}_0$	rad/s	$-8.8790*10^{-3}$	$-8.9950*10^{-3}$	$-8.7356*10^{-3}$
$\dot{\gamma}_0$	rad/s	3.453610^{-4}	9.673410^{-4}	$1.0680*10^{-3}$
$\dot{\lambda}_{v0}$	AU^{-5}/Day^2	$4.3455*10^{-3}$	$4.5582*10^{-3}$	$3.9247*10^{-3}$
t_{fb1}	Julian Date	2456669	2456673	2456669
r_{m1}	km	1290.85	263.71	457.76
β_1	radians	6.6100	6.2368	6.0001
α_1	radians	9.5651	9.7406	9.2750
γ_1	radians	0.1409	-1.4619	-0.2192
$\dot{\alpha}_1$	rad/s	$-1.2923*10^{-3}$	$-5.9511*10^{-3}$	$-8.7402*10^{-4}$
$\dot{\gamma}_1$	rad/s	$-1.9909*10^{-3}$	$-3.4922*10^{-3}$	$-2.3075*10^{-2}$
λ_{v1}	AU^{-5}/Day	0.7612	0.7069	0.6844
$\dot{\lambda}_{v1}$	AU^{-5}/Day^2	$3.6671*10^{-3}$	$2.9146*10^{-2}$	$-1.3869*10^{-3}$
Final Mass	kg	29990.17	29992.25	29994.04
		Constraints		
Eq. (A.65)$_x$	AU	$1.1273*10^{-3}$	$1.6366*10^{-2}$	$7.8281*10^{-10}$
Eq. (A.65)$_y$	AU	$2.6044*10^{-3}$	$1.3888*10^{-2}$	$5.1588*10^{-10}$
Eq. (A.65)$_z$	AU	$-2.5187*10^{-5}$	$7.1012*10^{-4}$	$2.0800*10^{-11}$
Eq. (A.66)	AU/Day^2	$-3.6553*10^{-2}$	$-1.8090*10^{-2}$	$-2.1437*10^{-10}$
Eq. (A.67)	$AU^{1.5}/Day^3$	$6.2895*10^{-5}$	$-1.1665*10^{-5}$	$-7.9756*10^{-13}$
Eq. (A.68)	$AU^{3.5}/Day^4$	$-4.3168*10^{-8}$	$1.0486*10^{-7}$	$3.8812*10^{-16}$
Eq. (A.69)	$AU^{4.5}/Day^5$	$-3.4440*10^{-10}$	$-1.5250*10^{-10}$	$-2.6072*10^{-18}$
Eq. (A.70)	$AU^{3.5}/Day^4$	$3.7825*10^{-8}$	$3.5150*10^{-9}$	$-7.8562*10^{-16}$
Eq. (A.71)	$AU^{4.5}/Day^5$	$1.1063*10^{-10}$	$-1.7159*10^{-9}$	$1.2661*10^{-18}$
Eq. (A.72)$_x$	AU	-0.8942	$9.0468*10^{-2}$	$6.7680*10^{-8}$
Eq. (A.72)$_y$	AU	1.8590	$9.3021*10^{-2}$	$9.3131*10^{-8}$
Eq. (A.72)$_z$	AU	-3.1985	-0.2830	$-1.2970*10^{-8}$
Eq. (A.73)$_x$	AU^{-5}/Day	0.1619	$2.3789*10^{-3}$	$-1.8433*10^{-8}$
Eq. (A.73)$_y$	AU^{-5}/Day	$-4.2146*10^{-2}$	$-2.2087*10^{-2}$	$-2.6753*10^{-8}$
Eq. (A.73)$_z$	AU^{-5}/Day	0.2065	0.1811	$4.6338*10^{-8}$
Eq. (A.74)	$AU^{1.5}/Day^3$	$1.0034*10^{-6}$	$2.8056*10^{-7}$	$-1.3207*10^{-13}$

The central difference derivatives diverged when 10,000 or less state transition matrix derivative iterations were used and converged when 11,000 or greater state transitions matrix derivative iterations were used before beginning to use central difference derivatives. Table A.5 shows the values of the free parameters when central difference derivatives began to be used to successfully determine the optimal values of the free parameters.

Earth-Saturn Constant Specific Impulse Transfer

The third example problem is the same as the second example problem except for two modifications. First, there is no gravity assist in this problem. Second, the solution method does not employ variational calculus to determine constraints and form a TPBVP problem. Instead, the kinematic boundary conditions are satisfied through the use of equality constraints and the transversality conditions are satisfied by minimizing the cost function using a sequential quadratic programming code.[31] This method requires one to determine the derivatives of the cost and constraint functions with respect to all of the free parameters. The accuracy with which the optimal trajectory can be found depends on the accuracy of these derivatives. The Euler-Lagrange equations are numerically integrated, and the continuous control still satisfies the Pontryagin Maximum Principle. The spacecraft is constrained to intercept the target planet at the final time, and the cost function is the total mass consumed.

To test the possible benefits of the state transition matrix method derivatives, a trajectory using a CSI engine to transport the spacecraft from Earth to Saturn is sought.

The engine parameters are the same as in the previous example. Applying Pontryagin's Maximum Principle again yields Eqs. (A.48) and (A.51) for the spacecraft state and its time derivative. The free parameters for this case are the initial time, final time, and the initial adjoint control parameters. Although the sequential quadratic programming code only directly enforced Eq. (A.72), an optimal trajectory must satisfy Eqs. (A.73) and (A.74) as well. Both state transition matrix derivatives and central difference derivatives were used to calculate an optimal trajectory starting from the same initial guess listed in Table A.6 using the sequential quadratic programming code.

Table A.6 Free Parameters For Earth-Saturn Constant Specific Impulse Trajectory

Parameters	Units	Initial Estimate	Converged Values Central Difference	Converged Values State Transition Matrix	Optimal Values
			Free Parameters		
t_0	Julian Date	2456952.78	2456925.77	2456965.48	2456964.83
t_f	Julian Date	2457589.79	2457636.91	2459477.13	2459455.70
α_0	radians	6.2981	3.4966	3.4193	3.3659
γ_0	radians	2.2007	3.5252	3.0690	3.0808
$\dot{\alpha}_0$	rad/s	$-7.9599*10^{-2}$	$2.4090*10^{-2}$	$-3.3591E*10^{-3}$	$-2.3463*10^{-3}$
$\dot{\gamma}_0$	rad/s	$1.4611*10^{-2}$	$-1.2437*10^{-2}$	$-3.6910*10^{-5}$	$4.7658*10^{-4}$
$\dot{\lambda}_{v_0}$	AU^{-5}/Day^2	$7.9702*10^{-2}$	$2.56780*10^{-2}$	$1.5106*10^{-2}$	$1.2577*10^{-2}$
Final Mass	kg	29964.94	29960.85	29988.72	29988.73
			Constraints		
Eq. $(A.72)_x$	AU	9.3835	$-3.5578*10^{-2}$	$8.2694*10^{-8}$	$2.6636*10^{-9}$
Eq. $(A.72)_y$	AU	10.8002	$7.9357*10^{-3}$	$-6.2508*10^{-6}$	$-5.9794*10^{-11}$
Eq. $(A.72)_z$	AU	-0.9918	$1.1228*10^{-3}$	$-1.4807*10^{-7}$	$-3.3001*10^{-11}$
Eq. $(A.73)_x$	AU^{-5}/Day	30.5139	-8.2630	-0.9056	$-3.2940*10^{-9}$
Eq. $(A.73)_y$	AU^{-5}/Day	25.6998	-15.1167	$9.6117*10^{-2}$	$2.0821*10^{-8}$
Eq. $(A.73)_z$	AU^{-5}/Day	-3.8537	-0.8742	-0.4560	$3.5364*10^{-10}$
Eq. (A.74)	$AU^{1.5}/Day^3$	$5.5250*10^{-5}$	$-5.1838*10^{-4}$	$4.9470*10^{-7}$	$1.1447*10^{-14}$

Table A.6 also shows the solution to which both derivative methods converged as well as the optimal solution. The optimal solution was determined by using the rootfinding method described in example problem two. The state transition matrix method derivatives were able to converge to nearly the optimal solution. The central difference derivative solution is extremely far from the optimal solution. In fact, the sequential quadratic programming code found the central difference solution using both central difference derivatives and state transition matrix derivatives. When using state transition matrix derivatives, the sequential quadratic programming code was able to continue past this solution in search of a better one. The central difference derivatives were not accurate enough for the sequential quadratic programming code to move past what should have been an intermediate non-optimal solution.

Figure A.14 shows the trajectory computed using the initial estimate of the free parameters as well as the solutions calculated using central difference derivatives and state transition matrix derivatives. The largest difference between the solution found using the state transition matrix derivatives and the solution found using central difference derivatives is that the state transition matrix solution consists of a thrusting segment followed by a coasting segment while the central difference solution is one continuous thrusting segment. The switching function for all three of the trajectories is shown in Figure A.15. Because the state transition matrix solution's switching function is positive for a much shorter time than the other two switching functions, the spacecraft thrusts for a shorter period of time on the state transition trajectory. Consequently, this trajectory consumes less mass.

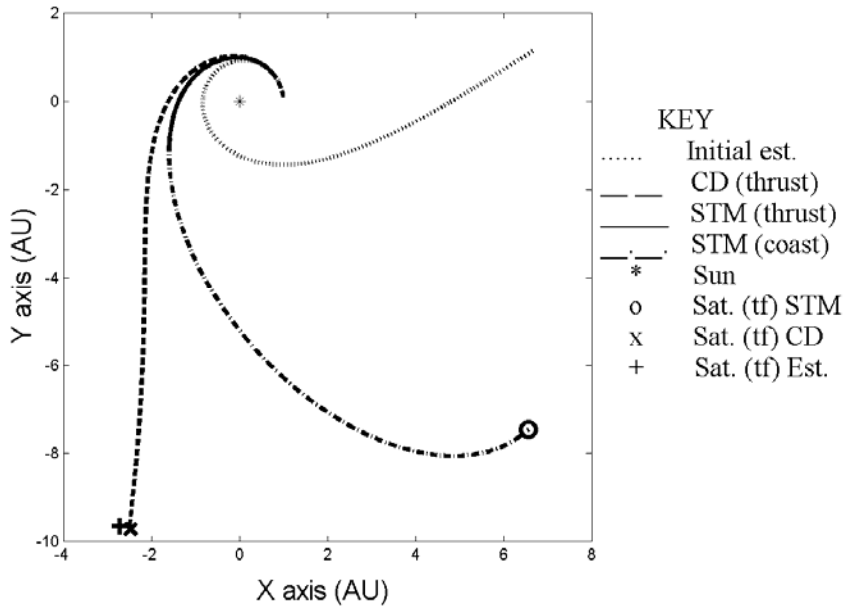

Figure A.14 Earth-Saturn Trajectories

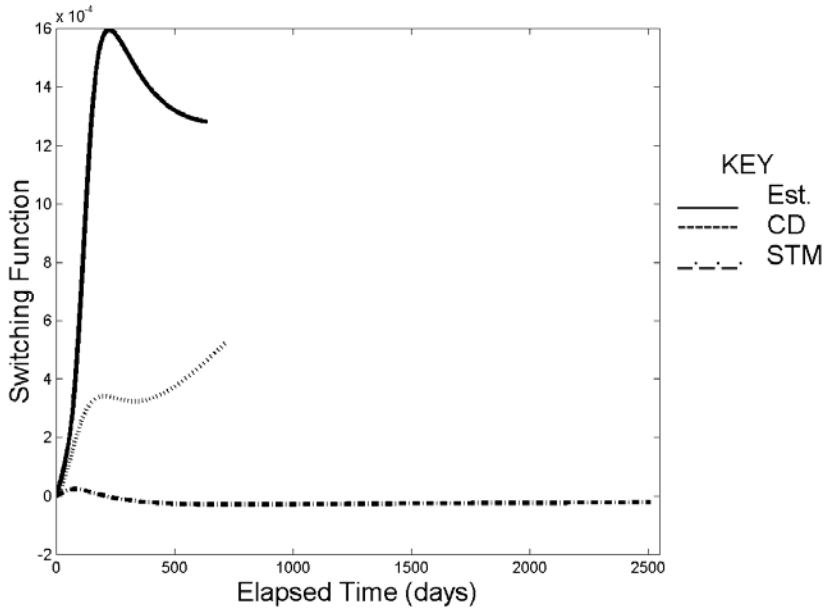

Figure A.15 Switching Structure for Earth-Saturn Trajectories

Appendix Conclusions

The state transition matrix method provides a tool to calculate the derivatives necessary to calculate optimal interplanetary trajectories even when the equations of motion and the spacecraft state are discontinuous. The partial derivative of the spacecraft state after the discontinuity with respect to the spacecraft state before the discontinuity must be known analytically. Using both sequential quadratic programming algorithms and rootfinding algorithms, the state transition matrix derivatives are shown to converge to the optimal solution from initial estimates of the free parameters where central difference derivatives fail to converge. The state transition matrix derivatives also do not require tuning of the perturbation step size.

The main disadvantage of using the state transition matrix to calculate derivatives is that it requires numerous analytic partial derivatives to be determined and coded. Whether the state transition matrix method or central difference method requires less total time (time required to derive conditions and move from initial estimates to final solution) depends on the number of solutions sought and the quality of the initial estimates for the free parameters.

Although the examples shown in this appendix only applied to gravity assist trajectories where the spacecraft state consisted of position, velocity, and mass or thrust-acceleration terms, the technique is general. These methods can be applied to any state space formulation where derivatives are necessary. The techniques from this chapter are used throughout this dissertation to determine numerical solutions. The solution process throughout this dissertation begins with a mass optimal solution. This mass optimal

solution is then walked to a mass plus observability optimal solution using these analytic derivatives.

APPENDIX B ADJOINT CONTROL TRANSFORMATION

The values of the position and velocity costates at the beginning of each trajectory segment are free parameters that must be optimized in order to determine the optimal trajectory. In order to obtain an initial estimate for these costates, an adjoint control transformation is used[33,34]. A frame is defined such that the first axis points along the spacecraft velocity, the third axis points along the orbital angular momentum vector of the spacecraft, and the second axis is defined so the system is right handed.

$$\begin{aligned} \hat{e}_1 &= \frac{\mathbf{v}}{v} \\ \hat{e}_2 &= \frac{\mathbf{h} \times \mathbf{v}}{|\mathbf{h} \times \mathbf{v}|} \\ \hat{e}_3 &= \frac{\mathbf{h}}{h} \end{aligned} \tag{B.1}$$

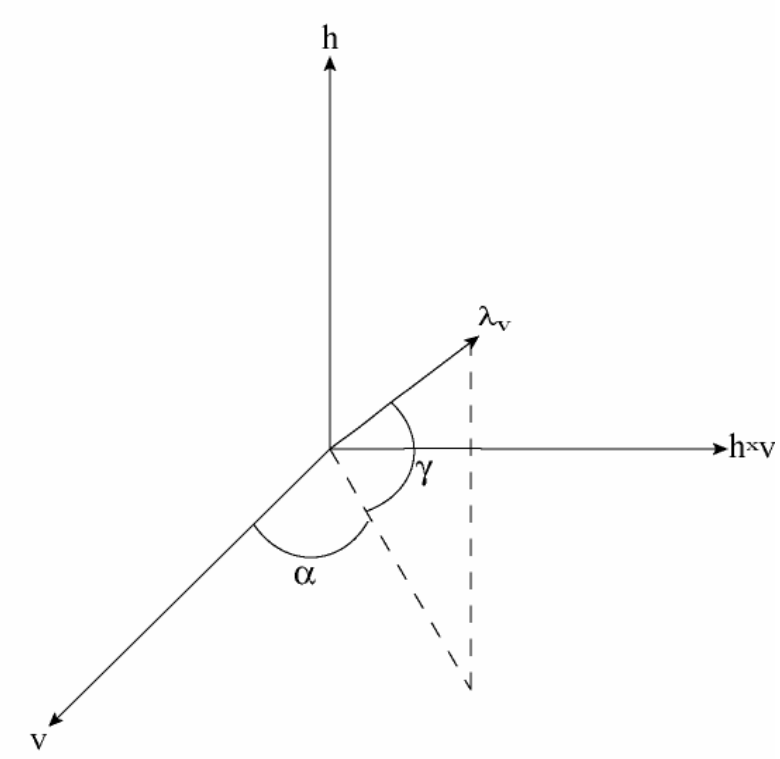

Figure B.1 Adjoint Control Transformation

The adjoint control transformation shown in Figure B.1 allows one to estimate the magnitude and direction of the costates in this vehicle-centered frame instead of requiring one to estimate the costates in the inertial Cartesian frame where the problem is solved. The initial velocity costate can thus be written as in Eq. (B.2). A transformation matrix can then be defined to express the costates on the inertial x, y, z bases as in Eqs. (B.4) and (B.5). Instead of estimating the initial value of the costates, the value of the adjoint control related variables α, γ, $\dot{\alpha}$, $\dot{\gamma}$, $\lambda_v(t_0)$, and $\dot{\lambda}_v(t_0)$ can be estimated. It is easier to determine an initial estimate of these parameters than it is to estimate the initial costates.[33,34]

$$\boldsymbol{\lambda}_{\mathbf{v}}(t_0)=\lambda_{\mathrm{v}}(t_0)\begin{pmatrix}\cos(\alpha)\cos(\gamma)\\ \sin(\alpha)\cos(\gamma)\\ \sin(\gamma)\end{pmatrix}\begin{matrix}\hat{e}_1\\ \hat{e}_2\\ \hat{e}_3\end{matrix} \tag{B.2}$$

$$\mathbf{R}=\begin{pmatrix}\dfrac{\mathbf{v}\cdot\hat{x}}{\mathrm{v}} & \dfrac{(\mathbf{h}\times\mathbf{v})\cdot\hat{x}}{|\mathbf{h}\times\mathbf{v}|} & \dfrac{\mathbf{h}\cdot\hat{x}}{\mathrm{h}}\\ \dfrac{\mathbf{v}\cdot\hat{y}}{\mathrm{v}} & \dfrac{(\mathbf{h}\times\mathbf{v})\cdot\hat{y}}{|\mathbf{h}\times\mathbf{v}|} & \dfrac{\mathbf{h}\cdot\hat{y}}{\mathrm{h}}\\ \dfrac{\mathbf{v}\cdot\hat{z}}{\mathrm{v}} & \dfrac{(\mathbf{h}\times\mathbf{v})\cdot\hat{z}}{|\mathbf{h}\times\mathbf{v}|} & \dfrac{\mathbf{h}\cdot\hat{z}}{\mathrm{h}}\end{pmatrix} \tag{B.3}$$

$$\boldsymbol{\lambda}_{\mathbf{v}}(t_0)=\lambda_{\mathrm{v}}(t_0)\mathbf{R}\begin{pmatrix}\cos(\alpha)\cos(\gamma)\\ \sin(\alpha)\cos(\gamma)\\ \sin(\gamma)\end{pmatrix}\begin{matrix}\hat{x}\\ \hat{y}\\ \hat{z}\end{matrix} \tag{B.4}$$

$$\begin{aligned}\boldsymbol{\lambda}_{\mathbf{r}}(t_0)=&\left[\lambda_{\mathrm{v}}(t_0)\mathbf{R}\begin{pmatrix}\dot{\alpha}\sin(\alpha)\cos(\gamma)+\dot{\gamma}\cos(\alpha)\sin(\gamma)\\ \dot{\alpha}\cos(\alpha)\cos(\gamma)+\dot{\gamma}\sin(\alpha)\sin(\gamma)\\ -\dot{\gamma}\cos(\gamma)\end{pmatrix}\right.\\ &\left.-\dot{\lambda}_{\mathrm{v}}(t_0)\mathbf{R}\begin{pmatrix}\cos(\alpha)\cos(\gamma)\\ \sin(\alpha)\cos(\gamma)\\ \sin(\gamma)\end{pmatrix}-\lambda_{\mathrm{v}}(t_0)\dot{\mathbf{R}}\begin{pmatrix}\cos(\alpha)\cos(\gamma)\\ \sin(\alpha)\cos(\gamma)\\ \sin(\gamma)\end{pmatrix}\right]\begin{matrix}\hat{x}\\ \hat{y}\\ \hat{z}\end{matrix}\end{aligned} \tag{B.5}$$

APPENDIX C GRAVITY ASSIST MODEL

The flyby is modeled as a zero sphere of influence patched conic where the velocity of the spacecraft changes instantaneously and the position of the spacecraft remains constant. The spacecraft is constrained to intercept the center of the flyby planet at the time of the gravity assist even though the flyby radius is non-zero. The cost difference of targeting the flyby radius instead of the center of the planet is minimal. The impulsive thrust engine is able to create a Δv parallel to v_∞ at the location that would be periapse of an unpowered flyby. Because the finite thrust engines are unable to provide an impulsive velocity change, Δv_{pow} is equal to zero for the finite thrust engine model. As a result, J is constant across the flyby. The flyby angle, β shown in Figure C.1, is the angle from the $(v_{\infty\,i} \times v_p) \times v_{\infty\,i}$ axis to the projection of $v_{\infty\,o}$ in the plane defined by the $(v_{\infty\,i} \times v_p) \times v_{\infty\,i}$ and $v_{\infty\,i} \times v_p$ axes. This angle determines which side of the planet the spacecraft flies past during the gravity assist. The flyby radius can be constrained to be greater than or equal to a minimum value. The velocity change during the flyby can be determined from Eqs. (C.1) to (C.7).[35]

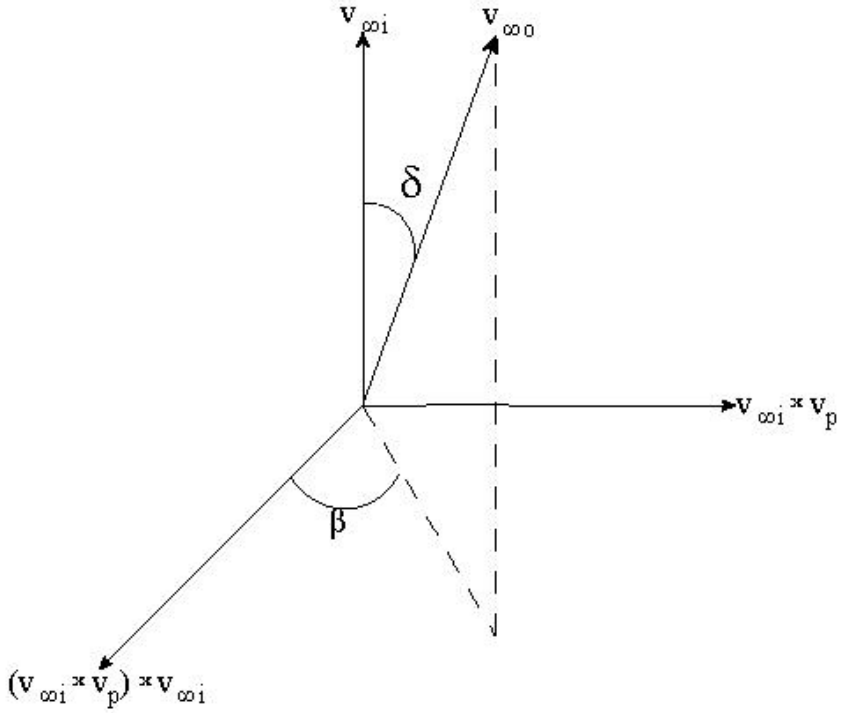

Figure C.1 Flyby Angle and Flyby Turn Angle

$$\sin\left(\frac{\delta_{\text{fb1}}}{2}\right) = \frac{\mu_{\text{fb}}}{\mu_{\text{fb}} + \text{r}_{\text{m}} \text{v}_{\infty_i}{}^2} \tag{C.1}$$

$$\sin\left(\frac{\delta_{\text{fb2}}}{2}\right) = \frac{\mu_{\text{fb}}}{\mu_{\text{fb}} + \text{r}_{\text{m}} \text{v}_{\infty_o}{}^2} \tag{C.2}$$

$$\text{v}_{\infty_o} = \text{v}_{\infty_i} + \Delta\text{v}_{\text{pow}} \tag{C.3}$$

$$\delta_{\text{fb}} = \frac{\delta_{\text{fb1}} + \delta_{\text{fb2}}}{2} \tag{C.4}$$

$$\mathbf{R}_{\text{fb}} = \begin{pmatrix} \dfrac{\mathbf{v}_{\infty_i} \cdot \hat{x}}{\mathrm{v}_{\infty_i}} & \dfrac{[(\mathbf{v}_{\infty_i} \times \mathbf{v}_p) \times \mathbf{v}_{\infty_i}] \cdot \hat{x}}{|(\mathbf{v}_{\infty_i} \times \mathbf{v}_p) \times \mathbf{v}_{\infty_i}|} & \dfrac{(\mathbf{v}_{\infty_i} \times \mathbf{v}_p) \cdot \hat{x}}{|\mathbf{v}_{\infty_i} \times \mathbf{v}_p|} \\ \dfrac{\mathbf{v}_{\infty_i} \cdot \hat{y}}{\mathrm{v}_{\infty_i}} & \dfrac{[(\mathbf{v}_{\infty_i} \times \mathbf{v}_p) \times \mathbf{v}_{\infty_i}] \cdot \hat{y}}{|(\mathbf{v}_{\infty_i} \times \mathbf{v}_p) \times \mathbf{v}_{\infty_i}|} & \dfrac{(\mathbf{v}_{\infty_i} \times \mathbf{v}_p) \cdot \hat{y}}{|\mathbf{v}_{\infty_i} \times \mathbf{v}_p|} \\ \dfrac{\mathbf{v}_{\infty_i} \cdot \hat{z}}{\mathrm{v}_{\infty_i}} & \dfrac{[(\mathbf{v}_{\infty_i} \times \mathbf{v}_p) \times \mathbf{v}_{\infty_i}] \cdot \hat{z}}{|(\mathbf{v}_{\infty_i} \times \mathbf{v}_p) \times \mathbf{v}_{\infty_i}|} & \dfrac{(\mathbf{v}_{\infty_i} \times \mathbf{v}_p) \cdot \hat{z}}{|\mathbf{v}_{\infty_i} \times \mathbf{v}_p|} \end{pmatrix} \tag{C.5}$$

$$\mathbf{r}(\mathrm{t}_{\text{fb+}}) = \mathbf{r}(\mathrm{t}_{\text{fb-}}) \tag{C.6}$$

$$\mathbf{v}(\mathrm{t}_{\text{fb+}}) = \mathbf{v}_{\mathrm{p}}(\mathrm{t}_{\text{fb}}) + \mathrm{v}_{\infty_o} \mathbf{R}_{\text{fb}} \begin{pmatrix} \cos(\delta_{\text{fb}}) \\ \sin(\delta_{\text{fb}})\cos(\beta) \\ s\,\mathrm{in}(\delta_{\text{fb}})\sin(\beta) \end{pmatrix} \tag{C.7}$$

REFERENCES

[1] Betts, J. T. "Survey of Numerical Methods for Trajectory Optimization", *Journal of Guidance, Control, and Dynamics*, Vol. 21, pp. 193-207, 1998.

[2] Lawden, D. E. *Optimal Trajectories for Space Navigation*, Butterworths, London, 1963.

[3] Jezewski, D. J. "Primer Vector Theory and Applications", NASA Technical Report R-454, Lyndon B. Johnson Space Center, Houston, TX, 1975.

[4] Vander Stoep, D. R. "Trajectory Shaping for the Minimization of State-Variable Estimation Errors" *IEEE Transactions on Automatic Control* Vol. AC-13, pp. 284-286, 1968.

[5] Schmidt, G. T. "A New Technique for Identification and Control of Systems with Unknown Parameters", Dissertation, Massachusetts Institute of Technology, 1970.

[6] Speyer, J. L., Hull, D. G., Tseng, C. Y., and Larson, S. W. "Estimation Enhancement by Trajectory Modulation for Homing Missiles" *Journal of Guidance, Control, and Dynamics*, Vol. 4, pp. 167-174, 1984.

[7] Hull, D. G., Speyer, J. L., and Tseng, C. Y. "Maximum-Information Guidance for Homing Missiles", *Journal of Guidance, Control, and Dynamics*, Vol. 8, No. 4, 1985, pp. 494-497.

[8] Hull, D. G., Speyer, J. L., and Burris, D. B. "Linear-Quadratic Guidance Law for Dual Control of Homing Missiles", *Journal of Guidance, Control, and Dynamics*, Vol. 13, No. 1, 1990, pp. 137-144.

[9] Oshman, Y. and Davidson, P. "Optimization of Observer Trajectories for Bearings Only Target Localization", *IEEE Transactions on Aerospace and Electronic Systems* Vol. 35, No. 3, pp. 892-902, 1999

[10] Seywald, H. and Kumar, R. "Desensitized Optimal Trajectories", AIAA/AAS Spaceflight Mechanics Meeting, AAS Paper 96-107, Austin, TX, 1996.

[11] Seywald, H. "Desensitized Optimal Trajectories with Control Constraints", AIAA/AAS Spaceflight Mechanics Meeting, AAS Paper 03-147, Ponce, Puerto Rico, 2003.

[12] Seywald, H. "Desensitized Optimal Orbit Insertion", AAS/AIAA SpaceFlight Mechanics Meeting, AAS Paper 04-215. Maui, HI, 2004.

[13] Mishne, D. ”Guidance Law for the Reconfiguration of Satellite Formation, in the Presence of Measurement Errors”, AIAA/AAS Astrodynamics Specialist Conference, AAS Paper 05-334, Lake Tahoe, CA, 2005.

[14] Zimmer, S., Ocampo, C. and Bishop, R. “Incorporating Observability Into Trajectory Optimization,” AIAA/AAS Spaceflight Mechanics Meeting, AAS Paper 05-132, Copper Mountain, CO, 2005.

[15] Zimmer, S., Ocampo, C. and Bishop, R. “Decreasing Semimajor Axis Uncertainty Through Trajectory Design,” AIAA/AAS Astrodynamics Specialist Conference, AAS Paper 05-333, Lake Tahoe, CA, 2005

[16] Zimmer, S., Ocampo, C. and Bishop, R. ”Decreasing Spacecraft Uncertainty Through Trajectory Design with Discrete Observation Measurements,” AIAA/AAS Astrodynamics Specialist Conference, AAS Paper 05-334, Lake Tahoe, CA, 2005.

[17] Zimmer, S. and Ocampo, C. “The Use of Analytical Gradients to Calculate Optimal Gravity Assist Trajectories,” *Journal of Guidance Control and Dynamics*, Vol. 28, no. 2, pp. 324-332, Mar.-Apr. 2005.

[18] Zimmer, S. and Ocampo, C. "Analytical Gradients for Gravity Assist Trajectories Using Constant Specific Impulse Engines," *Journal of Guidance Control and Dynamics,* Vol. 28, no. 4, pp. 753-760, Jul.-Aug. 2005.

[19] Hull, D. G. *Optimal Control Theory for Applications*, Springer, New York, 2003.

[20] Bishop, R.H., Burkhart, P. D., and Thurman, S. W. "Observability During Planetary Approach Navigation", *Advances of the Astronautical Sciences*, Vol. 82, Pt. 2, 1993, pp. 973-984.

[21] Prussing, J. E. "Equation for Optimal Power-Limited Spacecraft Trajectories," *Journal of Guidance, Control, and Dynamics*, Vol. 16, No. 2, 1993, pp. 391-393.

[22] Gelb, A. *et* al., *An Applied Optimal Estimation*, American Massachusetts Institute of Technology, Cambridge, MA, 1989.

[23] D'Amario, L. A., Byrnes, D. V., Sackett, L. L., and Stanford, R. H., "Optimization of Multiple Flyby Trajectories," *Advances in the Astronautical Sciences*, AAS Paper 79-162, Vol. 40, Pt. 2, 1979, pp. 695-729.

[24] Sauer, C. G. Jr. "Optimization of Interplanetary Trajectories with Unpowered Planetary Swingbys," *Advances in the Astronautical Sciences*, AAS Paper 87-424, Vol. 65, Pt. 1, 1987, pp. 253-272.

[25] Mirfakhraie, K. and Conway, B. "Optimal Cooperative Time-Fixed Impulsive Rendezvous," *Journal of Guidance, Control, and Dynamics*, Vol. 17, No. 3, 1994, pp. 607-613.

[26] Ocampo, C. A. and Rosborough, G. W. "Optimal Low-Thrust Transfers Between a Class of Restricted Three-Body Trajectories," *Advances in the Astronautical Sciences*, AAS Paper 93-681, vol. 85, Pt. 2, 1993, pp. 1547-1566.

[27] Gill, P., E., Murray, W., and Wright, M., H. *Practical Optimization*, Academic Press, London, 1981, Ch. 8.

[28] Hull, D. G. and Williamson, W. E. "Numerical Derivatives for Parameter Optimization," *Journal of Guidance and Control*, Vol. 2, No. 2, 1979, pp158-160.

[29] Hindmarsh, A. C. "Serial Fortran Solvers for ODE Initial Value Problems," URL:http://www.llnl.gov/CASC/odepack [cited October 18, 2005].

[30] Standish, E. M. "The JPL Planetary and Lunar Ephemerides DE405/LE405," URL:http://ssd.jpl.nasa.gov/iau-comm4/de405iom/de405iom.ps [cited October 18, 2005].

[31] "VF13AD", *Harwell Subroutine Library*, URL: http://hsl.rl.ac.uk/archive2002/hslarchive/packages/vf13/vf13.pdf [cited October 18, 2005].

[32] Casalino, L., Colosurdo, G. and Pastrone, D. "Optimization of ΔV Earth-Gravity-Assist Trajectories," *Journal of Guidance, Control, and Dynamics*, Vol. 21, No. 6, 1998, pp. 991-995.

[33] Dixon, L. C. W., and Biggs, M. C. "The Advantages of Adjoint-Control Transformations when Determining Optimal Trajectories by Pontryagin's Maximum Principle," *Aeronautical Journal*, March 1972, pp. 169-174.

[34] Zondervan, K. P., Wood, L. J. and Caughey, T. K. "Optimal Low-Thrust, Three-Burn Orbit Transfers with Large Plane Changes," *The Journal of the Astronautical Sciences*, Vol. 32, No. 3, 1984, pp. 407-427.

[35] Battin, R. H., *An introduction to the Mathematics and Methods of Astrodynamics, Revised Edition,* American Institute of Aeronautics and Astronautics, Reston, VA, 1999, Ch. 9.

VITA

Scott Zimmer was born in Joliet, Illinois in 1978. He is the son of Bob and Dorothy Zimmer. Scott has one older brother, Bart, who is attending Law School at the University of Michigan. Scott was the valedictorian of the class of 1997 at Joliet West High School. Scott attended the University of Illinois at Urbana-Champaign where he majored in Aeronautical and Astronautical Engineering. At Illinois, Scott worked in Professor Wayne Solomon's laser laboratory for two years. Scott was also co-director of the Engineering 100 program. In May 2001 Scott received his Bachelor of Science Degree from Illinois. In the fall of 2001, Scott began graduate school at the University of Texas at Austin. Scott married Erin Lehner of Joliet on August 10, 2002. At Texas, Scott has worked as both a research assistant and a teaching assistant. Scott has been advised by Professor Cesar Ocampo and Professor Robert Bishop while at Texas. He has also presented papers at several AIAA conferences and published articles in the *Journal of Guidance, Control, and Dynamics*. The majority of Scott's funding has come from a National Defense Science and Engineering Graduate Fellowship as well as the Thrust 2000 Fellowship program. Scott will remain at the University of Texas at Austin as a lecturer during Spring 2006. Scott will join The Aerospace Corporation in Chantilly, Virginia in the Summer of 2006.

Permanent Address: 3407 Pandola Avenue; Joliet, IL 60431

This dissertation was typed by the author.